

MULTICONFIGURATIONAL PERTURBATION THEORY: APPLICATIONS IN ELECTRONIC SPECTROSCOPY

BJÖRN O. ROOS, KERSTIN ANDERSSON,
MARKUS P. FÜLSCHER, PER-ÅKE MALMQVIST,
and LUIS SERRANO-ANDRÉS

Department of Theoretical Chemistry, Chemical Centre, Lund, Sweden

KRISTIN PIERLOOT

*Department of Chemistry, University of Leuven, Heverlee-Leuven,
Belgium*

MANUELA MERCHÁN

Departamento de Química Física, Universitat de València, Spain

CONTENTS

- Abstract
- I. Introduction
- II. Multiconfigurational Perturbation Theory
 - A. Zeroth-Order Hamiltonian
 - B. Multistate CASPT2
 - C. Intruder-State Problem
- III. Applications in Spectroscopy
 - A. Electronic Spectroscopy for Organic Molecules
 - 1. Basis Sets
 - 2. Problems and Limitations
 - 3. Solvation Effects
 - 4. Spectroscopy of Carbonyl Compounds: Formaldehyde and Acetone
 - 5. Interacting Double Bonds: Methylene-cyclopropene

6. Interacting Fragments: Biphenyl and Bithiophene
 7. Spectroscopy of Protein Chromophores
 8. Electronic Spectra of Radical Cations of Linear Conjugated Polyenes and Polycyclic Aromatic Hydrocarbons
- B. Electronic Spectroscopy for Transition Metal Compounds
1. Special Considerations
 2. Transition Metal Complexes with Cyanide and Carbonyl Ligands
 3. Cr_2 Molecule and Its Spectroscopy

IV. Summary

Acknowledgments

References

ABSTRACT

Applications of the complete active space (CAS) SCF method and multiconfigurational second-order perturbation theory (CASPT2) in electronic spectroscopy are reviewed. The CASSCF/CASPT2 method was developed five to seven years ago and the first applications in spectroscopy were performed in 1991. Since then, about 100 molecular systems have been studied. Most of the applications have been to organic molecules and to transition metal compounds. The overall accuracy of the approach is better than 0.3 eV for excitation energies except in a few cases, where the CASSCF reference function does not characterize the electronic state with sufficient accuracy.

Some of the more important aspects of the theory behind the method are described in the review. In particular, the choice of the zeroth-order Hamiltonian is discussed together with the intruder-state problem and its solution. A generalization of the method to a multistate perturbation approach is suggested. Problems specifically related to spectroscopic applications are discussed, such as the choice of the active space and the treatment of solvent effects.

The spirit is to show some of the results, but also to guide users of the approach by pointing to the problems and limitations of the method. The review covers some of the newer applications in the spectroscopy of organic molecules: acetone, methylenecyclopropene, biphenyl, bithiophene, the protein chromophores indole and imidazole, and a series of radical cations of conjugated polyenes and polyaromatic hydrocarbons. The applications in transition metal chemistry include carbonyl, nitrosyl, and cyanide complexes, some dihalogens, and the chromium dimer.

I. INTRODUCTION

The improvement in recent years of the methods and techniques of *ab initio* quantum chemistry has considerably increased the possibilities of

obtaining accurate theoretical information about spectroscopic properties of molecular systems and of their photochemistry (see, e.g., articles in Ref. 1). It is in particular the developments of the multiconfigurational approaches that have had a profound impact on the possibilities for large-scale applications in spectroscopy. The electronic structure for most ground-state molecules is rather simple, with the wavefunction dominated by a single (Hartree–Fock) configuration. The situation is different for the excited states. Here the energy separation between different electronic configurations is smaller, which results in larger mixing. Singly and doubly excited configurations close in energy are not uncommon. A typical case in organic systems results from the interaction of two C=C double bonds. The triplet excitations in each of them can couple to a singlet with an energy close to that of a singly excited singlet state in one of them. This has profound consequences for the lower part of the electronic spectrum of such systems, for example, in pyrrole, thiophene, and related system (for details, see the article by Roos et al. in Ref. 1).

Situations such as the one described above are normally treated using multiconfigurational (MC) SCF theories. Most MCSCF calculations are today performed within the framework of the complete active space (CAS) SCF scheme [2]. The generality of this approach makes it especially suitable for studies of excited states. The wavefunction is defined by selecting a set of active orbitals and is constructed as a linear expansion in the set of configuration functions (CFs) that can be generated by occupying the active orbitals in all ways consistent with an overall spin and space symmetry [full configuration interaction (CI)]. No assumptions are made regarding the character of the excited states (singly or multiply excited) or the shape of the molecular orbitals. The latter are optimized with the only limitations set by the chosen basis set. This can be done independently for each state but is more commonly done as an average over a set of excited states. The CASSCF method has been used to study a large number of spectroscopic problems for small and medium-sized molecules.

However, while the CASSCF method can handle the near-degeneracy problem in a balanced and effective way, it does not include the effects of dynamic (external) correlation. For small molecules it is possible to treat this problem using multireference (MR) CI or similar techniques. Two recent review articles in the electronic spectroscopy of diatomic [3] and triatomic [4] molecules provide good illustrations of the present state of the art. The MRCI method is in principle capable of very high accuracy. It is also very general and can treat any type of electronically excited state. However, the computational effort increases steeply with the number of correlated electrons. It is therefore not a method that can be used for larger molecules. An illustration is given by a recent MRCI study

of the electronic spectrum of the pyrimidine molecule, which failed due to the size bottleneck [5].

An alternative approach for the treatment of dynamic correlation effects within the multiconfigurational framework was developed six years ago [6, 7], based on an earlier suggestion [8]. The idea was to use second-order perturbation theory. As all configurations with large coefficients were included into the CASSCF wavefunction, the presumption was that it should be possible to obtain an accurate estimate of the contributions from the remainder of the full CI space by means of low-order perturbation theory, where the CASSCF wavefunction acts as the zeroth-order approximation (the reference function). A perturbation method is also size consistent and can therefore be applied to systems with many electrons without loss of accuracy (in practice, it turns out that the approach is only "almost size consistent," but this has no practical consequences, since the nonadditive terms give very small contributions to the correlation energy [9]). The algorithm for the solution of the first-order equations has a complicated structure, and an effective implementation is possible only if one can compute effectively up to fourth-order density matrices for the CASSCF wavefunction. This problem was solved using the split unitary group approach [10]. The resulting method was named CASPT2 and has been added to the MOLCAS quantum chemistry software [11]. All results that will be presented here have been obtained using this program. The CASPT2 method has been applied to a large body of chemical problems. Provided that extended basis sets are used and the active space of the CASSCF reference function is properly chosen, it gives highly accurate relative energies for a broad range of chemical problems (for a recent review, see Ref. 12). Due to the general nature of the reference function, the method works equally well for ground and excited states and for electronic states that are not well characterized by a single configuration. The applications in electronic spectroscopy have been especially rewarding, since alternative methods exist only for small molecules. The results obtained for excited states of organic molecules have recently been reviewed [13].

The present review is concerned with general aspects of applications of the CASSCF/CASPT2 method in molecular spectroscopy. We first introduce the reader to the method. This is brief; we refer readers to the original papers and the thesis of Andersson [14] for details. The pitfalls of the method are discussed with special emphasis on the intruder-state problem. The applications in spectroscopy are divided into two parts. One deals with recent results obtained for organic systems and the other with transition metal compounds. For each of these types of application, we discuss the general requirements that have to be fulfilled to obtain

accurate results. These include the choice of active space, basis set, and so on. The final discussion emphasizes the limitations of the method and where future work should be concentrated to increase the range of applications and the effectiveness of the approach.

II. MULTICONFIGURATIONAL PERTURBATION THEORY

The (hopefully converging) series of results from any systematic iterative method defines the partial sums of a perturbation series. We consider the approximate solution to the electronic Schrödinger equation. In this context a Taylor series expansion in one perturbation parameter is almost always implied:

$$\hat{H} = \hat{H}_0 + \lambda \hat{H}_1, \quad (1)$$

where \hat{H}_0 is a simplified operator, which can be chosen on grounds of expediency, and λ is the formal perturbation parameter.

In particular, state-specific methods produce a state function and an energy:

$$\begin{aligned} \hat{H}(\lambda)\Psi(\lambda) &= E(\lambda)\Psi(\lambda) \\ \Psi(\lambda) &= \Psi_0 + \sum_1^{\infty} \lambda^k \Psi_k \\ E(\lambda) &= E_0 + \sum_1^{\infty} \lambda^k E_k \end{aligned} \quad (2)$$

as functions of λ , expressed as Taylor expansions, and we are usually interested only in the value $\lambda = 1$.

By contrast, effective Hamiltonian methods produce a stable subspace and an effective Hamiltonian matrix:

$$\begin{aligned} \hat{H}(\lambda)\Psi(\lambda) &= \Psi(\lambda)\mathbf{H}^{\text{eff}}(\lambda), \\ \Psi(\lambda) &= \Psi_0 + \sum_1^{\infty} \lambda^k \Psi_k, \\ \mathbf{H}^{\text{eff}}(\lambda) &= \mathbf{H}_0 + \sum_1^{\infty} \lambda^k \mathbf{H}_k, \end{aligned} \quad (3)$$

where Ψ is now a row array of wavefunctions. The space spanned by Ψ_0 is called the model space. For $\lambda = 1$, the exact energies are obtained as the eigenvalues of the matrix \mathbf{H}^{eff} . The state-specific perturbation series is

thus a special case of the effective Hamiltonian method, with a one-dimensional model space.

If any of the functions of λ above is not analytic for all arguments $|\lambda| \leq 1$, the perturbation series of that function does not converge. We will be concerned only with the conventional situation where the wavefunction is contained in a finite (but potentially huge) space spanned by Slater determinant functions constructed by a finite set of orbitals, or equivalently, such determinants precombined into configuration functions (CFs). From the point of view of this article, the Hamiltonian \hat{H} is thus not the exact electronic Hamiltonian but is its projection in the CF space. Our aim is thus to construct a perturbation theory that approximates the full CI result in this space. The FCI equations are algebraic equations, and lack of convergence of the perturbation series is then caused by near coincidence of energies of model functions with functions outside the model space, which are in this context called intruders.

In this article we deal exclusively with the CASPT2 method, where the series expansions are truncated to first order in wavefunctions, and second order in energy. Intruders are tolerable if they do not contribute to the energy at this level. We assume that the reader has some familiarity with the CASSCF method, which is used to obtain the root function. More information can be obtained in earlier review articles [2, 12, 13]. The equations to be solved, to the second order, are simple:

$$\begin{aligned} \hat{H}_0 \Psi_0 &= E_0 \Psi_0, \\ E_1 &= \langle \Psi_0 | \hat{H}_1 | \Psi_0 \rangle, \\ (\hat{H}_0 - E_0) \Psi_1 &= -(\hat{H}_1 - E_1) \Psi_0, \\ E_2 &= \langle \Psi_1 | \hat{H}_1 | \Psi_0 \rangle. \end{aligned} \tag{4}$$

The Ψ_1 wavefunction is restricted to be orthonormal to Ψ_0 , which gives the equation system a unique and well-conditioned solution if there is no intruder. Obviously, the first equation is normally not to be solved for Ψ_0 . Instead, that wavefunction is given, and \hat{H}_0 is designed to have it as an eigenfunction.

There are a number of important differences between single-determinant root functions and multiconfigurational root functions. One of the most important is that a one-electron operator cannot in general have a multiconfigurational Ψ_0 as an eigenfunction. Consider first the ordinary Møller–Plesset perturbation series: The \hat{H}_0 operator is chosen to be $\hat{H}_0 = \hat{F}$, the Fock operator of Hartree–Fock theory. The orbitals are usually chosen to diagonalize \hat{F} . The solution of the perturbation

equations will preserve the number of excited electrons, so the first-order wavefunction can involve only single and double excitations. Similarly, the n th order involves $1-2n$ excited electrons. A zero-electron excitation is never produced, because of orthogonality.

From a formal point of view, the simplest multiconfigurational extension again uses a diagonal, one-electron \hat{H}_0 . However, this is simple only when the *space of interacting determinants* is small enough. This contains the set of determinants that are produced by single and double excitations from those determinants that are used in the root wavefunction. Moreover, it requires that \hat{F} has Ψ_0 as eigenfunction, which is possible for a multiconfigurational wavefunction only if all the active orbitals have the same orbital energy (quasidegenerate perturbation theory). For general purposes it is advantageous to work with CASSCF wavefunctions. There are then typically 10^{10} interacting determinants, and also the quasidegenerate \hat{H}_0 is rarely adequate.

By contrast, CASPT2 uses orbital excitation operators applied to the root wavefunction to express the perturbation function. Apart from the root function itself, this generates the singly excited wavefunctions $\{\hat{E}_{pq}\Psi_0\}$, the doubly excited wavefunctions $\{\hat{E}_{pqrs}\Psi_0\}$, and so on. These lists are here written in a general way—in practice, many of the terms listed are zero, and the rest may be linearly dependent. Furthermore, perhaps surprising at first, in contrast to the ordinary single-configurational case, the space spanned by the doubly excited wavefunctions contains the singly excited ones. This set of functions, orthonormalized against the CAS-CI space, will be called the first-order interacting (FOI) space. In CASPT2, the number of independent variables is roughly, as for MP2, equal to the number of occupied pair of orbitals, times the number of virtual pairs. This small number has been obtained at the price of complexity: In order to make Ψ_0 an eigenfunction of \hat{H}_0 , we must use a projection operator $\hat{P}_0 = |\Psi_0\rangle\langle\Psi_0|$. To have Ψ_1 contained in the doubly excited space, there is a further projection. Due to the linear dependencies, the equation systems are overcomplete. Finally, the equation system does not have a diagonal equation matrix, but a dense one, often with a poor condition number and important nondiagonal elements.

Those complications are technical. For details, we refer to the original work [6, 7, 14], and to a recent review article [12]. Understanding the program from a functional point of view requires merely these pertinent facts: It is an ordinary MP perturbation theory, taken to second order in energy. Due to its use of a multiconfigurational root function, the equations may take a longer time to solve, but the rewards are a general applicability (regardless of multiplicity and symmetry, also for excited states) and often a higher accuracy as well since important correlation is

already built into the root function. Two important issues follow immediately from the wider range of applications. The definition of \hat{H}_0 will be suitably extended to multiconfigurational cases in the next section. Then the intruders must be dealt with—they are rare in near-closed-shell applications but are common among excited states, and occasionally appear during bond-breaking and similar near-degenerate situations.

A. Zeroth-Order Hamilton

In single-determinant perturbation theory, all formulas can be evaluated either by diagram techniques or by simple algebra. The energy, or any other quantity, at any level of perturbation theory, is obtained by a short sequence of operations, either of matrix multiplication type, or else division by energy denominators. This simplicity arises from the fact that every matrix element in the formulas will be a product of basic integrals, divided by such denominators, times a product of Kronecker deltas in the orbital indices. In the CASPT2 case, this remains true for those orbital indices that refer to either inactive or secondary orbitals in the CASSCF: those that are always doubly occupied, or not occupied at all, in the root (or reference) function. However, all formulas that involve active orbitals, which are those with different occupancy in different terms in the reference function, will be quite complicated. This is true already for the simplest possible zeroth-order Hamiltonian: the Møller–Plesset-like ansatz, which uses a Fock matrix (suitably generalized). The special case of a quasidegenerate Fock matrix is simpler still but is useful only for very simple references of the ROHF type, where all active orbitals are singly occupied and symmetry equivalent.

The \hat{H}_0 operator must be simple, but it must also be a reasonable approximation to \hat{H} for wavefunctions in the interacting space. If \hat{H} had, in fact, been expressible as a one-electron operator $\hat{f} = \sum f_{pq} \hat{a}_p^\dagger \hat{a}_q$, with matrix elements unknown to us, the matrix elements could be obtained by the formula $f_{pq} = -\langle \Phi | [[\hat{H}, \hat{a}_q^\dagger], \hat{a}_p]_+ | \Phi \rangle$, for any arbitrary normalized wavefunction. If it is not an exact one-electron operator, this formula can be used for a specific Φ —in our case we will choose the root function Ψ_0 —or an average of several Φ functions or an ensemble of wavefunctions, to obtain an approximation. In particular, if Ψ_0 is a component of a set of symmetry-equivalent degenerate states, and if we require \hat{H}_0 to preserve this symmetry, we must use the average over the members of this degenerate set.

In our previous work [6, 7], the operator defined above was evaluated for the average over the spin of Ψ_0 , since we require that \hat{H}_0 does not break spin symmetry. The result is

$$f_{pq} = h_{pq} + \sum_{rs} D_{rs} [(pq|rs) - \frac{1}{2}(pr|sq)], \quad (5)$$

where spatial orbitals and the spin-summed density matrix \mathbf{D} are used, as a consequence of the spin summations. \mathbf{h} is the core Hamiltonian, and for a closed-shell wavefunction, this Fock matrix is identical to the conventional one used in Hartree–Fock theory. The extension of the Fock matrix to general correlated wavefunctions has been used before in other contexts. It interpolates between two matrices: the eigenvalues (with opposite sign) of one are ionization energies, and the eigenvalues of the other are electron affinities, both in the sense of the extended Koopmans theorem. We have for some time used the term *standard Fock matrix* for this matrix and suggest this as a suitable and highly needed name, since a host of other named matrices have been suggested for various purposes. We thus regard CASPT2 as an extension of the Møller–Plesset method, which allows CASSCF reference functions.

Multiconfigurational perturbation theory as outlined above has been applied successfully to a large number of chemical problems (see Refs. 12 and 13 and references therein). The zeroth-order Hamiltonian has thus turned out to be a good choice for a broad range of problems. However, in a systematic test of geometries and binding energies of 32 molecules containing first-row atoms [15], it was noticed that wavefunctions dominated by an open-shell configuration were favored over wavefunctions dominated by a closed-shell configuration. This led to dissociation energies underestimated with between 3 and 6 kcal/mol times the number of extra electron pairs formed. It would be desirable to give a more balanced treatment of these two kinds of wavefunctions for a more accurate determination of dissociation energies and excitation energies.

One deficiency can be seen in the case of a high-spin open-shell wavefunction. If the condition that \mathbf{f} should not be symmetry breaking is relaxed, by replacing \mathbf{D} with the spin density matrix and using spin orbitals, we arrive at

$$f_{pq}^{\alpha} = h_{pq}^{\alpha} + \sum_{r=1}^{N^{\beta}} [(\phi_p^{\alpha} \phi_q^{\alpha} | \phi_r^{\alpha} \phi_r^{\alpha}) + (\phi_p^{\alpha} \phi_q^{\alpha} | \phi_r^{\beta} \phi_r^{\beta}) - (\phi_p^{\alpha} \phi_r^{\alpha} | \phi_r^{\alpha} \phi_q^{\alpha})] \\ + \sum_{r=N^{\beta}+1}^{N^{\alpha}} [(\phi_p^{\alpha} \phi_q^{\alpha} | \phi_r^{\alpha} \phi_r^{\alpha}) - (\phi_p^{\alpha} \phi_r^{\alpha} | \phi_r^{\alpha} \phi_q^{\alpha})], \quad (6)$$

$$f_{pq}^{\beta} = h_{pq}^{\beta} + \sum_{r=1}^{N^{\beta}} [(\phi_p^{\beta} \phi_q^{\beta} | \phi_r^{\beta} \phi_r^{\beta}) + (\phi_p^{\beta} \phi_q^{\beta} | \phi_r^{\alpha} \phi_r^{\alpha}) - (\phi_p^{\beta} \phi_r^{\beta} | \phi_r^{\beta} \phi_q^{\beta})] \\ + \sum_{r=N^{\beta}+1}^{N^{\alpha}} (\phi_p^{\beta} \phi_q^{\beta} | \phi_r^{\alpha} \phi_r^{\alpha}), \quad (7)$$

where \mathbf{h}^α and \mathbf{h}^β are the matrix representations of \hat{h} in the spin α and spin β orbital spaces, the N^α electrons of α spin are described by the spatial orbitals ϕ_p^α , and the N^β electrons of β spin are described by the spatial orbitals ϕ_p^β . Just as the spin-summed standard Fock matrix coincides with the conventional one in the closed-shell case, the matrix displayed above coincides with the conventional spin-orbital Fock matrix when evaluated for a high-spin ROHF wavefunction. This Fock matrix is different for α and β spin, and since a systematic component in the CASPT2 error is associated with open shells, it could be hypothesized that this difference could be important to preserve. However, it turns out that a spin-dependent Fock matrix cannot be used with properly spin-coupled wavefunctions.

Consider, for instance, the dissociation of N_2 into two ground-state (e.g., ^4S) N atoms. The local effects of the exact Hamiltonian on one of the N atoms (its spectrum, for instance) is the same also when it is considered as one part of a molecule with large enough interatomic distance. This locality property must be shared by the zero-order Hamiltonian if the perturbation theory is to be size consistent. But the local state of the N atom, during dissociation of the molecule from the ground ($^1\Sigma_g^+$) state, is not described by a wavefunction: It is a mixed state, containing four different spin projections. This mixed state is what any size-consistent Hamiltonian will see, locally. It must treat each spin component in an equal way. The naïve use of a spin-dependent Fock matrix would actually have almost no effect on the ground-state dissociation of the N_2 molecule. It would have the intended effect on the high-spin $^7\Sigma$ case, which could be used at the dissociation limit since it has the same energy, but that is not a possible way out for intermediate interatomic distances.

However, there is another important difference between the α and β electrons in the high-spin case: The *open* α orbitals are populated, the *open* β are not; thus the open α orbitals should use orbital energies appropriate for ionization, while the β ones should be appropriate for electron affinity. To use distinct orbital energies for active orbitals, depending on whether an electron is added or removed, is a principle that would work for arbitrary spin-coupled cases. It is not possible for a strictly one-electron operator. Several ways to approach this problem have been suggested:

1. Two-electron operators can be added to \hat{H}_0 . A small number of important terms were suggested by Murray and Davidson for open-shell perturbation theory [16] and later by Kozłowski and Davidson for more general multiconfiguration perturbation theory [17]. Such formulas, which

we will call *OPT2-like*, can all be written as $\hat{H}_0 = \sum \varepsilon_p \hat{n}_p + \eta_p \hat{n}_p (2 - \hat{n}_p)$ with somewhat different definitions of the parameters ε_p and η_p (\hat{n}_p is the number operator for orbital p). The OPT2-like schemes lack orbital invariance. This is problematic in low-spin ROHF cases, since it is not invariant even to rotations among symmetry-equivalent orbitals. It is also problematic for more general MCSCF root functions, since near-degeneracy gives the orbital set an unlimited sensitivity to small changes in geometry or to conditions at distant parts of a molecule, and the variations in orbitals representation affect the second-order energy.

2. Because of the orbital dependence of the OPT2 scheme, Kozłowski and Davidson have also suggested a scheme called IOPT [18], where the distinction between added and removed active orbitals is achieved by a term involving the *sum* of active orbital occupation. However, this scheme has very large size consistency errors [9].

3. A more comprehensive set of two-electron operators can be included. Inclusion of terms involving four active orbitals gives a Hamiltonian that is exact within the CAS-CI space. As a side effect, it has Ψ_0 as eigenfunction, without projections. It turns out that while the preliminary stages of the CASPT2 method become much more complicated by the extra terms, the final iterative equation solution is simplified. This method is thus quite reasonable for small active spaces and is presently investigated by Dyll [19]. However, it is not invariant to orbital rotation between, for example, an inactive and a fully occupied active orbital.

4. We said earlier that simplicity demands a one-electron \hat{H}_0 . This is not quite true, of course: Corrections of a very general nature can be defined operationally, by manipulating the matrix elements or the energy denominators, rather than by first defining operators and then computing their matrix elements. This is straightforward in a determinant or CF formulation, but using the FOI space, it is no longer trivial to ensure that the operator defined is Hermitian, or that a "small" correction gives small effects on the correlation energy. We have made a large number of experiments with this kind of correction but have failed to find one that combines simplicity, orbital invariance, and size consistence while taking due account to the strong nonorthogonality and overcompleteness of the set of excited wavefunction terms.

5. The average implied in the standard Fock matrix is not necessarily the best compromise between ionization energy/electron affinity of active orbitals. In a number of applications, the contribution to the second-order correlation energy is much larger for a few excitations from open shells to low-lying virtual orbitals than the contributions from exciting

into the open shells. A better compromise is then to keep closer to the ionization-energy-type Fock matrix, which in our high-spin example is the f^α . For ROHF perturbation theory, this has been recognized for a long time. Modified Fock matrices suitable for CASPT2 have been studied by Andersson [20].

In CASSCF theory, with changes in conformation or perturbations (including also the perturbation of one group in a molecule due to distant groups), there may be large changes in orbitals due to rotations between inactive and heavily occupied (at that conformation) orbitals, or between weakly occupied (at that conformation) correlating orbitals and virtual ones. Also, while rotations within the active space are irrelevant to the CASSCF wavefunction, attempts to make them more strictly defined via canonicalization schemes fail because these schemes do not in general yield orbitals that vary slowly enough with geometry or perturbation. Because of this, we feel that representation invariance is an issue of decisive importance. Dyall's scheme is attractive and has many important invariance properties, but it does depend on the subdivision into inactive/active orbitals, also for fully occupied orbitals. We have tried the last of the alternatives listed above, since this can be made representation independent.

In Ref. 20 several choices of a Fock operator for a general CASSCF reference state were discussed. They were all constructed such that for our high-spin example, the f^α Fock matrix is obtained for the open orbitals. These modified Fock operators were constructed with the aid of a matrix \mathbf{K} , defined as

$$K_{pq} = \sum_{rs} (\mathbf{Dd})_{rs} (pr|sq), \quad (8)$$

where $\mathbf{d} = 2 \cdot \mathbf{1} - \mathbf{D}$ is a hole density matrix. In the classical open-shell cases, with occupation numbers only 0, 1, or 2, this matrix is called the *open-shell exchange matrix* and denoted \mathbf{K} or \mathbf{K}° . The more general extension defined above has many applications, and we suggest that the term *open-shell exchange matrix* can be used for it as well. In terms of this matrix, the three choices of *open-shell corrected* Fock matrices discussed in Ref. 20 are

$$\mathbf{g}_1 = -\frac{1}{4}(\mathbf{DKd} + \mathbf{dKD}), \quad (9)$$

$$\mathbf{g}_2 = -\frac{1}{2}(\mathbf{Dd})^{1/2}\mathbf{K}(\mathbf{Dd})^{1/2}, \quad (10)$$

$$\mathbf{g}_3 = -\frac{1}{2}(\mathbf{Dd})\mathbf{K}(\mathbf{Dd}). \quad (11)$$

The major effect of introducing a correction to the Fock matrix is an enlarged energy gap between the active and secondary orbitals. The enlargement is small for CASSCF wavefunctions dominated by a closed-shell configuration and larger for other kinds of wavefunctions. Since the correction does not affect the inactive-inactive and secondary-secondary subblocks of the Fock matrix, the energy gap between the inactive and active orbitals will consequently be reduced. The enlarged energy gap between the active and secondary orbitals will lead to larger energy denominators for the most relevant contributions to the second-order energy. The result is smaller absolute values of the second-order energy for reference functions with many open shells. However, if inactive orbitals high in energy are present, the decreased energy gap between them and the active orbitals may lead to contributions to the second-order energy with small energy denominators.

It has often been assumed that the MCSCF Fock matrix can be used as \hat{H}_0 for multiconfiguration root functions. This works for a few simple open-shell cases but is in general wrong. The MCSCF Fock matrix, which is used to find energy-optimized orbitals in MCSCF (such as CASSCF), is

$$f_{pq}^{\text{MCSCF}} = \sum_r h_{pr} D_{rq} + \sum_{rst} (pr|st) P_{rq, st}, \quad (12)$$

where $P_{qr, st}$ is the two-electron spin-free density matrix. The optimization criterion is that this matrix is symmetric. First, there is an obvious occupation number dependence that must be eliminated: The orbital energy of a strongly occupied orbital becomes twice as large as that of the standard Fock matrix. The correlating orbitals, which should be very high in energy, are multiplied with low occupation numbers and have thus numerically small, and in fact, *negative* eigenvalues. The naïve interpretation of this phenomenon is that $\mathbf{f}^{\text{MCSCF}}$ is a valid one-electron Hamiltonian matrix but in a nonorthogonal basis set with overlap matrix \mathbf{D} , so that a more reasonable eigenvalue equation would be $\mathbf{f}^{\text{MCSCF}} \psi = \epsilon \mathbf{D} \psi$. However, any realistic experiment shows that the orbital energies so obtained, which may be regarded as approximate ionization energies (with negative sign) in the sense of the extended Koopmans theorem, will behave as expected only for orbitals with high occupation number. For weakly occupied ones, the energy starts to *go down*. It never reaches positive values, and has in fact (if the EKT is valid) an upper limit that is the exact negative of the lowest ionization energy, in the basis-set limit.

For the weakest occupied orbitals, it makes sense to interchange particles and holes. The resulting analog to the MCSCF Fock matrix is then $2\mathbf{f} - \mathbf{f}^{\text{MCSCF}}$, and the hole density matrix is, as before, $\mathbf{d} = 2 \cdot \mathbf{1} - \mathbf{D}$.

A physically meaningful eigenvalue equation is $(2\mathbf{f} - \mathbf{f}^{\text{MCSCF}})\psi = \varepsilon(2 \cdot \mathbf{1} - \mathbf{D})\psi$, which gives Koopmans type of *electron affinities* (with reversed sign) as eigenvalues, but only for weakly occupied orbitals. For the strongly occupied orbitals, the energies go *up* to high values.

The counterintuitive behavior of the electron orbital energies for high occupation number, and of hole orbital energies for low occupation number, are simple examples of a fairly general phenomenon: the selection effect. When adding, removing, or exciting electron(s), the result is a new unnormalized wavefunction with another energy. The energy difference is not just an approximate sum of orbital energies, since the new wavefunction is not obtained by simply changing orbital occupations up and down. In addition, we must select that part of the correlated wavefunction that gives a nonzero result. As an example, consider $\Psi_0 = |\cdots(c_1\psi_i\bar{\psi}_i - c_2\psi_u\bar{\psi}_u)\rangle$, where a bonding orbital is correlated by double excitations to an antibonding ($c_1 \gg c_2$). The excitation operator \hat{E}_{iu} provides a wavefunction term $\alpha|\cdots(\bar{\psi}_i\psi_u - \psi_i\bar{\psi}_u)\rangle$ with an estimated excitation energy $\varepsilon_u - \varepsilon_i$, just as expected. But *so does* \hat{E}_{iu} . Instead of the expected energy difference, we get its negative. In fact, the expected result would imply that the excitation changes the occupation numbers as $n_i \leftarrow n_i + 1$, $n_u \leftarrow n_u - 1$, which is nonsense in this case since $n_i \approx 2$ and $n_u \approx 0$. This is never observed for single-determinant root functions. Of course, the complete picture is complicated by non-diagonal and two-electron terms, but we wish only to give a simple qualitative explanation to a counterintuitive selection effect in the use of multiconfiguration root functions. The same phenomenon also explains why $\mathbf{f}^{\text{MCSCF}}$ fails to give proper orbital energies for weakly occupied orbitals, even if the occupation number dependence has been divided off.

Adding the two eigenvalue equations removes the \mathbf{D} matrix dependence. Divided by 2, the result is the standard Fock matrix eigenvalue equation. This has sometimes been taken to mean that the *eigenvalues* of this are just the arithmetic mean of approximate negative ionization potentials (IPs) and electron affinities (EAs). However, it is obvious that in making this average, the first equation contains negative IPs weighted with the occupation number n , and the second, negative EAs weighted by $(2 - n)$. Thus when n goes toward either 0 or 2, the equation remains well behaved and the eigenvalues have the proper Koopmans interpretation.

B. Multistate CASPT2

As already mentioned, there is a so-called effective Hamiltonian approach to multiconfiguration perturbation theory. This approach is often

applied with the complete active space as the model space. We have avoided this formulation and use a single-root perturbation theory, primarily because of the advantages in using the FOI space, and also to minimize complications involving intruders. However, the relative amplitude of the configurations in the CAS-CI space is then unalterable. A slight different CASSCF wavefunction would have been the optimal choice for the root function. In principle, the CASSCF wavefunction can be reoptimized, but this is not without complications and is probably not a convergent procedure for excited states. An alternative is then to use the effective Hamiltonian approach but with only a small space of CASSCF wavefunctions rather than a large space of configuration functions.

One of the major advantages of the CASSCF/CASPT2 approach is that excited electronic states of molecular systems can be obtained almost as easy as ground electronic states. By changing the nuclear coordinates, one can generate entire potential surfaces that contain information of chemical interest such as equilibrium structure, reaction paths, and so on. Such potential surfaces do not normally cross each other, but they do at points of high symmetry and also along the conical intersection paths, which are curves or hypercurves of dimension $N - 2$, where N is the total number of internal coordinates. When the energy surfaces cross or come near each other, this is often highly significant to spectroscopic properties and to reaction probabilities. In a region of conformations where a state crossing occurs, there is no bound to the derivative of the state function with respect to coordinates. Rapid changes occur in all properties and transition moments.

It is thus of importance that crossings and avoided crossings are treated as accurately as possible. Single-state perturbation methods are not generally applicable, due to strong divergence. They can still be useful if truncated at very low order in perturbation theory. CASPT2 will still give useful results in such situations, provided that the crossing states are included in the CAS-CI, so that they do not interact with the root function. However, the accuracy of the result is often impaired. Rapid changes in the root function occur where the potential surfaces cross at the CASSCF level. This is rarely at the same geometry as for the correlated wavefunction. The rather abrupt changes in second-order correlation energy can give rise to multiple minima, unphysical, repeated curve crossing, and other unwanted phenomena [21].

Apart from the qualitative errors that are obvious in near-crossing situations, there is also the question of precision. As an example, among the many molecular spectra that have been computed by CASPT2, there are a handful of energies with untypically large errors. These seem to be

caused by erroneous mixing, at the CASSCF level, of wavefunction terms with different dynamic correlation.

The effective Hamiltonian formalism avoids these drawbacks by treating several zeroth-order functions at once. These functions span the model space, and they are the basis of a matrix Hamiltonian. The energies are obtained as eigenvalues of this matrix, so if the matrix elements are smooth functions of geometry, the drawbacks above can be avoided. In particular, different energy surfaces do not normally cross, but when they do, this is dealt with in a stable manner by the final diagonalization of the effective Hamiltonian matrix, not by the series expansion. Actually, the reference functions in CASPT2 are CASSCF wavefunctions, which are not smooth functions of geometry everywhere but are subject to large and rapid changes where the CASSCF energy surfaces cross. However, these changes amount to rotations within the model space, which can be shown not to affect the result.

Assume that we have decided on some particular zeroth-order Hamiltonian, as simple as possible, for which we require that

$$\hat{H}_0 \Psi_0^i = E_0^i \Psi_0^i, \quad i = 1, \dots, n, \quad (13)$$

where n is the dimension of the model space. Here Ψ_0^i are CASSCF wavefunctions, and \hat{H}_0 is similar to the one used for single-state CASPT2. From the reference functions, we form new functions by adding a perturbation part. In the intermediate normalization, the perturbation added to a Ψ_0^i function is orthonormal to *all* the reference functions. This has the consequence that we cannot require that the new functions solve individual Schrödinger equations. Instead, we require that the interesting eigenfunctions can all be obtained as linear combinations of the perturbed functions. This indirect formulation allows the perturbation expansions to converge also in curve-crossing situations.

The general procedure is most easily described in terms of a few operators. Define the projectors $\hat{P} = \sum_1^n |\Psi_0^i\rangle\langle\Psi_0^i|$ and $\hat{Q} = \hat{1} - \hat{P}$, and use a *wave operator* $\hat{\Omega}$ to write the perturbed functions $\Psi^i = \hat{\Omega}\Psi_0^i$. Instead of the Schrödinger equation, we write

$$\hat{H}\hat{\Omega}\Psi_0^i = \hat{\Omega}\hat{H}^{\text{eff}}\Psi_0^i, \quad (14)$$

where \hat{H}^{eff} is an operator acting entirely *within* the model space (i.e., only its action on functions in the model space is relevant), and it maps any such function into the model space. For any Ψ that can be expressed as a linear combination of reference functions, it now follows from linearity that if $\hat{H}^{\text{eff}}\Psi = E\Psi$, then also $\hat{H}\hat{\Omega}\Psi = E\hat{\Omega}\Psi$. A set of n solutions

to the complete Schrödinger equation can thus be obtained by solving the eigenvalue problem for the operator \hat{H}^{eff} . A matrix representation is used in practice, but the operator formulation is practical for working out and concisely denote perturbation schemes and shows explicitly that the procedure is invariant to rotations among the CASSCF wavefunctions. The matrix \mathbf{H}^{eff} obeys

$$H_{ij}^{\text{eff}} = \langle \Psi_0^i | \hat{H}^{\text{eff}} | \Psi_0^j \rangle ,$$

$$\hat{H}^{\text{eff}} \Psi_0^j = \sum_i \Psi_0^i H_{ij}^{\text{eff}} . \quad (15)$$

The wave operator and \hat{H}^{eff} are not completely specified. For our purposes it is simplest to set $\hat{\Omega} \hat{Q} = \hat{H}^{\text{eff}} \hat{Q} = \hat{0}$. The perturbation equations are obtained by the ansatz $\hat{\Omega} = \hat{P} + \sum_1^\infty \lambda^k \hat{\Omega}_k$. A convenient relation is the *Bloch* equation

$$[\hat{\Omega}, \hat{H}_0] \hat{P} = \hat{H}_1 \hat{\Omega} \hat{P} - \hat{\Omega} \hat{P} \hat{H}_1 \hat{\Omega} \hat{P} , \quad (16)$$

which gives the perturbation equations to all orders by substituting the expansion of $\hat{\Omega}$, replacing \hat{H}_1 by $\lambda \hat{H}_1$, and collecting terms of equal order. In computation this will give a matrix commutator equation at each order. It is most easily solved in a basis where \hat{H}_0 is diagonal, where it simplifies to division by energy denominators. Each denominator is the energy difference between one \hat{H}_0 eigenfunction in the model space, and one outside it. Any degeneracy in the model space is thus irrelevant.

Multiplying Eq. (14) from the left by \hat{P} gives $\hat{P} \hat{H} \hat{\Omega} \hat{P} = \hat{H}^{\text{eff}}$. Inserting the $\hat{\Omega}$ expansion gives

$$\hat{H}^{\text{eff}} = \sum_{k=0}^{\infty} \lambda^k \hat{H}_k^{\text{eff}} = \hat{P} \hat{H}_0 \hat{P} + \lambda \hat{P} \hat{H}_1 \hat{P} + \sum_{k=2}^{\infty} \lambda^k \hat{P} \hat{H}_1 \hat{\Omega}_{k-1} \hat{P} . \quad (17)$$

For CASPT2, the equations to second order are

$$\langle \Psi_0^i | \hat{H}_0^{\text{eff}} | \Psi_0^j \rangle = \langle \Psi_0^i | \hat{H}_0 | \Psi_0^j \rangle = E_0^i \delta_{ij} , \quad (18)$$

$$\langle \Psi_0^i | \hat{H}_1^{\text{eff}} | \Psi_0^j \rangle = \langle \Psi_0^i | \hat{H}_1 | \Psi_0^j \rangle , \quad (19)$$

$$\langle \Psi_0^i | \hat{H}_2^{\text{eff}} | \Psi_0^j \rangle = \langle \Psi_0^i | \hat{H}_1 \hat{\Omega}_1 | \Psi_0^j \rangle . \quad (20)$$

The zeroth-order eigenfunctions are identical to $\{\Psi_0^i\}_{i=1}^n$ and their energies are equal to E_0^i . At the first-order level the matrix $\langle \Psi_0^i | \hat{H}_0^{\text{eff}} + \hat{H}_1^{\text{eff}} | \Psi_0^j \rangle = \langle \Psi_0^i | \hat{H} | \Psi_0^j \rangle$ should be diagonalized. If Ψ_0^i are CASSCF

wavefunctions with a common orbital set, this matrix is already diagonal and the first-order energies are identical to the CASSCF energies (E_{CAS}^i). Finally, at the second-order level the matrix $\langle \Psi_0^i | \hat{H}_0^{\text{eff}} + \hat{H}_1^{\text{eff}} + \hat{H}_2^{\text{eff}} | \Psi_0^j \rangle = E_{\text{CAS}}^i \delta_{ij} + \langle \Psi_0^i | \hat{H}_1 \hat{\Omega}_1 | \Psi_0^j \rangle$ should be diagonalized. For obtaining the second-order energy we have to determine $\hat{\Omega}_1$ from the lowest-order Bloch equation:

$$[\hat{\Omega}_1, \hat{H}_0] \hat{P} = \hat{H}_1 \hat{P} - \hat{P} \hat{H}_1 \hat{P}. \quad (21)$$

To make the solution of this equation as simple as possible, we define the zeroth-order Hamiltonian in a similar way as for the single-state case (see Refs. 6 and 7) using various projection operators. This will then allow us to express

$$\hat{\Omega}_1 \Psi_0^i = \sum_{I=1}^M C_I^i |I\rangle, \quad |I\rangle \in V_{SD}, \quad (22)$$

where V_{SD} is the space spanned by single and double replacement states generated from all the n states Ψ_0^i and M its dimension. Equations (21) and (22) together give the following system of equations:

$$\sum_{J=1}^M \langle I | E_0^i - \hat{H}_0 | J \rangle C_J^i = \langle I | \hat{H}_1 | \Psi_0^i \rangle \equiv V_I^i, \quad I = 1, \dots, M, \quad (23)$$

from which the expansion coefficients C_I^i can be determined. Equation (23) is similar to the one for single-state CASPT2. The difference lies in the space V_{SD} . For a multistate CASPT2 this space will be approximately n times larger than the space obtained in single-state CASPT2. Using the definitions above, the matrix representation of the second-order effective Hamiltonian can be expressed as

$$\langle \Psi_0^i | \hat{H}_0^{\text{eff}} + \hat{H}_1^{\text{eff}} + \hat{H}_2^{\text{eff}} | \Psi_0^j \rangle = E_{\text{CAS}}^i \delta_{ij} + \sum_{I=1}^M C_I^i V_I^{i*} = E_{\text{CAS}}^i \delta_{ij} + \mathbf{V}^{i*} \mathbf{C}^j. \quad (24)$$

The final step in a multistate CASPT2 calculation is a diagonalization of the matrix in Eq. (24), which gives the energy of the states under consideration up to second order. We have used here a formulation where \hat{H}^{eff} and \mathbf{H}^{eff} are non-Hermitian. However, this is of no computational importance as long as \mathbf{H}^{eff} is a small matrix. The increase in computational cost will be due primarily to the increased number of variables: the size of the system of linear equations in CASPT2 will be proportional to the

number of states. Since in many cases two reference functions are sufficient, this does not dramatically increase the computational time or storage. We are presently coding a CASPT2 version with an effective Hamiltonian. It will be of special interest for studies of avoided crossings but also for cases where one can expect that a single optimized CASSCF reference function has the wrong shape due to lack of dynamic correlation (e.g., for negative ions).

C. Intruder-State Problem

The success of a low-order perturbation treatment is vitally dependent on the strength of the perturbation. Fast convergence is obtained only for weak perturbations. In addition, E_0 —the eigenvalue of \mathbf{H}_0 corresponding to Ψ_0 —should not be close to any other eigenvalue. If this happens for a function in the FOI space, the second-order energy will become divergent. Such intruder states seldom appear in the normal Møller–Plesset perturbation theory, which is used primarily for molecules in their ground state. The CASPT2 approach is, however, frequently used also for excited states. Here it is not uncommon to find intruder states. To realize why they appear, one has to understand the structure of the CI space in which the wavefunction is expanded. The initial partitioning of the occupied molecular orbitals into an inactive and an active part defines the CAS-CI space as all the CFs that are obtained by distributing the active electrons among the active orbitals in all possible ways consistent with a given space and spin symmetry. The CASSCF wavefunction is expanded in this CI space. The orthogonal complement does not interact with the CAS wavefunction and will consequently not appear in the first order wavefunction. The CFs in the FOI space will have at least one electron in the external (virtual) orbital space and/or at least one hole in the inactive space,

Assume now that one orbital, which is important for the description of the electronic spectrum of the system, is missing from the active space (it may be inactive or external). Excitations involving this orbital will then belong to the FOI space. It is not unlikely that the zeroth-order energy for one or several of the CFs where this orbital is excited (to or from) will have low energies and may act as intruder states in a CASPT2 calculation. Clearly, the remedy to the problem is in this case to include the orbital in the active space.

It is, however, not always possible to solve the problem so easily. The active space may already be at the limit of what the method can handle (normally, 12–14 orbitals) and further extension is then not possible. A typical case are calculations with extended basis sets, which include diffuse or semidiffuse functions. Such basis sets give rise to a number of

Rydberg-like states. Calculations, which aim also at describing excited states of Rydberg type, will have most of the diffuse functions in the active space. However, it often happens that some diffuse electronic states are left in the FOI space. The energy lowering due to dynamic correlation is usually smaller for diffuse states than for the more compact valence excited states. At the zeroth-order level, the diffuse states will therefore be artificially stabilized with respect to other excited states, and accidental degeneracy may occur, even if these states are much higher in energy when dynamic correlation corrections have been added. This situation is rather common in CASPT2 calculations on excited states. However, the interaction element coupling the intruder state with Ψ_0 is often very small. Thus the contribution to the second-order correlation energy may be without importance even if the energy denominator is small. In such cases it may be allowed to disregard the contribution of the intruder state. Another possibility is to delete the diffuse orbital that causes the problem. It has been shown in a number of cases that virtually identical results are obtained whether the orbital is deleted from the virtual or added to the active space [22].

Even if intruder states most commonly appear in calculations on excited states, there are a few cases where it also happens for ground-state energy surfaces. An especially pathological system is the chromium dimer. With an active space of 12 orbitals (Cr $3d$ and $4s$) and 12 active electrons, several intruder states appear in the region around the minimum on the ground-state potential curve (for details, see Refs. 14 and 23). They have their origin in orbitals of mainly $4p$ character. The best solution to the problem would have been to include these orbitals in the active space since they are rather close in energy to the $4s$ orbitals. However, such a procedure would have resulted in an active space consisting of 18 orbitals, which is far beyond the capability of the present computer implementation. It was shown in a recent study of Cr_2 that a useful potential curve could be constructed by excluding the rather narrow regions where the intruder states appeared [23], but this is clearly an unsatisfactory solution to the problem. There are two main reasons why intruder states show up in the potential curve for Cr_2 . One is the low energy of the $4p$ orbitals. The second is the strongly degenerate character of the CASSCF wavefunction with six weak chemical bonds. The occupation numbers of several of the active orbitals are as a consequence close to 1. As discussed in Section II.B, such a situation leads to a diminished energy gap between the active and virtual orbitals and thus increases the possibility for intruder states. For Cr_2 it was possible to reduce the problem by introducing a modification in \hat{H}_0 , which stabilized the active orbitals [23, 24]. As discussed earlier, the modification intro-

duced by Andersson [25] cannot be adopted generally. It stabilizes the active orbitals, which makes the energy difference to the inactive orbitals smaller. Thus the method will work only when all valence electrons are active (as in Cr_2). It will not work in cases where one can expect that the energy difference between active and inactive orbitals is small. In such cases the modification will increase the probability for intruder states.

A very simple way to avoid near-degeneracies in the zeroth-order Hamiltonian is to introduce a level shift [26]. \hat{H}_0 is then replaced with $\hat{H}_0 + \varepsilon \hat{P}_I$, where ε is a small positive number and \hat{P}_I is the projection operator for the FOI space. The first-order equation with the shifted Hamiltonian is

$$(\mathbf{H}_0 - (E_0 - \varepsilon)\mathbf{S})\tilde{\mathbf{C}} = -\mathbf{V}, \quad (25)$$

where $\tilde{\mathbf{C}}$ is the new first-order CI vector (the expansion vector for Ψ_1 in the FOI space). It is easy to derive a formula for the level-shifted second-order energy in terms of $\tilde{\mathbf{C}}$ and \mathbf{C} ,

$$\tilde{E}_2 = E_2 + \varepsilon \mathbf{C}^\dagger \mathbf{S} \tilde{\mathbf{C}}. \quad (26)$$

\mathbf{C} can be written as $\tilde{\mathbf{C}} + o(\varepsilon)$ provided that ε is small compared to the eigenvalues of \mathbf{H}_0 , which will be the case if there are no intruder states. If the intruder states have been removed by the level shift, it is possible to make an approximate *a posteriori* correction of the second-order energy to an assumed unshifted calculation without the intruder state. The correction is obtained from Eq. (26) by replacing \mathbf{C} with $\tilde{\mathbf{C}}$,

$$E_2 \approx \tilde{E}_2 - \varepsilon \tilde{\mathbf{C}}^\dagger \mathbf{S} \tilde{\mathbf{C}}, \quad (27)$$

which can be written as

$$E_2 \approx \tilde{E}_2 - \varepsilon \left(\frac{1}{\tilde{\omega}} - 1 \right), \quad (28)$$

where $\tilde{\omega}$ is the weight of the CASSCF reference function in a normalized zeroth plus first-order function. The correction is given by $E_2 - \tilde{E}_2$, which we shall call the LS (level-shift) correction.

The procedure above can work only if the effect of the level shift is negligible in the stable case when no intruder state appears. Otherwise, we have introduced a new parameter into the model over which we have no control. The behavior of the level-shifted CASPT2 approach has recently been tested in a series of calculations on the N_2 and Cr_2 molecules [26]. The first test was performed on the potential curve for the

$X^1\Sigma_g^+$ ground state of N_2 . An ANO-type basis set of size $5s4p3d2f$ was used [27]. The active space consisted of the eight orbitals generated from the nitrogen valence orbitals with 10 active electrons. Calculations were performed at 19 points spread around the minimum of the potential curve, and the spectroscopic constants were obtained by numerical solution of the vibrational Schrödinger equation. The results obtained with different level shifts ε are illustrated in Table I. This table contains two entries, one where the shift was applied [Eq. (25)] without LS correction and one where this correction was added to \hat{E}_2 . In the first case we see an almost linear increase of the second-order energy with the level shift (the slope is about 0.05). The computed spectroscopic constants are, however, affected surprisingly little. Between a shift of zero and 0.2 hartree, the bond distance decreases 0.0009 Å, the stretching frequency increases 8 cm^{-1} , and the bond energy increases with 0.106 eV. The LS corrected second-order energy removes almost all these changes. The total second-order energy only changes 0.6 millihartree, the bond energy 0.016 eV, the frequency 1 cm^{-1} , and the bond distance 0.0001 Å. Considering the general accuracy of a second-order perturbation treatment,

TABLE I
Effect of the Level Shift in the Zeroth-Order Hamiltonian on the Spectroscopic Properties of the Ground-State Potential of N_2

Shift (H)	r_e (Å)	ω_e (cm^{-1})	D_e (eV)	Δ_e^a
<i>Without the LS Correction</i>				
0.00	1.1036	2324	9.21	—
0.05	1.1033	2326	9.24	2.7
0.10	1.1031	2328	9.27	5.3
0.20	1.1027	2332	9.32	10.3
0.50	1.1017	2342	9.42	23.7
<i>With the LS Correction</i>				
0.00	1.1036	2324	9.21	—
0.05	1.1036	2324	9.21	0.041
0.10	1.1035	2324	9.22	0.158
0.20	1.1035	2325	9.23	0.589
0.50	1.1031	2329	9.28	3.029
<i>Experimental^b</i>				
—	1.0977	2359	9.91	—

^a Shift in millihartrees with respect to the CASPT2 energy without a level shift.

^b From Ref. 212.

these effects of the level shift are clearly negligible. Even a level shift as large as 0.5 hartree gives rise to very small shifts in computed properties. The conclusion is that a small level shift will not affect computed properties if the second-order energy is LS corrected and there are no intruder states. The computed bond energy for N_2 is 0.7 eV smaller than the experimental value, which corresponds to 0.23 eV per electron pair. This is an illustration of the systematic error in the CASPT2 approach discussed earlier: The bond energy is underestimated with 4–6 kcal/mol per electron pair. Notice that application of the level shift (without LS correction) decreases this error. That is because the shift will have a larger effect when the eigenvalues of \mathbf{H}_0 are smaller, as is the case for the nitrogen atom compared to the nitrogen molecule.

To study what happens if there is an intruder state, we performed level-shifted calculations on an excited ($A^3\Sigma_u^+$) of N_2 , for which an intruder state crosses the potential curve close to the minimum [7]. The details of the calculations were the same as for the ground state. The result is shown in Table II and is also illustrated in Fig. 1, which shows the potential curve for three values of the level shift: 0.00, 0.05 and 0.10

TABLE II
Effect of the Level Shift in the Zeroth-Order Hamiltonian on the Spectroscopic Properties of the ($A^3\Sigma_u^+$) Excited State of N_2

Shift (H)	r_e (Å)	ω_e (cm ⁻¹)	D_e (eV)	Δ_e^a
<i>Without the LS Correction</i>				
0.00	1.3095	1340	3.36	—
0.05	1.2917	1427	3.38	3.0
0.10	1.2931	1433	3.38	6.9
<i>With the LS Correction</i>				
0.00	1.3095	1340	3.36	—
0.05	1.2874	1378	3.40	-1.3
0.10	1.2931	1427	3.38	-0.35
<i>2π_g Orbitals Added to the Active Space^b</i>				
0.00	1.2953	1409	3.30	—
<i>Experimental^c</i>				
—	1.2866	1461	3.68	—

^a Shift in millihartrees with respect to the CASPT2 energy without a level shift.

^b Data from Ref. 7.

^c From Ref. 212.

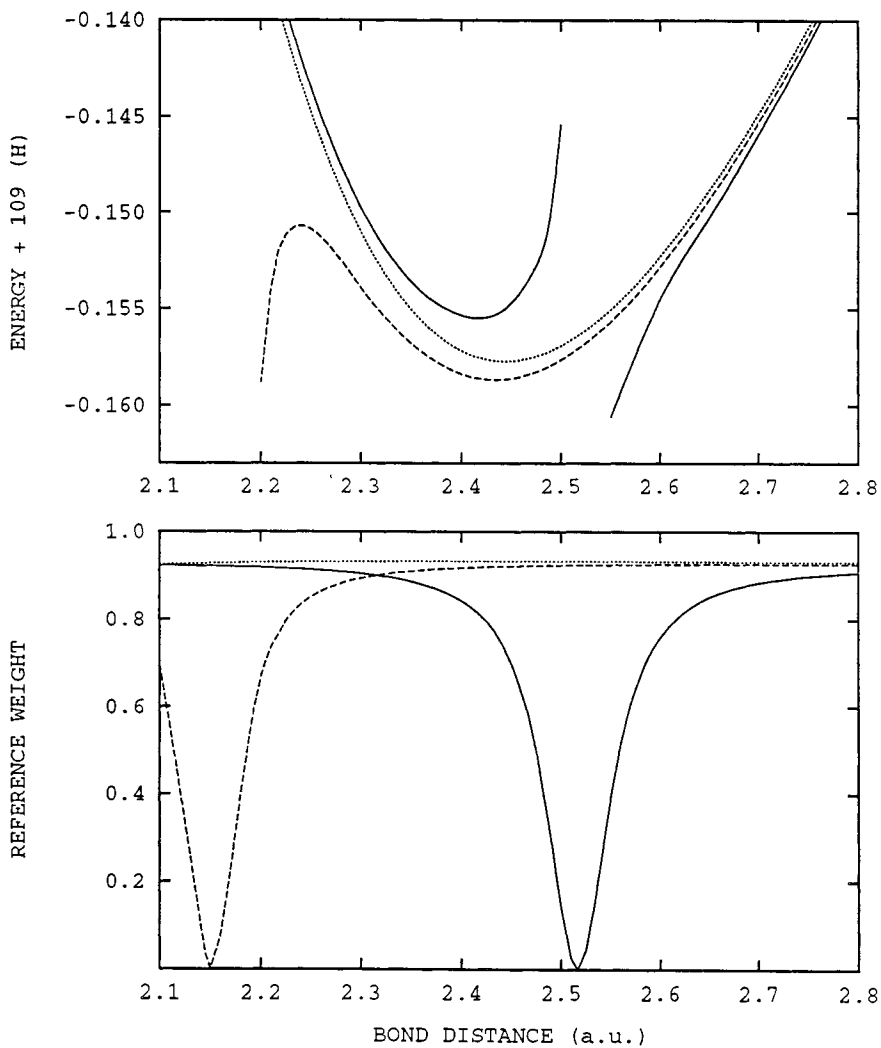


Figure 1. Potential curves for the $(A^3\Sigma_u^+)$ excited state of N_2 for three values of the level shift: 0.00 (solid line), 0.05 (dashed line) and 0.10 a.u. (dotted line). The LS correction has been applied. The lower diagram gives the corresponding weight of the CASSCF reference function.

hartree and the weight, ω , of the corresponding CASSCF reference function. The appearance of the intruder state is clearly seen for the unshifted potential as a singularity at a bond distance of about 1.36 Å. The weight ω drops to zero at this point. The spectroscopic constants presented in Table II have been obtained by fitting the potential only to the points for which the reference weight is acceptable. It is clear from the figure that such a procedure is rather meaningless when intruder states appear in the potential close to the minimum. It must be regarded as fortuitous that the results presented in Table II do not have larger errors.

A level shift of 0.05 hartree (with LS correction) moves the intruder state to shorter internuclear distances. It will, however, still affect the region around the minimum. A level shift of 0.10 hartree will remove the intruder entirely and the potential curve is now normal in the minimum region with constant weight of the reference function, which indicates a balanced description of the dynamic correlation effects. Away from the intruder-state region, the effect of the level shift on the total energy is less than 1 millihartree. The spectroscopic constants obtained with the level-shifted potential are of the same quality as those obtained for the ground state. We conclude that intruder states can be removed by applying a level shift together with the LS correction. The result of such a calculation will be similar to those obtained by incorporating the intruder state into the active space, which is the ideal (but often impossible) solution to the problem. It must, however, be emphasized that the level-shifted CASPT2 method will work only in cases where the interaction between the intruder state and the reference function is weak. Strongly interacting states should be included into the CAS space by increasing the number of active orbitals. In the N_2 case it was possible to remove the intruder state by adding the two $2\pi_g$ orbitals to the active space [7]. The resulting spectroscopic parameters are very similar to those obtained by the level-shift method (cf. Table II).

A severe test of the level-shifted CASPT2 procedure is Cr_2 . Previous studies of this molecule have shown that a number of intruder states appear along the ground-state potential curve [14]. Modifying the zeroth-order Hamiltonian only partially solved the problem, and it was only by avoiding the intruder state regions that approximate spectroscopic constants could be computed for Cr_2 [23]. Not surprisingly, intruder states also appeared frequently for the excited-state potential curves [24]. The chromium dimer has been studied here using the same basis set as was used in Ref. 23: ANO $8s7p6d4f$. The active space comprised the chromium $3d$ and $4s$ orbitals and corresponding electrons. The $3s$ and $3p$ electrons were included in the CASPT2 treatment, and relativistic

corrections were added as in the earlier work. About 25 points on the potential curve were computed with a spacing of 0.05 a.u. around the minimum. Calculations were performed for three values of the level shift: 0.05, 0.10, and 0.20 a.u.

The resulting potential curves are shown in Fig. 2 and the computed spectroscopic constants are given in Table III. Corresponding results without level shift have been presented in the earlier work (cf. Fig. 5 and Table 2 in Ref. 23). As can be seen in the figure, there are at least three intruder states in the region around the minimum. A level shift of 0.05 a.u. does not remove them. A level shift of 0.10 a.u. gives a potential curve without intruder states, but the dip in the CASSCF weight in the minimum region shows that they still influence the potential. A constant weight is obtained with a level shift of 0.20 a.u. As in previous work, the spectroscopic constants for the case with intruders present have been obtained by using only those parts of the potential curve where the CASSCF weight is large. The bond distance computed in this way is reasonable, as is the bond energy. The harmonic frequency is, however, 100 cm^{-1} too large. Increasing the level shift from 0.05 to 0.10 brings the computed frequency to the experimental value (cf. Table III). The bond distance has, however, increased. The weight is still low in the region around minimum, which makes the LS correction large. Using 0.20 a.u. instead makes the calculation stable. The computed bond energy and the frequency are now close to experiment. The excellent agreement with experiment may, however, be somewhat fortuitous, as indicated by preliminary results obtained with a large basis set containing *g*-type functions. We refer to the original article for details [26].

The examples above indicate that a level-shifted CASPT2 method with LS correction is a promising approach to deal with the intruder state problem. The results obtained for the challenging system Cr_2 are surprisingly accurate. They show once again that the CASPT2 approach is capable of giving accurate structural and energetic data for complex electronic states once the intruder state problem has been removed.

III. Applications in Spectroscopy

The CASPT2 approach has been used in a large variety of applications ranging from molecular structure determinations in ground and excited states [15] to calculations of binding energies of transition metal compounds [28, 29]. There is, however, little doubt that the most spectacular success of the new approach has been in electronic spectroscopy and photochemistry. Up until now, a lot of effort has been put into the refinement of computational methods for molecular ground states and it

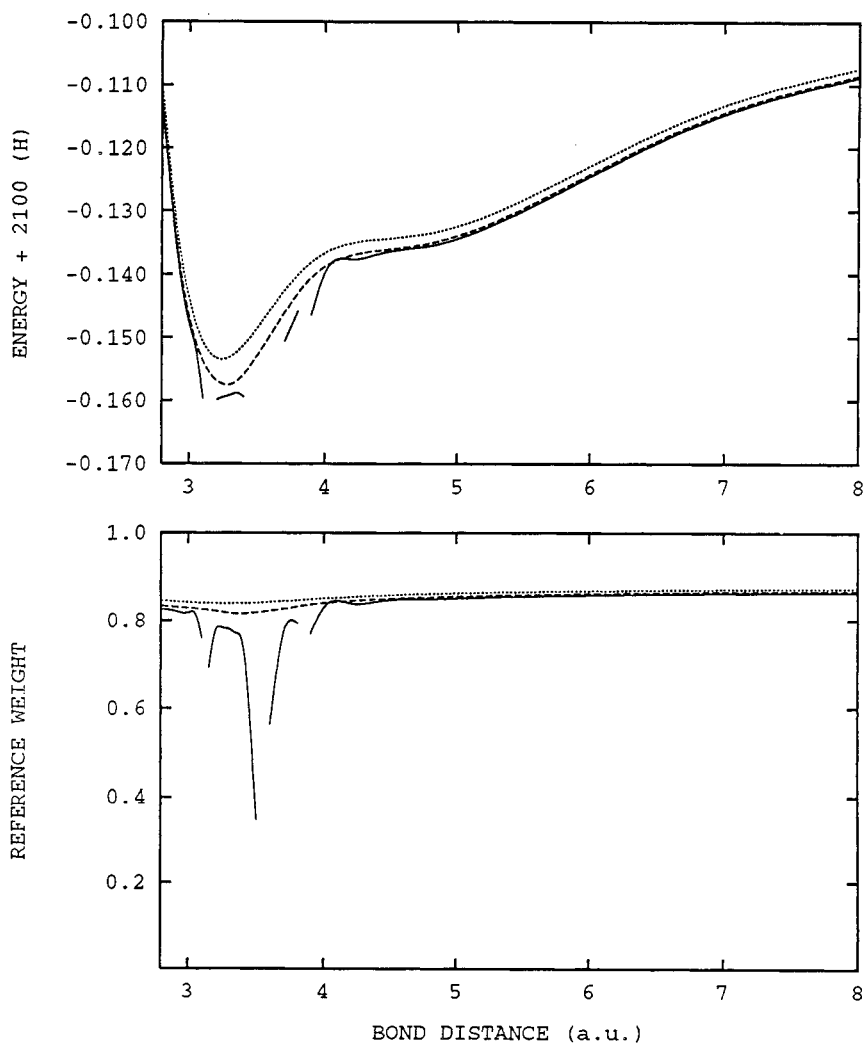


Figure 2. Potential curves for the ground state of Cr_2 for three values of the level shift: 0.05 (solid line), 0.10 (dashed line) and 0.20 a.u. (dotted line). The LS correction has been applied. The lower diagram gives the corresponding weight of the CASCF reference function.

TABLE III
Effect of the Level Shift in the Zeroth-Order Hamiltonian on the Spectroscopic Properties of the Ground State of Cr₂ (Including Relativistic Corrections)

Shift (H)	r_e (Å)	ω_e (cm ⁻¹)	$\Delta G_{1/2}$ (cm ⁻¹)	D_0 (eV)	Δ_e^a
<i>Without the LS Correction</i>					
0.05	1.713	496	478	1.38	—
0.10	1.717	470	457	1.31	10.2
0.20	1.712	459	448	1.16	30.6
<i>With the LS Correction</i>					
0.05	1.707	597	531	1.56	—
0.10	1.736	488	475	1.53	2.5
0.20	1.714	482	467	1.42	6.6
<i>Experimental</i>					
—	1.679 ^b	481 ^c	452	1.44 ^d	—

^a Shift in millihartrees with respect to the CASPT2 energy with a level shift of 0.05 a.u.

^b From Ref. 213.

^c From Ref. 214.

^d From Ref. 215.

is today possible to obtain accurate results for many molecular properties. Most of the approaches are based on the Hartree–Fock approximation as the reference for the estimation of correlation contributions. In contrast, much less effort has been put into the development of efficient computational tools for the excited states. The CI singles approach (singly excited configurations with respect to a HF reference function) has been advocated as a simple and systematic tool for larger molecules [30]. The method is, however, too approximate and limited to be of any practical value. Attempts to include correlation effects by means of perturbation theory have not been successful. The only general tool is multireference CI, but this approach has severe limitations, as pointed out above. Recent attempts to extend the coupled cluster methods to excited states are promising, but so far they are limited to states dominated by single excitations with respect to a HF reference [31].

Early applications of the CASPT2 method to the electronic spectrum of the nickel atom [32] and the benzene molecule [33] were promising and showed that the method gave the same accuracy for excited states as for ground-state properties. This was expected, since the generality of the CASSCF reference function makes the second-order approximation equally valid for all states. The positive surprise was the high accuracy.

Excitation energies were computed with errors less than 0.2 eV in both cases. This was a higher accuracy than any of the earlier calculations on Ni and benzene had achieved. The CASPT2 method has during the last three years been applied to a large number of electronic spectra. Some of the earlier applications in organic chemistry have already been reviewed [13]. Here we discuss additional applications in organic systems but also the electronic spectroscopy of transition metal compounds, where the demands on the approach are different.

A. Electronic Spectroscopy for Organic Molecules

As mentioned above, one of the first applications of the CASPT2 method was the electronic spectrum of the benzene molecule. This study was successful and gave results of higher quality than had been obtained using large-scale MRCI techniques [34]. It was quite clear that the reason for the larger errors obtained in the earlier studies were the difficulties these *ab initio* methods had in treating the dynamic correlation effects. Benzene and molecules of similar size contain many valence electrons, all of which must be included in the correlation treatment. Extensive basis sets are necessary to account for the correlation effects. In a conventional configuration interaction (CI) approach the size of the CI expansion consequently becomes large. Of special importance are the σ - π correlation effects, which manifest themselves as a dynamic polarization of the σ framework. These correlation effects are state dependent and omitting them leads to erratic predictions of relative energies.

A recent multireference (MR) CI study of the electronic spectrum of pyrimidine [5] showed that large CI expansions were needed to converge the results for the excitation energies. Convergence could actually not be achieved without extending the length of the CI expansion beyond the limits set by the MRCI program [about 3 million configuration functions (CFs)]. The remaining error in the computed excitation energies was in some cases 0.4 eV. Although this error might be acceptable, the test showed that the MRCI method is not a practical tool for studies of electronic spectra of larger organic molecules.

Why is the more approximate CASPT2 method more successful in electron spectroscopy than the more elaborate MRCI method? One answer is that the correlation treatment is based on a full CASSCF reference instead of a (often small) selected set of configurations. The result is a more balanced treatment of different excited states. Another difference is that the simpler CASPT2 method can be used with larger basis sets, which gives a wider area of application and increased accuracy. It is also a size-extensive approach, which is necessary in application to larger systems where many electrons have to be correlated (there are

small size-extensivity violating terms in \hat{H}_0 , but they are of no practical importance). The method has been used to estimate correlation contributions to excitation energies in as large molecules as porphyrin with 114 correlated electrons [35]. The general experience is that the CASPT2 method, when applied to electronic spectroscopy of organic molecules, yields excitation energies with an accuracy of 0.3 eV or better. A few exceptions to this rule exist [36]. They are usually due to an inappropriate description of the CASSCF reference function. An example is valence–Rydberg mixing, which may be incorrectly described by the CASSCF wavefunction, due to errors in relative energies at this level of approximation.

The CASPT2 applications in organic spectroscopy have recently been reviewed [13]. The applications discussed included linear polyenes (from ethene to octatetraene), five-membered rings and norbornadiene (systems with two interacting double bonds), benzene and benzene derivatives, the porphyrin molecule, charge transfer in aminobenzonitriles, and the nucleic acid base monomers cytosine, thymine, uracil, and guanine. Here we review continued applications, including dimeric systems such as biphenyl and bithiophene, one more example of interacting double bonds: the methylenecyclopropene system, formaldehyde and acetone, imidazole and indole, and a series of aromatic cations and anions (Fig. 3). However, before describing these applications, we discuss some of the general features and problems that have to be considered. They include the choice of basis set and active orbitals, problems with intruder state, valence–Rydberg mixing, and so on. One section deals with the solvent effects on the electronic spectra.

1. Basis Sets

The basis set, inevitably, represents a compromise between the accuracy of a calculation and the computational effort. Recent improvements in calculating two-electron repulsion integrals [37, 38] combined with the atomic natural orbital (ANO) basis sets introduced by Almlöf and Taylor [39] now allow the use of large primitive sets routinely. Two such libraries of basis sets have been constructed by Widmark et al. [27, 40] and Pierloot et al. [41] and are derived from van Duijneveldt's [42] primitive basis sets. The larger set, for convenience called ANO-L, includes (8s4p3d) primitives for hydrogen and (14s9p4d3f) for the atoms Li–Ne. The smaller primitive set, hereafter referred to as ANO-S, has the following size: H(7s3p) and Li–Ne(10s6p3d). Unless stated otherwise, the ANO-L basis sets are applied in the present calculations.

ANO-type basis sets are based on a general contraction scheme and thus offer a route to high-quality one-particle basis sets without making

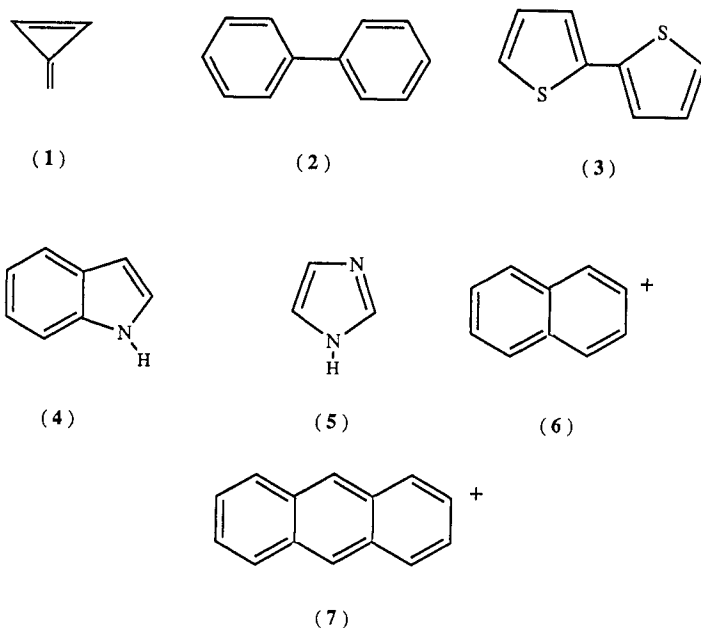


Figure 3. Structure formulas for methylenecyclopropene (1), biphenyl (2), bithiophene (3), indole (4), imidazole (5), naphthalene⁺ (6), and anthracene⁺ (7).

the wavefunction calculation unfeasible. Moreover, they can be improved systematically by progressively increasing the number of contracted functions. In general, if the basis sets are contracted to TZP (triple-zeta plus polarization) quality in the valence space (e.g., for first-row atoms the contracted size would be $4s3p1d$), the resulting basis sets are optimal to treat relative correlation and polarization effects in the valence space, as has been shown in a number of applications.

It is, however, also clear that quantitative results can be obtained only when the basis sets are large enough to treat the different types of excited states on a comparable level of accuracy. This means that the basis set must be able to describe equally well valence and Rydberg states, and flexible enough to cover states of an ionic nature at the same time as less diffuse covalent states.

A test of the basis-set effects on the excitation energy and transition moments of vertically excited singlet states in pyrazine has been published [43]. Table IV shows some recent data on the basis-set dependency of the excitation energy for the lowest vertically excited singlet states of neutral butadiene and its positive and negative ions. In accord with the previous results, we conclude that basis sets of the contracted size ($4s3p1d/2s$)

TABLE IV
Basis-Set Effects on the Excitation Energies (eV) of Butadiene and Its Ions^a

State	ANO-S (3s2p1d/2s)	ANO-S (4s3p1d/2s)	ANO-S (4s3p2d/2s)	ANO-S (4s3p2d/2s1p)	ANO-L (4s3p2d/2s1p)	ANO-L (4s3p2d1f/2s1p)
<i>Neutral Butadiene</i>						
1^1B_u	6.07	6.06	6.00	5.98	6.02	6.07
1^1A_g	6.34	6.16	6.11	6.09	6.10	6.07
<i>Butadiene Radical Cation</i>						
1^2A_u	2.42	2.41	2.41	2.40	2.40	2.39
2^2A_u	4.18	4.14	4.14	4.12	4.11	4.09
<i>Butadiene Radical Anion</i>						
1^2B_g	2.50	2.23	2.20	2.21	2.24	2.24
2^2B_g	3.26	2.87	2.84	2.85	2.72	2.67

^a The geometry of butadiene in the different electronic states has been computed at the ROHF/MP2 level of approximation using 6-31G* basis sets. Excitation energies have been computed with the CASSCF/CASPT2 method.

appear to be an optimal compromise between the quality and size of a calculation. The novel aspects are that it hardly makes any difference whether ANO-L or ANO-S sets are used. Moreover, for the butadiene cation the valence description can even be reduced to DZP (double-zeta plus polarization) quality.

If one is about to study the electronic spectrum of a neutral molecule in the ultraviolet region, say up to 8 eV, a large number of states will be included of which some may be Rydberg states. As the excited electron approaches the ionization limit it will move in very diffuse orbitals, resembling the hydrogenic functions and with radial maximum several times larger than the size of the molecule. Obviously, standard basis sets need to be supplemented with an adequate set of Rydberg ANO basis functions. In numerous applications it has been found that it is advantageous to add such basis sets routinely, even if one is not interested in the Rydberg states. Recently, we demonstrated [44] that the neglect of Rydberg states may lead to a significant artificial mixing of Rydberg and valence states.

The present method to obtain the Rydberg basis functions is based on the universal Gaussian basis sets devised by Kaufmann et al. for representing Rydberg and continuum wave functions [45], and the contraction coefficients are obtained in the following way: A CASSCF wavefunction for the cation lowest in energy is determined with the uncontracted, extra basis set placed at the center of charge. From the

resulting set of MOs, the lowest virtual orbitals of each angular momentum component are selected and used to construct an averaged density matrix, which is then diagonalized. The resulting natural orbitals are used as basis functions for the Rydberg states.

The uncontracted Rydberg basis sets typically include eight Gaussian functions per angular function. This large number of primitives is needed to describe properly the region of space where the excited electron penetrates the charge distribution of the remaining molecular core.

Finally, in calculations of electronic spectra of negatively charged systems, the extra electron may orbit in a large number of diffuse states before dissociation. However, the potential felt by the electron at large distances will not be a central field. Consequently, these diffuse orbitals cannot be approximated by hydrogen atom-like functions. Therefore, the most promising way to obtain accurate results for negatively charged systems is, apparently, to augment the atomic basis sets and to test for saturation of one-particle space.

2. *Problems and Limitations*

CASPT2 is not a black-box technique. It is demanding on the user, who has to know enough chemistry and quantum chemistry to be able to choose an appropriate active space. It may sometimes be necessary to experiment with different active spaces to check that the results are converged with respect to this parameter. The output of the calculations has to be inspected carefully for intruder states. When intruder states appear, appropriate steps must be taken to remove them. There are limitations to what applications are possible and the user must be aware of that and must be able to judge the quality of the calculation. In this section we discuss some of the problems and limitations of the method and give some illustrations that might be helpful for other users of the CASPT2 method.

One of the severe bottlenecks of the CASPT2 approach is the size of the active space. It is very hard to perform calculations with more than 12 active orbitals when the system has no symmetry. With symmetry it is possible to extend the practical limit to 13 or 14, but above that the calculations become too heavy. When studying only one energy surface, it is rare that more than 12 active orbitals are needed to describe the near-degeneracies in the system. Calculations in spectroscopy are, however, more demanding. Different orbitals are active in different excited states. Most electronic spectra have Rydberg states mixed in with the valence states. Thus Rydberg orbitals have to be included. As an example, consider the molecule methylenecyclopropene (MCP) [(1) in Fig. 3], the spectrum of which is discussed in more detail below. A

minimum set of valence active orbitals is 4. To this must be added nine Rydberg orbitals ($3s$, $3p$, and $3d$), which gives a total of 13. More orbitals may have to be added if intruder states appear in the calculations. The calculation would hardly be possible without symmetry. However, since the molecule has C_{2v} symmetry, it is possible to divide up the Rydberg orbitals such that calculations in different symmetries are made with the appropriate subset that contributes to excited states within that symmetry. The selection is illustrated later in Table V, which shows that it was in no case necessary to use more than nine active orbitals.

The problem was solved in a somewhat different way in a recent study of the phenol molecule [46]. The calculations of the excited states in this molecule were subdivided into three groups: the valence $\pi \rightarrow \pi^*$ states, Rydberg $\pi \rightarrow \pi^*$ states, and $\pi \rightarrow \sigma^*$ states. The molecule was assumed to be planar. For the valence states, the orbitals and the CASSCF states were obtained by minimizing the average energies of the lowest seven A' states. Three Rydberg orbitals had been obtained in earlier pilot studies and were deleted from the MO basis. The 21 occupied sigma orbitals were inactive, and the active space consisted of nine π orbitals: the oxygen lone pair, the six-ring π , and two extra-valence orbitals, which were needed to avoid intruder state problems (see also the earlier study of the benzene molecule [33]). The key to the problem is here the identification of the Rydberg orbitals and the exclusion of them from the one-electron basis. A similar approach was used in a recent study of the valence excited states of uracil, thymine, and cytosine [44, 47].

The $\pi \rightarrow \pi^*$ Rydberg states were computed by starting out from

TABLE V
CASSCF Wavefunctions (Number of Active Electrons) Used for Valence and Rydberg Transitions in Methylene cyclopropene

Wavefunction ^a	State	Number of Configurations ^b	N_{states} ^c
CASSCF(0301)(4)	${}^3B_2(2b_1 \rightarrow 1a_2^*)$	9	1
CASSCF(0301)(4)	${}^3A_1(2b_1 \rightarrow 3b_1^*)$	6	1
CASSCF(0501)(4)	${}^1A_1(2b_1 \rightarrow 3p_x, 3d_{xz}, 3b_1^*)$	65	4
CASSCF(5301)(4)	${}^1B_1(2b_1 \rightarrow 3s, 3p_z, 3d_{z^2}, 3d_{x^2-y^2})$	175	5
CASSCF(0311)(6)	${}^1B_1(4b_2 \rightarrow 1a_2^*)$	9	1
CASSCF(0302)(4)	${}^1B_2(2b_1 \rightarrow 1a_2^*, 3d_{xy})$	22	2
CASSCF(0331)(4)	${}^1A_2(2b_1 \rightarrow 3p_y, 3d_{yz})$	57	3
CASSCF(1301)(6)	${}^1A_2(8a_1 \rightarrow 1a_2^*)$	9	1

^a Within parentheses the number of active orbitals of symmetry a_1 , b_1 , b_2 , and a_2 of the point group C_{2v} .

^b Number of configurations in the CASSCF wavefunction.

^c States included in the average CASSCF calculation.

orbitals obtained in a calculation on the cation. First, a CASSCF calculation was performed, where the 21 occupied sigma orbitals were frozen, and the oxygen lone-pair orbital inactive, with 12 π -orbitals active, for the average of the 12 lowest A' states. This resulted in an optimized active orbital set containing the six valence π orbitals, three correlating orbitals, and three well-formed Rydberg orbitals. Six Rydberg states (excitations out of the two highest occupied π -orbitals to the $3p\pi$ and the two $3d\pi$ orbitals) were identified, and for each the natural orbitals were extracted and used as a *state-specific* orbital set for a set of CASCI calculations (CASSCF without orbital reoptimization) again using nine active orbitals. The type of orbitals in the active space is now different: Each orbital set contains only that state-optimized Rydberg orbital which must be present, and there are minor variations of the correlating orbitals, depending on which of the two ion rests the state contains.

The $\pi \rightarrow \sigma^*$ Rydberg states were obtained from a CASSCF with the 21 occupied sigma orbitals, and also the oxygen lone pair, inactive. The active space comprised six sigma orbitals and the six ring valence π orbitals, and the average energy of the lowest 12 states was minimized. The orbital optimization produced six Rydberg orbitals of σ symmetry. The 12 states were each used as the root state for subsequent CASPT2 calculations, without reoptimization. In all, 25 electronic states were determined for phenol, 13 of A' and 12 of A'' symmetry.

The validity of the CASSCF/CASPT2 method for computing excitation energies and properties of the excited states relies on the possibility of obtaining a valid reference function for the perturbation treatment. This is not always a trivial task. The reason is that the dynamic correlation energy is normally different in different excited states. Its effect on the excitation energy is usually small and positive for Rydberg states, it is negative and sometimes large for valence excited states. The ordering of the states is, as a result, different at the CASSCF level before the dynamic correlation energy has been added. At this level states may appear which are not going to remain in the final list, since they are not well characterized (higher Rydberg states, for example, for which there are no appropriate basis functions). A good example is given in the study of the furan molecule [48]. It was decided to include four 1A_1 states in the study, three valence states and one Rydberg state. A four-state average CASSCF calculation gave, however, only two valence states (the ground state and one excited state). The two other states were of Rydberg character. It was not until eight states were included in the averaging that the third valence state was found, with an energy of 10.6 eV relative to the ground state. The calculation was then repeated,

but now with a weight of the four desired states nine times larger than that of the other states. The final CASPT2 calculation gave three valence excited states and one Rydberg state in the energy range 0–7.8 eV. The decrease in the excitation energy was 2.9 eV for the fourth state, while it was only 0.2 eV for the Rydberg state. This and similar examples show that it is important to know in advance the general structure of the excited states of interest. The CASSCF calculations must be set up such that they are included among the resulting wavefunctions. It may be necessary to perform several CASSCF calculations in order to arrive at a state-averaged optimization emphasizing only those states for which the CASPT2 calculations will be performed.

Sometimes it may be difficult to know in advance how to construct the active orbital space, because the near-degeneracies in the system are not known and/or the space that would be satisfactory is too large to be possible. Guidance can then be obtained by performing restricted active space (RAS) SCF calculations on the excited states of interest (the RASSCF method is described in Refs. 10 and 49). The RASSCF method is characterized by a greater flexibility in the CF space used to build the wavefunction. Instead of a single active space, three subspaces are distinguished, RAS-1, RAS-2, and RAS-3. A certain number of active electrons are distributed among the three orbital spaces but now with the added restriction that at most a specified number of holes are allowed in the RAS-1 space and at most a specified number of electrons in RAS-3. One way to use this in spectroscopic applications is to diminish the size of the RAS-2 space to an absolute minimum and, instead, add orbitals to the RAS-1 and RAS-3 spaces. An extreme but often useful calculation is to have an empty RAS-2 space and to allow only single and double excitations from RAS-1 to RAS-3 (SDCI). The point is, of course, that it is possible to use many active orbitals in this way. Inspection of the natural orbital occupation numbers will then give information about the important near-degeneracies, which have to be included into the CASSCF calculation that precedes CASPT2.

The procedure above was used in a recent study of the lower excited states of free-base porphyrin [35]. This molecule has 24 π orbitals and 24 π electrons. It is clearly impossible to have all these orbitals and electrons active. Therefore, an SDCI-type RASSCF calculation was first performed with the 24 π orbitals active. The occupation numbers were then used as a guidance in a series of CASSCF/CASPT2 calculations on the excited states. It was possible to increase the active space in a systematic way until the computed excitation energies had converged. There is no guarantee that this is always possible, however. If not, the CASSCF/CASPT2 method cannot be used to study the electronic spectrum. One

such example is C_{60} . The minimum active space that can be used contains 15 orbitals and the calculation is thus outside the limits of the method. Other difficult cases are discussed in section III.B.

3. Solvation Effects

For isolated molecules of modest size, electronic excitation spectra can be predicted accurately by ab initio methods. On the other hand, such spectra may be of only limited relevance to bench chemists, who usually perform their experiments in a solvent. In this section we describe how solute-solvent interactions are included in the theoretical treatment of the electronic spectra within the present computational approach.

A microscopic description of solvation effects can be obtained by statistical mechanical simulation techniques or by a supermolecule approach. Through the advent of femtosecond time-resolution spectroscopy, this viewpoint has gained attraction. In the supermolecule approach, the surrounding solvent molecules are included in the quantum mechanical system. For studies of electronic excitations by statistical mechanics models, the solvent molecules are treated classically, but the quantum mechanical equations for the solute includes the solvent-solute interactions, resulting in a hybrid method [50, 51]. However, these methods are computationally demanding. In contrast, at the phenomenological level the solvent is regarded as a dielectric continuum, and there are a number of approaches [52-58] based on a classical reaction field concept. Typically, these methods are not more complicated than corresponding calculations for molecules *in vacuo*, except that self-consistency may require iteration. Here we use a modified version of the self-consistent reaction field (SCRf) approach of Bernhardsson et al. [59] to predict the shifts in band positions upon solvation.

Assuming that the solute is placed into a spherical cavity of radius a , Kirkwood derived a closed expression for the energy of the system,

$$E = E^0 - \frac{1}{2} \sum_{l,m} c_l M_l^m M_l^m \quad (29)$$

Here M_l^m is the real component m of a 2^l -pole moment of order l . The reaction field factor c_l is

$$c_l = - \frac{l!(l+1)(\epsilon-1)}{(l+1)\epsilon+l} \frac{1}{a^{2l+1}} \quad (30)$$

and depends on the dielectric permittivity ϵ of the solvent. Similar formulas may be derived for more general cavity shapes, but with much

larger number of multipoles and with coefficients to be determined for each case.

In the derivation of Eq. (29) and (30), equilibrium between the electronic state of the solute and the reaction field has been assumed. This condition is not fulfilled for an electronic excitation. The time dependence is approximated by partitioning the reaction field factor into two parts, which give a slow and fast component, respectively, of the reaction field. The reaction field is coupled to the average charge density of the quantum mechanical system, and the coupled equations are iterated to self-consistency. For a relaxed state such as the ground state in an absorption spectrum, the total dielectric constant is used, and the full reaction field is determined by the solute density. For excited states, however, that fraction of the reaction field which is due to slow relaxation processes is held fixed, and only the remainder is determined by the excited-state density, using the dielectric constant ϵ^∞ . The slow reaction field is obtained as the fraction $(c_i - c_i^\infty)/c_i$ of each individual 2^l -pole component. c_i^∞ is the reaction field factor using $\epsilon^\infty \approx n^2$ and n is the refraction index for some suitable frequency in the infrared or visible range.

A repulsive potential between the solute and the cavity walls is added to the reaction field(s). This repulsion is due to exchange interaction between the solute and the solvent molecules, which is modeled as

$$E_{ex} = \iiint \rho(r, \theta, \phi) f(r) d\phi d\theta dr, \quad (31)$$

where ρ denotes the electron density of the solute and $f(r)$ a penalty function of the form

$$f(r) = \sum_i \beta_i \exp[\alpha_i (r - R_i)^2] \quad (32)$$

and r, θ , and ϕ are polar coordinates relative to the cavity center. The $f(r)$ is only a function of the distance to the center and helps to confine the electron density to the cavity. Matrix elements of this function over a CGTO basis are easily programmed and are part of the standard repertoire of our integral program [11]. For our purposes we found four terms sufficient.

The excitation $2^1A_1 \leftarrow 1^1A_1$, from the ground state to the next singlet valence state of aminobenzonitrile (ABN) and dimethyl-ABN (DMABN) was used as test cases. Due to the larger dipole moment in the excited state, the transitions shift to the red in dipolar media for ABN [60] as well as for DMABN [61]. The latter has a larger shift, measured in several

solvents with ϵ up to 38.8 (Acetonitrile), which makes it a better example.

The geometries of ABN and DMABN were optimized at the CASSCF level of approximation [62]. ANO-S basis sets contracted as C, N[3s2p1d]/H[2s] were used. The cavity radius was optimized to minimize the absolute energy of the ground state at the CASSCF level of theory. This gave $a = 13.0a_0$ for ABN in diethylether, and $14.2a_0$, $13.8a_0$, and $13.5a_0$, for DMABN in cyclohexane, *n*-butylchloride, and acetonitrile, respectively.

The left side of Fig. 4 shows the CASPT2 energy diagram for the isolated molecule. We have found no experimental gas-phase excitation energy. The right-hand side shows the energy levels in a butyl chloride solution ($\epsilon = 9.65$). There, the computed excitation energy is 4.32 eV, in excellent agreement with experiment (4.3 eV; see Ref. 61). Upon solvation, all energy levels are lowered. The lowering is larger for the larger dielectric constants, and is larger for the excited state than for the ground state. For acetonitrile, with $\epsilon = 38.8$, the ground state is stabilized by 0.04 eV, but the excited state by 0.14 eV, giving a total red shift of 0.10 eV. The experimental shift is somewhat larger, 0.2 eV, in this case, but the experimental shifts are not very precise, and we conclude that the results are in agreement with experiment. The dipole moments of the ground and the excited states, 6.6 D and 14.2 D, respectively, are increased by the reaction field and reach 7.0 D and 15.2 D, respectively, in acetonitrile. They all have the same direction, parallel to the C_2 axis of the molecules.

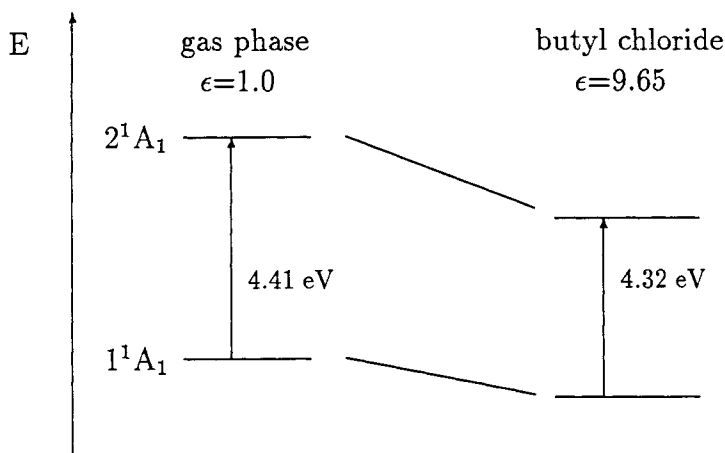


Figure 4. Solvation effects in the DMABN molecule.

This method was also used to study the electronic spectrum of imidazole. Section III.A.7 is devoted to the excited states of chromophores in proteins, and the imidazole results are presented there.

4. Spectroscopy of Carbonyl Compounds: Formaldehyde and Acetone

Aldehydes and ketones are important chromophoric groups, which play a central role in many different areas of chemistry. Formaldehyde is the prototype molecule for these kinds of compounds. Its electronically excited states have therefore been investigated extensively both experimentally and theoretically (see Refs. 63–65 and references cited therein). Acetone is the simplest aliphatic ketone. It is probably the best experimentally studied system of this group of important organic systems. The interpretation of its electronic spectrum has been and remains a subject of experimental interest [66–73]. In contrast to formaldehyde, acetone has been much less studied theoretically, undoubtedly due to the larger size of the molecule. To our knowledge there exist only two previous *ab initio* studies [74, 75]. Formaldehyde, on the other hand, is frequently used for testing new theoretical methods developed to treat excited states, because of its apparent simplicity and the numerous studies available.

At present there is consensus in the assignments of the vertical transitions of the low-energy part of the formaldehyde and acetone spectra, which are supported by CASSCF/CASPT2 calculations [65, 76]. However, the location and nature of all but the lowest singlet excited states of valence character is still one of the unresolved key problems of small carbonyl compounds. Qualitatively, the interpretation of the valence electronic transitions of the carbonyl chromophore involves a bonding π orbital of CO, a nonbonding $2p_y$ orbital on oxygen (hereafter named n_y), and an antibonding π^* orbital between C and O. Within the C_{2v} symmetry, with the z axis along the C–O bond, the lowest-energy electron promotion is from the HOMO, the b_2 nonbonding n_y orbital, to the b_1 antibonding π^* orbital resulting in the $^{1,3}A_2(n_y \rightarrow \pi^*)$ states. The $^{1,3}A_1(\pi \rightarrow \pi^*)$ states for the carbonyl group are expected to appear at energies similar to those found for the corresponding states in ethylene. However, the position of the 1A_1 valence state has not yet been determined unambiguously. At the CASPT2 level, the vertical transition energy for the valence $^1A_1(\pi \rightarrow \pi^*)$ state was computed to be above the $3s$, $3p$, and $3d$ members of the lowest Rydberg series, and the oscillator strengths were large for both formaldehyde and acetone. It is assumed that the $(\pi \rightarrow \pi^*)$ transition probably takes the form of a broad, undetected feature, underlying the somewhat congested Rydberg region between 7 and 12 eV, in the same way as the Rydberg transitions of

ethylene are superimposed on the broad singlet valence transition. Indeed, inspection of the electron energy-loss spectra of formaldehyde shows that the spectral peaks above ≈ 8 eV, corresponding to Rydberg series converging on the first ionization limit, are positioned on a nonzero background [77]. The band origin of the ($\pi \rightarrow \pi^*$) state is therefore expected to appear close to 8 eV. The CASPT2 results indicate a more complex structure in this region, although it may be noted that the computed lowest excitation energy for the planar geometry is 7.84 eV [65]. For acetone, two-photon photoacoustic spectroscopy gives evidence of a coupling between this valence state and the 1A_1 ($n_y \rightarrow 3p_y$) Rydberg state [71]. Similar evidence is obtained from two- and three-photon resonantly enhanced multiphoton ionization (REMPI) spectra of the $3p$ Rydberg transitions [73].

Knowledge about the vertical transitions is not enough for a full understanding of the spectroscopy of formaldehyde and acetone. The complicated photochemistry of formaldehyde has been described in recent papers by Hachey et al. [63, 64]. The interaction between the Rydberg and valence excited states in acetone has recently been studied with the CASSCF/CASPT2 method [76]. In principle, this can only be fully achieved with access to the full energy hypersurfaces, an obviously difficult task. We did not attempt to perform such a study. However, one of the main features expected for the equilibrium geometry of the 1A_1 ($\pi \rightarrow \pi^*$) excited state is a considerably increased CO distance compared to the ground state, since the excitation is from a bonding to an antibonding orbital. The energy was computed as a function of the CO bond length for the four lowest electronic states of 1A_1 symmetry, the ground state, the $n_y \rightarrow 3p_y$, and the $n_y \rightarrow 3d_{yz}$ Rydberg states, and the $\pi \rightarrow \pi^*$ valence state, which are placed vertically at 7.26, 7.91, and 9.16 eV, respectively. An active space (2230) with six active electrons was employed. It comprised the CO σ, σ^* (2000) and π, π^* (0200) orbitals, the lone pair, n_y , and $3p_y$ and $3d_{yz}$ Rydberg orbitals.

The computation of the CO-stretch potential energy curves is not straightforward with the present theoretical approach. The reason is the interaction of Rydberg and valence excited states. The reference functions for the perturbation calculation of the correlation energy are determined at the CASSCF level of approximation. However, at this level the interaction of the various states are grossly in error, since the dynamic correlation effects for the valence excited states are normally larger than for the Rydberg states. In the region of the crossing, the reference functions will therefore not describe correctly the mixing of the various states. This error cannot be corrected by a second-order treatment, since higher-order terms that mix the different reference functions

will be important. Only a multistate theory, which includes the mixing in the perturbation treatment, can solve this problem. The problem does not arise for the vertical transitions since there is no Rydberg–valence mixing in acetone at the ground-state equilibrium geometry.

The interaction between Rydberg and valence excited states can be assumed to be weak and only important close to the crossing points of the corresponding potential curves. One solution is to neglect the coupling by performing the calculations in such a way that the two types of states do not appear together. This approach was used in the calculation of the potential curves for the 1A_1 excited states. For CO distances shorter than 1.5 Å, $\pi \rightarrow \pi^*$ is the fourth excited state at the CASSCF level. Calculations with the active space (2230) and six active electrons were performed in this region. The CASSCF state average calculation included three roots (the ground state and the $n_y \rightarrow 3p_y$ and the $n_y \rightarrow 3d_{yz}$ states). The $3p_x$ and $3d_{xz}$ orbitals were deleted from the MO space to avoid intruder state problems from excitations to these orbitals from the occupied π orbital. The $\pi \rightarrow \pi^*$ excited-state potential was obtained with the active space (2200), which does not include the n_y and Rydberg orbitals. Only the four electrons of the CO bond were active. The state average calculation included only two roots. The same two Rydberg orbitals of π symmetry were deleted. The two results give an indication of the stability of the approach. First, the two potential curves for the ground state were virtually identical. Second, the computed vertical excitation energy for the $\pi \rightarrow \pi^*$ state was 9.20 eV, which is only 0.04 eV larger than the value obtained with the larger active space, which was used for all the vertical transitions. This illustrates again that the CASPT2 results are stable with respect to modifications in the active space as long as they do not grossly change the structure of the CASSCF reference function.

The resulting potential curves are shown in Fig. 5. The computed curves cross each other, but in the figure the avoided crossings have been indicated by introducing a small separation. The minimum of the ground-state curve is found for $r(\text{CO}) = 1.226$ Å with $\nu_3(\text{CO}) = 1698$ cm^{-1} , which can be compared to the experimental results (1.222 Å, 1731 cm^{-1}) [73, 78]. The 2^1A_1 state has a double minimum potential. The inner minimum is dominated by the $3p_y$ Rydberg state with an equilibrium bond length slightly shorter than that of the ground state. The outer minimum is the $\pi \rightarrow \pi^*$ state. It is located 7.42 eV above the ground state. The outer minimum is the $\pi \rightarrow \pi^*$ state. It is located 7.42 eV above the ground state at a CO distance of 1.58 Å. The excitation energy has thus decreased 1.78 eV compared to the vertical value.

The next state also has a double minimum potential along this coordinate. It contains contributions from all three diabatic curves. The

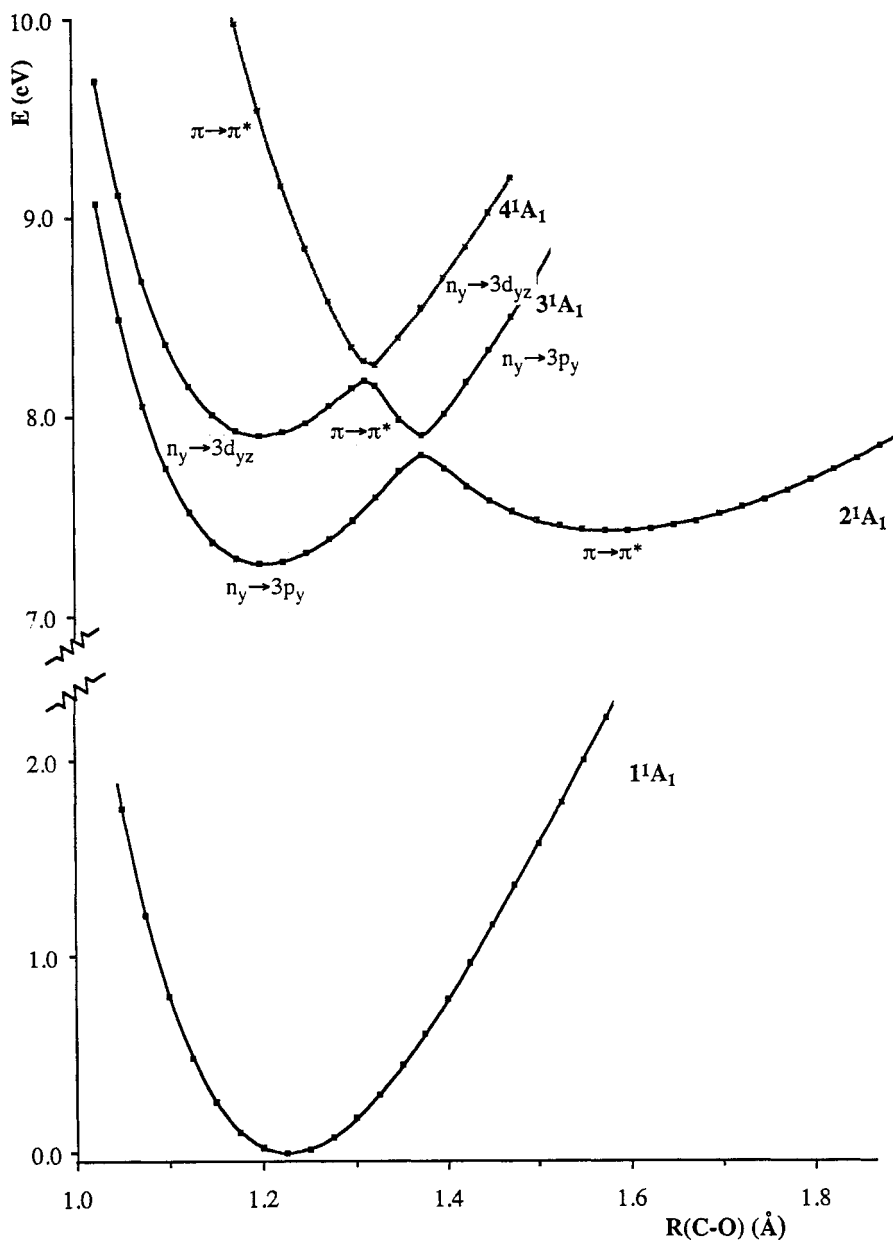


Figure 5. Potential curves for the $1A_1$ states in acetone as a function of the CO bond length.

inner minimum is dominated by the $3d_{yz}$ Rydberg state, while the outer minimum is due to the avoided crossing between the $\pi \rightarrow \pi^*$ and the $3p_y$ states. The upper state is a combination of the wings of the $\pi \rightarrow \pi^*$ state and the $3d_{yz}$ state. The result is one sharp minimum at 1.32 \AA , 8.26 eV above the ground state.

The transition moments for the three excitations from the ground state are smoothly varying functions of the CO distance. For the diabatic $3p_y$ Rydberg state the values vary from about 0.11 at short distances to 0.00 at $r(\text{CO}) = 1.5 \text{ \AA}$. The corresponding values for the $3d_{yz}$ Rydberg state are 0.59 to 0.45, and for the $\pi \rightarrow \pi^*$ state 1.26 to 0.75 [at $r(\text{CO}) = 1.95 \text{ \AA}$]. We used these data to perform a vibronic analysis, treating the system as a diatomic molecule. This is obviously a crude approximation, since it neglects all couplings to other modes and treats only the CO stretch frequency. Nevertheless, such a study might give some insight into the intensity distribution for excitations from the ground state to the three excited states. Since this calculation neglects all vibronic coupling between the three excited states, only the lowest vibrational quantum numbers were considered. The rovibrational Schrödinger equation was solved and the intensities were computed by numerical integration. Only excitations out of the $v'' = 0$ ground-state level were considered. This analysis shows that the bands of the 2^1A_1 system should be weak. The largest intensity is obtained for the 0–0 transition at 7.25 eV . The two lowest vibrational modes are entirely confined to the Rydberg part of the potential. It is only the third state that has any contribution from the $\pi \rightarrow \pi^*$ potential. But here the Franck–Condon overlap is small. The largest intensity for bands below 8.0 eV is found for the 0–0 transition to the 3^1A_1 state, which occurs at 7.9 eV . This is the $3d_{yz}$ transition. Appreciable intensity contributions from the $\pi \rightarrow \pi^*$ excited state appear only for the 4^1A_1 potential and start at 8.35 eV .

Recent theoretical studies of formaldehyde by Hachey et al. [64] and by the present authors [65] have revealed more features of the potential surfaces. The similarity between formaldehyde and acetone makes it possible to draw conclusions for the latter molecule based on the results obtained for formaldehyde, especially since the results obtained here for the 1A_1 states are similar in quality to those obtained by Hachey et al. The 1B_1 ($\sigma \rightarrow \pi^*$) potential has a minimum at $r(\text{CO}) = 1.47 \text{ \AA}$ and crosses the $^1A_1(\pi \rightarrow \pi^*)$ surface close to this point. Bending the CH_2 group out of the plane causes them to mix. The optimum bending angle was computed to be 46° . At shorter distances the 1B_1 surface mixes strongly with the ($n_y \rightarrow 3d_{xy}$) transition. It is likely that a similar situation obtains in acetone. Thus out-of-plane modes in combination with the CO stretch will allow for mixing of the 1A_1 and 1B_1 states. This will

complicate the vibrational spectrum further, compared to the simplified analysis performed above.

In addition, the bent $2^1A'$ ($\sigma \rightarrow \pi^*$, $\pi \rightarrow \pi^*$) surface can perturb the 1B_2 ($n_y \rightarrow 3s$) state [63]. The equilibrium geometry for the 1A_2 ($n_y \rightarrow \pi^*$) state is likewise expected to be bent (in formaldehyde the bending angle is 31° [65]). The results obtained by Hachey et al. for H_2CO shows that the 2^1A_2 ($n_y \rightarrow 3p_x$) potential is crossed by the 1B_1 ($\sigma \rightarrow \pi^*$) potential. Thus the dipole-forbidden transition to the 1A_2 state can become vibrationally allowed, borrowing intensity from the interfering 1B_1 state via modes of b_2 symmetry.

Assuming the two molecules to be similar, we conclude that $n_y \rightarrow$ Rydberg states may mix through vibronic interactions with the valence excited states of 1A_1 and 1B_1 symmetry. The large transition moment of the 1A_1 ($\pi \rightarrow \pi^*$) state can consequently be used to give intensity to Rydberg states of 1A_1 , 1B_1 , and 1B_2 symmetry. Direct observation of the $\pi \rightarrow \pi^*$ state is, on the other hand, difficult, due to the small Franck–Condon factors for the lower vibrational levels.

5. Interacting Double Bonds: Methylene cyclopropene

We have shown [13, 79, 80] that the electronic spectra of *cis*-1,3-butadiene [81], cyclopentadiene, aromatic five-membered heterocycles [48, 79], and norbornadiene [80] can be understood on the basis of a model with two interacting double bonds. Cyclopentadiene (CP) is the prime example of a ring-shaped molecule with a conjugated π -electron system, and its structure can be related to that of short polyenes such as *cis*-1,3-butadiene (CB) and the simplest heterocycles, such as pyrrole (PY), furan (FU), and thiophene (TP). In the series, *cis*-1,3-butadiene, cyclopentadiene, norbornadiene (NB), the latter is the most complex system, with the two ethylenic units coupled through indirect conjugation and π , σ interaction. One more system will be added here to the set of molecules with two interacting double bonds: methylenecyclopropene (MCP) [(1) in Fig 3] the simplest cross-conjugated π -electron system.

MCP, the archetype of nonalternant hydrocarbon known as the fulvenes, is a molecule of considerable theoretical and experimental interest [82–90]. It was synthesized and characterized for the first time in 1984 Billups et al. [84] and Staley and Norden [85] independently. An ultraviolet (UV) spectrum was included in the latter study. The electric dipole moment and heavy-atom molecular structure were reported two years later [88]. The experimental value of the dipole moment, $\mu = 1.90 \pm 0.02$ D, remarkably large for such a small molecule, which has been related to the strong transfer of π -electron density out of the ring due to the two double bonds interacting in a T-type arrangement. The

lowest adiabatic (8.15 ± 0.03 eV) and vertical (8.41 ± 0.05 eV) ionization potentials have been determined by photoelectron spectroscopy [89]. Most of the *ab initio* work has focused on the ground state of the molecule [86–89]. In the early study performed by Johnson and Schmidt [82] on the sudden polarization effect of the system, the low-lying excited states of planar MCP were characterized at the MCSCF level. A limited atomic basis set of double-zeta quality was used.

For the qualitative description of the electronic transitions it is helpful to consider the interaction of two independent ethylenic moieties. The interaction of the degenerate bonding, π_b , and antibonding, π_a , MOs of two ethylenic units results in the following four MOs: $\pi_1 = \pi_b + \pi_b$, $\pi_2 = \pi_b - \pi_b$, $\pi_3 = \pi_a + \pi_a$, and $\pi_4 = \pi_a - \pi_a$. With the geometrical arrangement in NB as reference, they lead to the orbital ordering $a_1(\pi_1)$, $b_1(\pi_2)$, $b_2(\pi_3)$, and $a_2(\pi_4)$ of the C_{2v} point group. Based on this structure the following valence singlet states can be expected and were actually obtained for NB. The one-electron promotions $\pi_2 \rightarrow \pi_3$ and $\pi_1 \rightarrow \pi_4$ yield two states of A_2 symmetry, while $\pi_1 \rightarrow \pi_3$ and $\pi_2 \rightarrow \pi_4$ give two states of B_2 symmetry. The corresponding electronic configurations are nearly degenerate and mix to form B_2^- and B_2^+ states. The minus state has the lowest energy and low intensity, while the plus state is pushed up and carries most of the intensity. There is an additional state of A_1 symmetry formed by two electron replacements, mainly the $(\pi_2)^2 \rightarrow (\pi_3)^2$ doubly excited configuration. Similar arguments can be used to rationalize the electronic transitions found in related systems as the five-atom rings (CP, PY, FU and TP) and *cis*- and *trans*-butadiene (CB and TB).

Due to the perpendicular arrangement of the double bonds in MCP, the two antibonding π_a ethylenic MOs cannot interact, since they have different symmetry. Interaction is, however, possible between the π_b MOs. In increasing order of orbital energies, the π -valence orbitals are: $1b_1(\pi_1)$, $2b_1(\pi_2)$, $1a_2(\pi_3)$, and $3b_1(\pi_4)$. The SCF orbital energies show that configurations involving the first occupied π orbital will not play a significant role in the description of the low-lying excited states. The $1b_1$ MO is around 5.8 eV below the HOMO, $2b_1$, which has a Koopmans' ionization potential of 8.1 eV (C[4s3p1d]/H[2s1p] results). Electronic states dominated by excitations out of the $1b_1$ MO will consequently not appear in the low-energy part of the spectrum. Two π -derived low-lying singlet and triplet valence excited states can therefore be expected in MCP: $2b_1 \rightarrow 1a_2$ gives rise to a state of B_2 symmetry and the excitation $2b_1 \rightarrow 3b_1$ results in a state of A_1 symmetry. Due to the localization of the $1a_2$ MO on the two carbon atoms of the ring, the transition from the ground state to the first singlet excited state, 1B_2 ($2b_1 \rightarrow 1a_2$), is expected with low intensity, contrary to the case of short polyenes in which the

corresponding feature is the most prominent. With both the $2b_1$ and $3b_1$ MOs spread on the four carbon atoms, the valence transition to the 1A_1 ($2b_1 \rightarrow 3b_1$) state is expected to be most intense. In addition, because of the high ring strain inherent in its molecular structure, the σ and σ^* orbitals of MCP are expected to be shifted significantly relative to those of unstrained hydrocarbons. Indeed, the HOMO-1 ($4b_2$) describes the σ C-C bonds adjacent to the double bond in the cyclic part of the molecule. Valence features involving σ MOs therefore had to be included in description of the electronic spectrum of MCP. Rydberg states arising from excitations out of the HOMO are predicted to be interleaved among the valence excited states.

The ground-state geometry determined in gas phase by microwave spectroscopy [88] was employed. Calculations were carried out within C_{2v} symmetry, placing the molecule in the yz plane with z axis bisecting the HCH angle. The ANO-L type C $[4s3p1d]/H[2s1p]$ basis set was used, supplemented with a $1s1p1d$ set of Rydberg functions, placed in the charge centroid of the 2B_1 state of the MCP cation. The active spaces used and the type of states computed are listed in Table V.

The active space comprising the π -valence MOs (0301) was used in the computation of the low-lying 3B_2 and 3A_1 states. For the study of the singlet excited states the active space was extended to include the corresponding Rydberg orbitals as appropriate. The results of the study are presented in Table VI. *Ab initio* transition energies obtained in previous calculations at the MCSCF level [82] are also included. The computed dipole moment for the ground state at the single-state optimized CASSCF (0301) level, 1.80 D, is in agreement with experiment, 1.90 D [88]. Three valence singlet states, 1B_2 , 3B_1 , and 4A_1 , were located below 7 eV. As expected, the lowest singlet excited state is of B_2 symmetry. The computed intensities for the two lowest valence transitions (both involving excitations to the $1a_2$ MO) are relatively low. The third valence transition represents the most intense feature of the system. The expectation values of x^2 , y^2 , and z^2 reveal the valence nature of the 1B_2 and 3B_1 states, while the 4A_1 state is somewhat more diffuse. The 1B_2 and 3B_1 states have opposite polarity to that of the ground state, due to the promotion of an electron into the $1a_2$ orbital entirely localized on the three-membered ring. Due to the ionic nature of the 4A_1 valence state, its computed dipole moment is high, 4.81 D, with the same polarity as the ground state [a carbanion center (CH_2^-) attached to a cyclopropenyl cation]. Comparison of the CASSCF and CASPT2 results demonstrates the importance of dynamic correlation effects to the excitation energies. The largest dynamic correlation contribution corresponds to the 4A_1 valence state, 1.22 eV. It is therefore not surprising

TABLE VI
Calculated Excitation Energies (eV) and Other Properties of the Vertical Excited States of Methylene cyclopropene

State	CASSCF	CASPT2	μ^a	Total ^b			Oscillator Strength	Other Results MCSCF ^c
				$\langle x^2 \rangle$	$\langle y^2 \rangle$	$\langle z^2 \rangle$		
Ground state (1^1A_1)	—	—	-1.80	-20.0	-15.2	-16.9	—	—
Singlet states								
$1^1B_2(2b_1 \rightarrow 1a_1^*)$	4.71	4.13	+2.07	-22.6	-18.8	-14.4	0.0093	4.71
$1^1B_1(2b_1 \rightarrow 3s)$	5.04	5.32	+2.19	-41.7	-36.5	-32.8	0.0028	—
$1^1A_2(2b_1 \rightarrow 3p_y)$	5.28	5.83	+1.23	-34.7	-66.2	-25.6	Forbidden	—
$2^1B_1(2b_1 \rightarrow 3p_z)$	5.52	5.84	+1.58	-36.7	-32.2	-64.0	0.0275	—
$2^1A_1(2b_1 \rightarrow 3p_x)$	5.00	5.85	+0.78	-71.7	-30.7	-26.7	0.0670	—
$3^1B_1(4b_2 \rightarrow 1a_2^*)$	7.29	6.12	+0.01	-22.2	-15.8	-15.8	0.0064	—
$2^1A_2(2b_1 \rightarrow 3d_{yz})$	5.94	6.54	-1.86	-37.6	-74.4	-70.1	Forbidden	—
$4^1B_1(2b_1 \rightarrow 3d_{zz})$	6.14	6.55	-5.78	-42.0	-54.3	-86.6	0.0012	—
$5^1B_1(2b_1 \rightarrow 3d_{x^2-y^2})$	6.19	6.62	-0.31	-82.1	-64.5	-30.5	0.0005	—
$3^1A_1(2b_1 \rightarrow 3d_{xz})$	5.77	6.71	-0.46	-84.2	-34.8	-74.5	0.0062	—
$2^1B_2(2b_1 \rightarrow 3d_{xy})$	6.53	6.75	-0.58	-80.4	-75.7	-29.6	0.0035	—
$4^1A_1(2b_1 \rightarrow 3b_1^*)$	8.04	6.82	-4.81	-32.2	-17.7	-21.6	0.5840	9.36
Triplet states								
$1^3B_2(2b_1 \rightarrow 1a_1^*)$	3.50	3.24	+0.97	-20.3	-17.2	-15.0	—	3.32
$1^3A_1(2b_1 \rightarrow 3b_1^*)$	4.72	4.52	-0.85	-20.8	-15.6	-18.2	—	4.87

^a Dipole moment (CASSCF) in Debye (experimental value for the ground state is -1.90 a.u. [88]).

^b Expectation value (CASSCF) of x^2 , y^2 , and z^2 (in a.u.).

^c MCSCF results employing a double-zeta basis set from Ref. 82.

that previous MCSCF calculations using a small atomic basis set [82] placed this state energetically too high, at 9.36 eV.

The calculated vertical transition energy from the ground to the 1^1B_1 ($2b_1 \rightarrow 3s$) Rydberg state is 5.32 eV. It is a weak transition. The $3p$ Rydberg states, 1^1A_2 , 2^1B_1 , and 2^1A_1 , have similar excitation energies. The 2^1A_1 state is placed at 5.85 eV above the ground state. The oscillator strength for the corresponding transition is around 0.07. It is actually the second most intense feature of the spectrum. The five members of the $3d$ series have been computed to lie in the energy range 6.54–6.75 eV. The dipole-allowed $3d$ transitions have lower intensities than the $3p$ transitions. In contrast to the $3s$ and $3p$ Rydberg states (cf. Table VI), the $3d$ states have the same polarity as the ground state. The singlet–triplet gaps are computed to be 0.89 and 2.30 eV for the 1^3B_2 and 1^3A_1 states, respectively. MCP has the smallest singlet–triplet splitting for the HOMO \rightarrow LUMO excited state (0.89 eV), as compared to the related systems NB (1.86 eV), CP (2.12 eV), and CB (2.77 eV). It is an additional reflection of the different (localized) nature of the LUMO in MCP.

As far as we are aware, no gas-phase spectroscopic data are available for comparison. The UV spectrum of MCP in *n*-pentane at -78°C is, however, available [85]. It displays a broad low-intensity band at 4.01 eV, a more narrow low-intensity band at 5.12 eV, and a strong band at 6.02 eV. The position of the first band is strongly solvent dependent, 4.49 eV in methanol at -78°C . The solvation effects are smaller for the other absorption bands; 5.00 and 5.90 eV in methanol, respectively. Therefore, comparison of the calculated (gas-phase) results with the available experimental data in solution has to be done with caution. The presence of a condensed medium perturbs the electronic transitions in several ways. Rydberg states are precluded and bands are usually broad with low resolution. The observed bands of the UV spectrum reported by Staley and Norden [85] should therefore be related to the computed valence transitions. The first band can be identified with the lowest vertical singlet–singlet transition, computed at 4.13 eV in gas phase. The fact that the energy of the excitation increases in a more polar solvent is consistent with the change of sign of the dipole moment (from -1.80 D to $+2.07$ D), which makes the interaction with the solvent repulsive in the upper state during the time scale of the excitation. A broad band is also expected due to strong relaxation effects in the solvent. A bathochromic shift is expected for the $1^1A_1 \rightarrow 4^1A_1$ transition since the dipole moment of the 4^1A_1 state is 3 D larger than that of the ground state and with the same sign. Finally, comparison between the observed and calculated intensities of the three valence transitions located below 7 eV supports the identification of the weak band centered at 5.12 eV in *n*-pentane, with the

second valence transition, which has a computed vertical energy of 6.12 eV in the gas phase. The dipole moment is, however, small and one would not expect a solvent red shift of 1 eV. It is, however, possible that other effects than the solvent are important for the differences between the spectrum of MCP in gas phase and solution. One possibility is the nonvertical nature of the transitions. Johnson and Schmidt [82] have calculated the low-lying diradical and zwitterionic states of 90° twisted MCP. The exocyclic π -bond twisting leads to a pronounced stabilization with respect to the correlated states of planar MCP. The equilibrium geometries of the excited states are, in general, expected to be twisted. The importance of this phenomenon has been demonstrated in ethylene, and it is by now well established that the maximum of the π - π^* valence band, which occurs at 7.66 eV [91], does not correspond to the vertical transition, which has a best theoretical estimate of about 8 eV [92], but instead, to a somewhat twisted molecule. Another possible source of error in the description of the 4^1A_1 state is related to the increased spatial diffuseness of this state compared to the other valence excited states. In cases where there is an erroneous valence-Rydberg mixing at the CASSCF level, the CASPT2 does not lead to an improvement of the excitation energy, and larger errors are obtained (about 0.4 eV for the V state of ethylene and 0.3 eV for the lowest singlet-singlet transition of TB [36]). This possibility was checked in a series of calculations using different active spaces and different basis sets. Additional MRCI calculations were also performed to check the behavior of the CASPT2 approach itself. The result of all these studies (which will be reported in detail elsewhere [93]) unambiguously show that the vertical transition energy of the 4^1A_1 state is located around 7 eV.

To summarize, the main features of the electronic spectrum of methylenecyclopropene can be rationalized within the scheme of two interacting double bonds. The lowest triplet state is mainly described by the HOMO \rightarrow LUMO excitation. The energy difference between the π_3 and π_2 orbitals is about the same in MCP, NB, CP, and CB. This is reflected in similar values for the lowest singlet-triplet transition, 3.24, 3.42, 3.15, and 2.81 eV, respectively. The orbital energy model is too crude to allow a more detailed analysis of the small relative energy differences. The corresponding singlet excited state, 1^1B_2 , located at 4.13 eV, lies around 1 eV below the corresponding state in the related systems NB (1^1A_2 : 5.28 eV), and CP (1^1B_2 : 5.27 eV). Orbital energy differences are about the same as in the other diene systems [79]. Thus the explanation lies in the electron repulsion terms. The excitation moves the electron from an orbital, which is delocalized over all four atoms to an orbital entirely localized on the ring atoms. This greatly reduces the

size of the corresponding exchange integral, with a corresponding down shift of the energy for the singlet state and a small singlet-triplet separation.

The strongest vertical transition corresponds to the 4^1A_1 valence state, computed in the high-energy side of the spectrum above the $n=3$ Rydberg series, at 6.82 eV, is described primarily by the $\pi_2 \rightarrow \pi_4$ configuration, with a small valence-Rydberg mixing. No near degeneracy occurs with excitations involving the lowest π orbital, which can be rationalized considering the large orbital energy spacing with the remaining π orbitals. The T-type interaction between the two double bonds and the intrinsic strain of the molecule makes the system unique, with a valence state described primarily by one-electron promotion from the highest σ orbital (HOMO-1) to the LUMO present at a moderate energy, between the $3p$ and $3d$ Rydberg series. The shifts noted between the computed spectrum and the available UV spectrum in *n*-pentane and methanol are probably due to both the nonvertical nature of the valence bands and to solvent effects.

Taking into account that methylenecyclopropene is a highly reactive compound, the experimentally determined gas-phase spectrum might not be easily accessible for some time. The interplay between experiment and theory therefore has importance for gaining further insight into the properties of this fundamental nonalternant hydrocarbon.

6. *Interacting Fragments: Biphenyl and Bithiophene*

With the studies of the electronic spectra of basic systems as benzene [33] and thiophene [79] performed successfully, it was tempting to try to relate the electronic states of two such interacting fragments to those of the corresponding monomer. Two cases may occur: two weakly coupled π systems such as in biphenyl [(2) in Fig. 3] or stronger coupling as in bithiophene [(3) in Fig. 3]. In the former situation it was possible to identify the excited states with the excited states in benzene. The orbitals are only weakly perturbed and retain their benzene identity to a large extent. Bithiophene is different. The shorter CC link distance leads to dimer orbitals that are considerably modified. The HOMO and HOMO-1 orbitals in thiophene are close in energy and mix strongly when perturbed. It is thus not possible to identify the excitation pattern in the dimer from the orbitals of thiophene. The main features in the energy range up to 6 eV of both biphenyl [94] and bithiophene [95] have been analyzed from CASSCF wavefunctions and CASPT2 energies. The results have been used to assign the experimental spectra, resulting in agreement between computed and measured excitation energies.

Apart from the intrinsic interest of biphenyl (BP) and bithiophene

(BT), they also act as models of the conjugated organic polymers polyparaphenylene (PPP) and polythiophene (PT), respectively. As is discussed in detail elsewhere [96], the results for the electronic excited states of the cation and anion of BP can be used for interpreting the polaron states in doped PPP. The main features of the spectra are reviewed briefly below.

Biphenyl Molecule. Most calculations were performed for a planar molecule with D_{2h} symmetry. The molecule is placed in the yz plane with z as the long molecular axis. A structure optimized at the CASSCF level was used [97]. The active space comprised the 12 π -valence orbitals, with 12 π electrons active. The computed excitation energies and oscillator strengths are collected in Table VII. In this table the observed bands are also related to the calculated vertical excitation energies. When comparing the experimental and theoretical data, one has to keep in mind that the geometry of the ground state of BP depends on the phase. A planar structure with large oscillations has been derived for solid biphenyl at

TABLE VII
Calculated and Experimental Singlet-Singlet Vertical Excitation Energies and Oscillator Strengths in Planar Biphenyl

States	Excitation Energy (eV)			Oscillator Strength	
	CASSCF	CASPT2	Exp.	Calc.	Exp.
1^1B_{3g}	4.66	4.04	4.11(0-0) ^{a,b} 4.17 ^c 4.37(0-0) ^d	Forbidden	—
1^1B_{2u}	4.92	4.35	4.20 ^a 4.26(0-0) ^e 4.59 ^f 4.59 ^g	0.0005	0.02 ^f 0.01 ^g
1^1B_{1u}	6.62	4.63 ^h	5.21 ^f 4.80 ^g 4.95 ⁱ 4.92 ^j 5.02 ^k	0.6200	0.36 ^f 0.28 ^g
2^1B_{3g}	7.98	5.07	—	Forbidden	—
$1^1B_{2g}(3s)$	5.65	5.60	—	Forbidden	—
2^1B_{2u}	8.87	5.69	6.41 ^f 5.85 ^g 5.96 ^j	0.4300	0.65 ^f 0.43 ^g
2^1B_{1u}	8.51	5.76	6.41 ^f 6.16 ^g 6.14 ^l	0.8355	0.65 ^f 0.45 ^g
2^1A_g	6.40	5.85	5.64 ^c	Forbidden	—
3^1A_g	8.49	5.85	5.64 ^c	Forbidden	—

^a Crystal absorption spectrum at 4.2 K [98].

^b Two-photon excitation spectrum of crystal biphenyl [99].

^c Two-photon excitation spectrum in ethanol [103].

^d Supersonic jet laser spectroscopy [217].

^e Absorption spectrum in argon matrix [100].

^f Vapor spectrum [102].

^g Crystal transitions derived from the reflection spectra [102].

^h The value obtained with the true (twisted) ground-state geometry is 5.09 eV.

ⁱ Electron energy-loss spectrum for biphenyl deposited on a thin film of solid argon at 20 K [106].

^j The UV spectrum in stretched film [105].

^k Absorption spectrum in cyclohexane [104].

temperatures above 40 K. In solution, in the crystal below 40 K, and in the gas phase, nonplanar structures with different twist angles are found (see Ref. 97 for details). All this shows that the ground-state energy surface is flat with respect to the twist angle. Simple arguments based on the orbital shapes show that the excited states have a more profound minimum at the planar structure. The assumption of a planar ground state may therefore give too small vertical excitation energies. In one such a case (1^1B_{1u}) this was illustrated in the recent study by computing also the excitation energy at the true ground-state equilibrium geometry [97]. The difference was found to be 0.46 eV.

As is shown in Table VII, experimental data in crystal, in solution, and in the gas phase give evidence of two low-energy transitions. This is reproduced by the calculations. The symmetry assignments are in agreement with the experimental data for the biphenyl crystal [98, 99]. The transition energies obtained are consistent with the crystalline data [98, 99] and biphenyl trapped in argon matrix [100]. Correlation with experimental data in the gas phase is also good considering that BP adopts a twisted conformation in this phase. In the energy interval 4.52–4.58 eV, two long progressions of the torsional vibration have been observed in the one- and two-photon absorption spectra of biphenyl in a supersonic jet. The fact that the intensities of these progressions are reversed in one- and two-photon spectroscopies supports assignment to the 1^1B_{3g} and 1^1B_{2u} states, as discussed by Murakami et al. [101]. A previous vapor spectrum showed a weak band at 4.59 eV with polarization along the short molecular axis as determined from an analysis of the reflection spectra in the crystal [102]. This band is therefore assigned to the 1^1B_{2u} state. The small value computed for the oscillator strength of this state is supported by the low intensity of the observed band, which in addition is obscured by the next band of the vapor spectrum. In solution, the experimental information about the two lowest singlet excited states comes primarily from two-photon spectroscopy [103]. The lowest band, located at 4.17 eV in ethanol solution, has been found to correspond to a final state of B symmetry. Dick and Hohlneicher [103] have assigned this band to a 1^1B_3 state based on the similarity to the lowest bands of the two-photon spectrum of fluorene. The band at 4.17 eV is then attributed to our 1^1B_{3g} state. It should be noted that in D_{2h} symmetry the 1^1B_{2u} state is two-photon forbidden, but in D_2 symmetry, in which the state becomes B_2 , it is allowed.

The third singlet excited state is of B_{1u} symmetry with a CASPT2 computed excitation energy of 4.63 eV and an oscillator strength of 0.62. The vapor spectrum shows a band of medium intensity at 5.21 eV [102]. This band has been found to be polarized along the long molecular axis

and is located at 4.80 eV in crystalline biphenyl [102]. An energy difference of 0.4 eV is therefore observed for the excitation energies measured in the gas and crystal phases. Values around 5 eV have been reported for this band in the absorption spectrum measured in solution [104] and for biphenyl deposited on film [105, 106].

The variation in the position of the maximum of the band depending on the media can be related to the twist angle of the molecule in the different media. Thus, in the gas phase, where biphenyl has the largest twist angle, the excitation energy acquires its maximum value, while it is minimum in crystalline biphenyl, which has a planar geometry at room temperature. These experimental facts seem to suggest that the 1^1B_{1u} excited state is planar, considering the low barrier to rotation determined for the ground state [97, 107]. It is therefore clear why the computed value is smaller than all the experimental data and closer to the value in the crystal phase. To get more insight into the influence of the geometry on the computed excitation energy to the 1^1B_{1u} state, calculations were carried out using a twisted geometry for the ground state of biphenyl. These calculations place the 1^1B_{1u} (or 1^1B_1 in D_2) state at 5.09 eV ($f=0.58$), which is in agreement with the gas-phase value [102].

Dick and Hohlneicher have suggested that the bands observed at energies higher than 4.7 eV are related to final states of A symmetry [103]. Thus a sharp maximum at 4.7 eV and a shoulder at about 5.0 eV were assigned to a low-lying $1A$ (or $1A_g$) state [103]. An exhaustive investigation of the $1A_g$ states has been undertaken to explain the above-mentioned features of the two-photon spectrum. We have been unable to find a low-lying $1A_g$ state, despite increasing the number of roots in the average CASSCF calculation to seven. The first state of this symmetry appears at 5.85 eV. The previous assignment of the two-photon spectrum should therefore be revised. The 2^1B_{2u} and 2^1B_{1u} states are calculated to be close in energy, with computed values of 5.69 and 5.76 eV, respectively, which are in agreement with experimental findings [102, 105, 108] considering the fact that the upper states are planar.

Two optically forbidden states of A_g symmetry are found at 5.85 eV. These states clearly correspond to the intense two-photon absorption starting at 5.64 eV, which was related to states of A symmetry on the basis of the value of the two-photon polarization parameter [103]. The CASSCF wavefunction of the 2^1A_g state is described mainly by doubly excited configurations which have a total weight of 43%, with predominance of the doubly excited configuration HOMO \rightarrow LUMO. By contrast, the CASSCF wavefunction of the 3^1A_g state is described mainly by four singly excited configurations, involving the four highest occupied and four lowest unoccupied MOs.

To summarize, there is agreement between the spectrum computed and the large amount of spectral information. The theoretical data confirm the sensitivity of the excitation energies to the structure of the ground state, which varies from nearly planar in crystals to 44°C twisted in the gas phase. The appearance of the first Rydberg transition has been predicted. It has been shown that no excited state of 1A_g symmetry appears below 5.85 eV. As far as we are aware, this represents the first *ab initio* study of BP. Comparison with earlier semiempirical studies shows that they are not able to account for all features of the electronic spectrum of biphenyl (see the discussion in Ref. 94).

Bithiophene Molecule. Calculations were performed at the planar *trans* geometry (C_{2h} symmetry) and at the twisted *trans*-bithiophene conformation (C_2 symmetry) obtained at the MP2/6-31G* level [109]. In most calculations the active space comprised the 10 valence π orbitals. Because of intruder states, two orbitals (one of each π symmetry) had to be added for the 2^1A_g excited state in the twisted conformation. The 12 π electrons were active. The computed excitation energies and transition intensities for the planar and twisted forms are presented in Table VIII together with relevant experimental information.

Four excited states of 1B_u and two of 1A_g symmetry (1B and 1A in the twisted form) have been studied. The first 1B_u state is dominated by the HOMO \rightarrow LUMO excitation, but contains in addition a sizable contribution from HOMO $-2 \rightarrow$ LUMO. The same is true for the next 1B_u state even if there are now larger contributions from higher excitations. The first state of 1A_g symmetry corresponds mainly to the HOMO $-1 \rightarrow$ LUMO excitation but contains 23% double excitations. The character of being doubly excited is even larger in the next state of this symmetry (42%), and here it is the (HOMO) $^2 \rightarrow$ (LUMO) 2 that dominates the wavefunction.

The fact that the ground-state potential is flat [109] implies that variations in computed excitation energies for different geometries will reflect mostly the shape of the upper state potential. Comparison with experiment is complicated, since measured bands depend strongly on temperature and medium. It is not unlikely that the *cis* conformation is more stable than *trans* in polar media, since there is a large difference in dipole moment. It is only low-temperature gas-phase data that can be compared directly to the present results.

The potential curves for the excited states are different from those of the ground state. In the region of the *trans* conformer they have a distinct minimum at the planar geometry. The energy difference to the twisted geometry varies from 0.14 eV for the 2^1B_u state to 0.45 eV for the 2^1A_g

TABLE VIII
 Calculated and Experimental Singlet-Singlet Excitation Energies (eV) and Calculated
 Oscillator Strengths in Planar and Twisted *trans*-Bithiophene

	State				
	1^1B_u	2^1B_u	2^1A_g	3^1A_g	3^1B_u
<i>Planar Conformation</i>					
CASSCF	5.64	6.13	5.92	5.31	7.82
CASPT2	3.88	4.15	4.40	4.71	5.53
Oscillator strength	0.062	0.014	Forbidden	Forbidden	0.253
<i>Twisted Conformation</i>					
CASSCF	5.76	6.29	6.07 ^a	5.56	7.86
CASPT2	4.36	4.22	4.90 ^a	4.99	5.79
Oscillator strength	0.049	0.034	0.013	0.0014	0.172
<i>Experimental Energies</i>					
	3.86(0-0), ^b 3.67(0-0) ^c		4.96, ^d 5.02 ^{e,f}		6.46 ^e
	4.13, ^d 4.11, ^e 4.09 ^f		4.48(0-0) ^g		5.93 ^f

^a State computed using the active space (66) due to intruder-state problems.

^b Fluorescence excitation spectrum of bithiophene seeded into a supersonic helium expansion [110].

^c Fluorescence excitation spectrum of solid solutions of bithiophene in *n*-hexane at 4.2 K [218].

^d Gas-phase absorption spectrum at room temperature [110].

^e UV absorption spectrum in cyclohexane [104].

^f UV absorption spectrum in methanol [111].

^g Two-photon fluorescence excitation spectrum of a dilute solution of bithiophene in crystalline *n*-hexane at 77 K [112].

state. Since the potential for the ground state is flat, these energy differences are almost identical to the difference between the two sets of excitation energies given in Table VIII. As a result, the computed excitation energies for the planar conformation are close to the 0-0 transition energies. The computed "vertical" energies (those for the twisted form) are more difficult to relate directly to experimental data, again because the potential for the ground state is flat while the upper potential is not. It should be noted that the transition moments vary strongly with geometry.

Four excited states were found at low energies (below 5.0 eV). A third 1^1B_u state is found with energies around 5.5 eV (0-0 transition). The first

excited state is of 1B_u symmetry with a computed 0–0 energy of 3.88 eV. This is in agreement with the recent fluorescence excitation spectrum of Chadwick and Kohler [110], who place the 0–0 transition at 3.86 eV. The corresponding spectrum in solid solution of *n*-hexane places the band at 3.67 eV, corresponding to a solvent shift of -0.19 eV (this is almost exactly the red shift expected if the molecule is forced to be planar in the condensed phase). The second state is also of 1B_u symmetry. This possibility was not discussed earlier. The 0–0 energy is 4.15 eV. It has considerably lower intensity than the first state in planar geometry, but they become more similar when the molecule is twisted. Gas-phase absorption spectroscopy finds the first band with a peak at 4.13 eV [110]. The band is broad with several features on the low-energy side, and it is not unlikely that it contains more than one transition. Also ultraviolet (UV) absorption spectra in solution show the same band [104, 111].

The first band of 1A_g symmetry appears at 4.40 eV in the planar conformation. It is shifted to 4.90 eV when the molecule is twisted. The two-photon excitation spectrum of Birnbaum and Kohler [112] locates the 0–0 band of a state of 1A_g symmetry at 4.48 eV, which is again in agreement with the present result. It is discussed whether they see the first excited state of this symmetry or the second. The present results strongly indicate that it is the first, but the $3{}^1A_g$ state is only 0.31 eV higher in energy. Considering the error bars of the computed excitation energies (0.3 eV), it cannot be ruled out completely that it is the third state that is observed. Both states are forbidden for planar geometry but become allowed when the system is twisted. UV absorption spectroscopy finds a second band with a peak at about 5.0 eV [104, 110, 111]. This band probably contains both 1A_g transitions, which in the twisted conformation are almost degenerate.

The UV absorption spectra contain a third band with maximum at about 6.0 eV [104, 111]. The calculations assign this band to the third state of 1B_u symmetry, which is computed to have a 0–0 transition energy of 5.53 eV, which increases to 5.79 eV at the twisted geometry. The UV absorption spectra have been recorded in solution and direct comparison is therefore not possible, since the ground-state conformation of the molecule is not known. It is probable that it is *cis*, at least in polar solvents. But the assignment of the band is clear. A fourth 1B_u state has actually been calculated with an adiabatic energy of 6.02 eV (not included in Table VIII). The band at 6 eV is probably composed of both these transitions. The computed intensity for the latter state is, however, small.

The main features of the low-energy part of the electronic spectrum of bithiophene are understood. Corresponding studies of the ter-thiophene molecule are under way. Together, the results may be used to calibrate

data obtained with more approximate methods. Extrapolation to larger oligomers becomes possible by using data computed with simpler semiempirical methods adjusted to fit *ab initio* results obtained for the dimer and trimer.

7. Spectroscopy of Protein Chromophores

The main features of the near- and far-ultraviolet spectra of the proteins are related to the absorption properties of the aromatic amino acids phenylalanine (Phe), tyrosine (Tyr), tryptophan (Trp), and histidine (His) [113, 114]. The peaks observed in the absorption spectra up to 185 nm (6.70 eV) can be assigned to the excited states of the chromophore-acting molecules benzene, phenol, indole, and imidazole, respectively. In the present section we focus on the theoretical description of the most representative valence singlet excited states of the aromatic amino acid chromophores. As the results for benzene and phenol have been recently described [13, 46], only the results for indole, [(4) in Fig. 3] and imidazole [(5) in Fig. 3] are reviewed here [115, 116]. The theoretical results support the assignment of four $\pi \rightarrow \pi^*$ valence singlet states as responsible for the most relevant observed peaks: two low-lying and weaker states usually named 1L_b and 1L_a , the splitting of which depends on the specific system, and two higher 1B_b and 1B_a states with larger intensities. Imidazole (and therefore histidine) is different, however, with only two transitions below 7 eV.

It is the configurations related to the HOMO, HOMO - 1 and LUMO, LUMO + 1 orbitals that are responsible for the four singlet (and four triplet) states: the HOMO \rightarrow LUMO state, two states as a mixture of the nearly degenerate HOMO - 1 \rightarrow LUMO and HOMO \rightarrow LUMO + 1 configurations, and a final HOMO - 1 \rightarrow LUMO + 1 state [13, 117]. The relative order of the HOMO \rightarrow LUMO state and the antisymmetric combination of the two nearly degenerate configurations will depend on the relative energies of the corresponding orbitals and the strength of the interaction. Even in highly symmetric systems, such as naphthalene, the HOMO - 1 \rightarrow LUMO and HOMO \rightarrow LUMO + 1 excitations belong to the same symmetry and are able to interact; the other two excitations, HOMO \rightarrow LUMO and HOMO - 1 \leftarrow LUMO + 1, belong to another symmetry. In this case the large difference in energy prevents strong mixing of the two configurations. The intensities give a good measure of the strength of the interaction. The two low-lying states have low intensities, one because it is the antisymmetric combination of two configurations [118], the other because of the orbital structures and often because it contains a large fraction of doubly excited states. These are the *L* states as they were labeled by Platt [119]. The complementary states

are pushed up in energy and have larger intensity. They were labeled B states [119]. Obviously, in large systems, more combinations are available and the structure becomes more complex. Configurations involving other orbital excitations mix together with doubly excited states, leading to a complex multiconfigurational character of the states. In addition, lowering the symmetry permits further mixing among the configurations. This happens, for example, in indole and imidazole, and modifies the simple model.

Indole Molecule. Tryptophan is the most important emissive source in proteins, with the indole chromophore, [(4) in Fig. 3] responsible for its low-energy absorption bands [120]. The studies of the electronic spectrum of indole have focused almost exclusively on the position and nature of the two low-lying valence singlet states, 1L_b and 1L_a , due to their apparent degeneracy and their different behavior in solvents. While the sharp 1L_b band origin and maximum in gas phase were established at 4.37 eV [121, 122], the maximum (4.77 eV [122, 123] in gas phase) and the origin (estimated from 4.42 to 4.70 eV [123–126]) of the 1L_a state have been disputed, because of the strong overlap between the two bands. The properties of the bands are sensitive to solvent effects and to substitutions in the indole ring [120]. The less studied group of intense transitions in the domain from 216 to 192 nm (5.74 to 6.45 eV) has been related to the strongly allowed ${}^1B_{a,b}$ manifold in polyhexacenes [114, 122]. The data concerning the triplet and Rydberg states are not discussed here.

The ground-state gas-phase equilibrium geometry was optimized at the CASSCF level employing an ANO basis set [41] contracted to N, C/3s2p1d, H/2s. The molecule is planar and was placed in the xy plane. The calculations of the vertical electronic spectrum used a larger ANO basis set [27] contracted to C,N/4s3p1d, H/2s and supplemented with 1s1p1d Rydberg-type functions in the cation charge centroid. The active space included the eight valence π orbitals plus the nitrogen lone-pair orbital and appropriate Rydberg orbitals.

Naphthalene [127] can be used as a model for the general structure of the excited states. A previous CASSCF/CASPT2 study showed that the low-lying 1L_b state (1^1B_{3u}) at 4.03 eV is a mixture of the above-mentioned singlet excited configurations, leading to a weak band ($f=0.0004$). The opposite mixture of the same configurations gives the 1B_b (2^1B_{3u}) state at 5.54 eV, which has the largest intensity in the spectrum ($f=1.34$). The interaction is not as strong in the 1L_a (1^1B_{2u}) state ($f=0.050$) at 4.56 eV and the 1B_a (2^1B_{2u}) state ($f=0.31$) at 5.93 eV. Both are well represented by a single excitation, HOMO \rightarrow LUMO and HOMO $-1 \rightarrow$ LUMO $+1$, respectively.

Table IX presents the results for the valence π states in indole. The four states discussed, 1L_b , 1L_a , 1B_b , and 1B_a , computed at 4.43, 4.73, 5.84, and 6.44 eV, respectively (see also Table XII), are in agreement both in energies and intensities with the experimental data. The 1L_b state, at 4.43 eV ($f=0.05$), has the expected composition of the wavefunction: HOMO $-1 \rightarrow$ LUMO, 44% and HOMO \rightarrow LUMO + 1, 22%. As pointed out, it is the antisymmetric combination of the configurations that gives the low value of the oscillator strength. Both energy and intensity are in agreement with the experimental values, 4.37 eV [121, 122] and 0.05 [128]. The 1L_a state is composed mainly of the HOMO \rightarrow LUMO configuration, 54%. The computed excitation energy, 4.73 eV, agrees with experiment, 4.77 eV.

The most intense feature in the spectrum was computed at 5.84 eV ($f=0.46$). It is the 1B_b state, which has a wavefunction composed mainly of the HOMO $-1 \rightarrow$ LUMO, 11%, and HOMO \rightarrow LUMO + 1, 42%, configurations. Several peaks and shoulders in the region 5.80–6.02 eV [122, 129] have been assigned to the most intense band. Finally, the 1B_a state is computed at 6.44 eV ($f=0.26$), in agreement with the band observed at 6.35 eV [122, 129]. Both 1B_b and 1B_a bands have lower intensities here than they have in naphthalene, a consequence of the larger configurational mixing in the wavefunction due to the lowering of the symmetry. The computed CASSCF dipole moments give us some hints about the expected behavior of the various bands in the presence of polar solvents. The ground-state dipole moment is computed to be 1.86 D (experiment: 2.09 D [130]). The dipole moment for the 1L_b state, 0.85 D, differs, however, from experiment 2.3 D [131]. The difference is outside the error limits of the theoretical value. The computed dipole moment for the 1L_a state, 5.7 D, is in better agreement with experiment, 5.4 D [132]. For the 1B_b and 1B_a states the values computed are 3.8 and 1.8 D, respectively. The 1L_a and 1B_b can be expected to be more affected by environmental effects because of the larger changes in their dipole moments compared to the ground state. This is seen clearly in the experimental spectra [129].

A less intense state at 6.16 eV with 16% double excitations in the wavefunction, and two higher and intense states, also with important contributions from doubly excited configurations, complete the computed valence spectrum. The Rydberg states series are not going to be described here, but the beginning of two series were calculated at 4.85 eV ($5a'' \rightarrow 3s$ state) and 5.33 eV ($4a'' \rightarrow 3s$ state).

In addition to the energies and intensities we have also included the transition moment directions in Table IX. These quantities, obtained in UV or infrared (IR) linear dichroism experiments, have been used

TABLE IX
 Calculated and Experimental Excitation Energies, Oscillator Strengths, Dipole Moments (μ), and Transition Moment Directions for the $\pi \rightarrow \pi^*$ Excited Valence Singlet States in Indole

State	Excitation Energy (eV)		μ (D)	Oscillator Strength		TM Direction ^c (deg)	
	CAS	PT2		This Work	Expt. ^b	This Work	Expt. ^d
1 ¹ A'	—	—	1.86	—	—	—	—
2 ¹ A'	4.83	4.43	0.85	0.050	0.045	+37	+42 ± 5
3 ¹ A'	6.02	4.73	5.69	0.081	0.123	-36	-46 ± 5
4 ¹ A'	6.97	5.84	3.77	0.458	—	+16	0 ± 15
5 ¹ A'	6.74	6.16	0.93	0.003	—	+5	—
6 ¹ A'	7.35	6.44	1.80	0.257	—	-55	> ± 30
7 ¹ A'	7.52	6.71	2.34	0.138	—	-10	—
8 ¹ A'	7.98	6.75	1.12	0.245	—	-12	—

^a Experiments from Refs. [121–123 and 129].

^b From Ref. 128.

^c The molecule is placed on the xy plane. The ring-shared bond is the y axis. The x axis is defined to be the pseudosymmetry long axis of indole, which joins the end carbon of the pyrrole moiety with the midpoint of the ring-shared bond. Angles are defined counterclockwise from the x axis. The nitrogen is placed in the fourth quadrant.

^d Experimental data from Ref. 133.

extensively for identifying excited states. Among all the experimental data the most recent measurements [133] have been selected in Table IX to show the agreement between theory and experiment.

Imidazole Molecule. The absorption spectra of imidazole [(5) in Fig. 3] in various solvents exhibit a broad band with maximum around 207 nm (6.00 eV) [134–136], which is usually attributed to the first $\pi \rightarrow \pi^*$ transition. A second band was observed in the 195–178 nm (6.38–6.97 eV) region, with a modest dependency upon solvent and pH [136]. Several weak bands have been reported at low energies. Our calculations have assigned them as triplet states and they were described and discussed in the original paper [116]. The recent study by Caswell and Spiro [135] reported a broad absorption band envelope at 207 nm (6.00 eV) with two overlapping peaks at 218 nm (5.69 eV) and 204 nm (6.08 eV), which were assumed to correspond to two different $\pi \rightarrow \pi^*$ transitions.

The theoretical studies on imidazole are scarce. A recent MRCI study by Machado and Davidson [137] considered valence and Rydberg states together for the first time. On the other hand, the available experimental spectra of imidazole are limited to methanol, ethanol, and aqueous solutions and it is difficult to establish the effects of the solvent on the different transitions. The structure of the computed gas-phase spectrum differ from the spectra in a solvated medium. An unambiguous assignment of the main valence bands in the spectrum of imidazole thus requires consideration of such effects. The reaction field method, explained above, was employed with the CASSCF/CASPT2 method to analyze the influence of the solvent on the valence $\pi \rightarrow \pi^*$ states of imidazole and assign the most important features.

The experimental ground-state geometry [138] was used with the molecule in the xy plane. ANO basis functions contracted as C, N/4s3p1d, H/2s1p, were used, supplemented with 1s1p1d Rydberg functions in the cation charge centroid. The study of the electronic spectrum of imidazole involved $\pi \rightarrow \pi^*$, $n \rightarrow \pi^*$, and Rydberg states (in the gas phase). The optimal radius for the cavity in the reaction field calculations was computed to be 7.0 bohr in both water and ethanol.

Table X compiles the computed gas-phase excitation energies, oscillator strengths, and dipole moments for the valence singlet excited states of the imidazole molecule. Previous MRCI results by Machado and Davidson [137] are also included. Table XI lists the results obtained in the reaction field model. Three valence $\pi \rightarrow \pi^*$ and two valence $n \rightarrow \pi^*$ states have been found in the gas-phase spectrum up to 8.5 eV. In addition, the beginning of three Rydberg series have been computed from

TABLE X
Calculated Excitation Energies, Oscillator Strengths, and Dipole Moments (μ) for the Excited Valence Singlet States in Gas-Phase Imidazole

State	Excitation energy (eV)			μ (D)	Oscillator Strength	
	CAS	PT2	MRCI ^a		This Work	MRCI ^a
1 ¹ A'	—	—	—	3.70	—	—
1 ¹ A''(n π^*)	7.02	6.52	—	0.22	0.011	—
2 ¹ A'($\pi\pi^*$)	7.51	6.72	7.71	4.61	0.126	0.080
3 ¹ A'($\pi\pi^*$)	8.43	7.15	8.18	3.00	0.143	0.070
2 ¹ A''(n π^*)	8.42	7.56	—	2.79	0.013	—
4 ¹ A'($\pi\pi^*$)	10.06	8.51	—	3.85	0.594	—

^a CIR6 calculations from Machado and Davidson [137].

TABLE XI
Calculated and Experimental Excitation Energies, Oscillator Strengths, (f) and Dipole Moments (μ) for the Valence Singlet States of Imidazole in Gas Phase, Ethanol, and Water

State	Gas phase				Ethanol			Water		
	PT2 (eV)	f	μ (D)	Expt. ^a	PT2 (eV)	f	μ (D)	PT2 (eV)	f	μ (D)
1 ¹ A'(ground state)	—	—	3.70	—	—	—	4.09	—	—	4.07
2 ¹ A'($\pi\pi^*$)	6.72	0.126	4.61	6.0	6.32	0.036	3.61	6.32	0.024	3.57
3 ¹ A'($\pi\pi^*$)	7.15	0.143	3.00	6.5	6.53	0.307	3.42	6.53	0.275	3.41
4 ¹ A'($\pi\pi^*$)	8.51	0.594	3.85	—	7.48	0.600	4.76	7.48	0.561	4.75

^a Experimental excitation energies are the same in ethanol and water [135, 136].

the highest occupied orbitals 3a''(π), 2a''(π), and 15a'(n) to the 3s Rydberg orbital at 5.71, 7.10, and 7.10 eV, respectively. The details of this part of the spectrum are discussed elsewhere [116]. The gas-phase results place a n \rightarrow π^* state at 6.52 eV as the lowest singlet excited valence state with low intensity, while the two valence $\pi \rightarrow \pi^*$ singlet states appear at 6.72 and 7.15 eV with moderate intensities. The most intense transition is the third valence $\pi \rightarrow \pi^*$ state at 8.52 eV. Analysis of the wavefunction shows strong mixing of different configurations in the low-lying states. One of the most important consequences is the increase in intensity in both states and a general increase in the energies with respect to the other protein chromophores. The indole model can be related to the interacting double-bond model explained in the methylenecyclopropene section. In imidazole, however, the general model should be only considered an approximation. As an illustration, the ¹L_b state wavefunction is composed of not only the two configurations expected but three: HOMO \rightarrow LUMO, 37%; HOMO - 1 \rightarrow LUMO, 23%, and

HOMO \rightarrow LUMO + 1, 25%, while the corresponding weights for the 1L_a state are 53%, 24%, and 12%.

As the experimental spectra for imidazole are available only in the polar solvents water and ethanol, there is no knowledge of the solvent effects on the spectrum. The addition of the effects of the environment by using the reaction field method, as explained in an earlier section, emphasizes the sensitivity of the imidazole states to the presence of a polar solvent. The theoretical results are presented in Table XI. No important differences were found for the solvents water and ethanol within the present model. The calculated excitation energies were 6.32, 6.53, and 7.48 eV in both solvents. The experimental spectra have peaks at 6.0 and around 6.5 eV [135, 136] for both water and ethanol as solvents.

As can be inferred from the data in Table XI, solvation leads to large changes in dipole moments. For the $2^1A'$ state, the dipole moment drops by more than 1 D. The solvent effects already appear to be saturated for ethanol. We also note that these changes are much larger for imidazole than they were for the ABN molecule (see Section III.A.3). It should be pointed out that the theoretical model used is crude and is not expected to provide extremely accurate shifts in excitation energies and other properties. Some expectation values, as for example the dipole moments computed at the CASSCF level, turn out to be sensitive to various parameters, such as the basis set, the active space, and the number of roots selected in the CASSCF state average calculations. Test calculations [116] have shown, however, that in this specific case the large solvent shifts are an artefact of the CASPT2 method. Too large excitation energies are obtained in the gas phase, due to an incorrect mixing of Rydberg and valence excited states, similar to what has been observed in ethene and butadiene [36].

Electronic Spectra of Proteins. The chromophore groups in a protein form a complex system of molecular fragments differing in structure and position and contributing as a whole to the spectroscopic properties of the protein. The absorption spectrum of a protein can be related to the superposition of the spectra of its chromophore groups. The most characteristic features have been found in the region 220–190 nm (5.64–6.53 eV), where the peptide or the amide chromophores absorb, and the range around 280 nm (4.43 eV), in which tyrosine and tryptophan absorption occur [114]. When aromatic amino acids are present, the energy region typical of peptide and amide absorption shows intense features corresponding to the higher states of the aromatic chromophores. Table XII compiles our theoretical and the experimental results

TABLE XII
 Theoretical and Experimental Energies (eV) and Oscillator Strengths (in parentheses)^a for the Most
 Representative Valence Singlet Excited States of the Aromatic Amino Acids^b and Their Chromophores

State	Benzene		Phenylalanine,		Phenol		Tyrosine,	
	Theory	Expt.	Expt.	Theory	Theory	Expt.	Theory	Expt.
¹ L _b	4.84 (forb.)	4.90 (—)	4.85 (0.01)	4.53 (0.007)	4.51 (0.02)	4.51 (0.02)	4.51 (0.02)	4.51 (0.02)
¹ L _a	6.30 (forb.)	6.20 (—)	6.00 (0.16)	5.80 (0.005)	5.77 (0.13)	5.77 (0.13)	5.70 (0.15)	5.70 (0.15)
¹ B _b	—	—	—	6.50 (0.68)	—	—	—	—
¹ B _a	7.02 (0.82)	6.94 (1.05)	6.60 (1.00)	6.56 (0.78)	6.60 (1.1)	6.60 (1.1)	6.46 (0.71)	6.46 (0.71)
	—	—	—	—	—	—	—	—
Indole								
Tryptophan,								
Theory		Expt.	Expt.	Theory ^c		Expt.		Histidine,
¹ L _b	4.43 (0.05)	4.37 (0.05)	4.31 (—)	6.32 (0.02)	6.0 (—)	6.0 (—)	5.7–6.3 (0.11)	5.7–6.3 (0.11)
¹ L _a	4.73 (0.08)	4.77 (0.12)	4.60 (0.10)	6.53 (0.28)	6.5 (—)	6.5 (—)	5.7–6.3 (0.11)	5.7–6.3 (0.11)
¹ B _b	5.84 (0.46)	6.02 (—)	5.69 (0.62)	7.48 (0.56)	>7.0 (—)	>7.0 (—)	>7.0 (—)	>7.0 (—)
¹ B _a	6.44 (0.26)	6.35 (—)	6.35 (0.38)	— (—)	— (—)	— (—)	— (—)	— (—)

^a Oscillator strength values in amino acids have been normalized to unity for the most intense band of phenylalanine. They are used only for comparison.

^b Amino acids experimental data in neutral aqueous phase from Refs. 113 and 114. See also Refs. 13, 115, and 116 and the text.

^c Theoretical CASPT2 energies include the solvent effects in imidazole.

for the aromatic amino acids and their chromophores. There is agreement between the theoretical (see Refs. 13, 46, 115, and 116) and experimental results on the molecules benzene, phenol, indole, and imidazole for energies and intensities. Experimentally, a general lowering of the energies can be observed in the amino acids, due to substitutions in the rings and solvent effects. All experimental data for the amino acids have been obtained in aqueous solutions. In some cases, increased intensities are observed due to symmetry breaking, for instance, in going from benzene to phenylalanine. The basic structure of the excited states, as discussed above, is, however, easy to observe: two low-lying weak 1L_b and 1L_a states, with the second usually more intense and more affected by the solvent environment, and two high-lying, more intense 1B_b and 1B_a states, actually overlapped in phenylalanine and tyrosine. Energies and intensities reflect the nature of the states and the configurational mixing observed in their wavefunction. The most important deviation from this scheme appears in imidazole and also in histidine. Here the solvent effects have been included in the theoretical results due to the importance of the environment for the energy of the low-lying states. The observed spectrum has only a single broad absorption band between 5.7 and 6.3 eV, while the next band appears at 7.0 eV [113, 114]. The theoretical results suggest the presence of both 1L_b and 1L_a bands in the 5.7–6.3 eV band envelope.

8. *Electronic Spectra of Radical Cations of Linear Conjugated Polyenes and Polycyclic Aromatic Hydrocarbons*

Linear conjugated polyenes (LCP) and polycyclic aromatic hydrocarbons (PAH) as well as their ions are key reactants in many chemical processes or can be identified as transient species. They have rich and broad electronic spectra, ranging from the ultraviolet to the visible and near-infrared [139, 140]. The electronic spectra of linear conjugated polyenes have served as tests for computational chemistry ever since the first semiempirical calculations were performed and have been discussed extensively in literature. However, it was not until recently that accurate, theoretical predictions of excited-state properties were attained by *ab initio* calculations [36, 141].

The principal experimental techniques to characterize the LCP radical cations have been photoelectron spectroscopy (PES) and electron absorption (EA) in matrices [142–150]. The production of radicals in matrices is a slow process and hence EA probes the electronic structure of the chromophore at the equilibrium geometry of the radical ion. In PES the chromophore has no time to relax. However, even ionization results in a remarkable attenuation of the bond-length alternation in comparison with

the neutral polyenes, the difference in the excitation energies derived from PES and EA are marginal.

Recently, Fülischer et al. [151] presented calculations on excited states in LCP radical cations using the CASSCF/CASPT2 method and ANO-S basis sets contracted as C, N[3s2p1d]/H[2s]. The geometries of the LCPs were optimized at the RHF/MP2 and ROHF/MP2 level of approximation, respectively, using 6-31G* basis sets. The calculated excitation energies shown in Table XIII were accurate to 0.2 eV or better. For the 2^2A_u state of octatetraene the shift upon going from the cation to the neutral geometry has been calculated to 0.16 eV, in agreement with the experimental value 0.2 eV [145].

The wavefunctions of the LCP radical cations are of rather simple structure and are dominated by single excitations. The two lowest π -excited states of equal symmetry are characterized by configuration mixing of two competing single excited configurations: HOMO – 1 \rightarrow HOMO and HOMO \rightarrow LUMO. Since the LCP radical cations are electron deficient, the wavefunctions are compact and well described by basis sets of modest size. Rydberg states do not appear in the low-energy part of the spectrum.

TABLE XIII
 π Excitation Energies of Linear Conjugated Polyene Radical Cations

State	Photoelectron Spectrum			Electron Absorption Spectrum		
	ΔE_{calc}^a	ΔE_{expt}^b	f_{calc}^c	ΔE_{calc}^a	ΔE_{expt}^b	f_{calc}^c
All- <i>trans</i> -1,3-butadiene						
1^2A_u	2.36	2.40	0.049	2.47	2.30	0.014
2^2A_u	4.56	—	0.644	4.23	4.20	0.651
All- <i>trans</i> -1,3,5-hexatriene						
1^2B_g	1.93	1.96	0.073	1.98	1.96	0.013
2^2B_g	3.59	—	0.910	3.37	3.30	1.001
2^2A_u	3.26	—	Forbidden	3.45	—	Forbidden
All- <i>trans</i> -1,3,5,7-octatetraene						
1^2A_u	1.63	1.67	0.116	1.66	1.67	0.0158
2^2A_u	3.04	3.00	1.238	2.86	2.77	1.370
2^2B_g	2.88	3.16	Forbidden	2.99	—	Forbidden
3^2A_u	3.72	—	0.001	3.88	—	0.001

^a Calculated excitation energy in eV using the CASSCF/CASPT2 method.

^b Experimental excitation energy in eV taken from Ref. 145 and references therein.

^c Calculated oscillator strength.

It is suspected that 0.2% of interstellar carbon may exist in the form of PAH radical cations and suggested that they may be possible carriers of the visible, diffuse interstellar absorption band (DIB), which extends from 4000 Å into the near IR [152]. Encouraged by the results on the LCP radical cations, Schütz et al. [153] undertook to calculate the electronic spectra of PAH radical cations starting with naphthalene [(6) in Fig. 3] and anthracene [(7) in Fig. 3].

The naphthalene cation has been studied by absorption spectroscopy in solutions [154, 155], glasses [156–159], and matrices [160]. Gas-phase data stem from PES [161, 162] and multiphoton dissociation [163, 164] spectra. Recently, the 180- to 900-nm absorption spectrum of naphthalene⁺ formed by photoionization in a neon matrix has been reinvestigated [165]. These experiments show seven progressions, with peak maxima at 1.84, 2.72, 3.29, 4.06, 4.49, 5.07, and 5.57 eV. The excitation energies calculated by Schütz et al. for the cation geometry are shown in Table XIV. They are in agreement with experiment. The largest deviation amounts to 0.13 eV (2^2B_{2g}). Table XIV also shows the predicted PES, which matches experiment.

Unfortunately, the experimental information for anthracene⁺ is not as rich as for naphthalene⁺. Transitions to the lowest π -excited state occur at 1.1 eV and are dipole forbidden. In addition, PES [161, 162] predicts transitions at 1.76, 2.73, and 2.81 eV. The EA spectrum [166] of anthracene⁺ recorded in argon matrices agrees with the absorption maxima in organic glasses [140], and the vibronic fine structure is in accord with the Raman spectrum of polycrystalline anthracene [167] at room temperature. The CASSCF/CASPT2 calculations presented by

TABLE XIV
 π -Excited States of the Naphthalene Radical Cation

State	Photoelectron Spectrum			Electron Absorption Spectrum		
	ΔE_{calc}^a	ΔE_{expt}^b	f_{calc}^c	ΔE_{calc}^a	ΔE_{expt}^d	f_{calc}^c
1^2B_{1u}	0.73	0.73	Forbidden	0.98	—	Forbidden
1^2B_{2g}	1.78	1.90	0.052	1.90	1.84	0.044
1^2B_{3g}	2.63	2.68	0.017	2.64	2.72	0.001
2^2B_{1u}	3.47	—	0.068	3.28	3.29	0.087
2^2B_{2g}	4.01	—	0.078	3.94	4.07	0.051
2^2B_{3g}	3.99	—	Forbidden	3.98	—	Forbidden

^a Calculated excitation energy in eV using the CASSCF/CASPT2 method.

^b Experimental excitation energy in eV from Ref. 161.

^c Calculated oscillator strength.

^d Experimental excitation energy in eV from Ref. 165.

TABLE XV
 π -Excited States of the Anthracene Radical Cation

State	Photoelectron Spectrum			Electron Absorption Spectrum		
	ΔE_{calc}^a	ΔE_{expt}^b	f_{calc}^c	ΔE_{calc}^a	ΔE_{expt}^d	f_{calc}^c
1^1B_{3g}	1.13	1.12	Forbidden	1.30	—	Forbidden
1^2A_u	1.48	1.76	0.084	1.56	1.72	0.079
1^2B_{1u}	2.16	—	0.002	2.03	2.19	0.010
2^2B_{2g}	2.56	2.73	Forbidden	2.66	—	Forbidden
2^2B_{1u}	2.66	2.81	0.070	2.75	2.89	0.063
2^2A_u	3.15	—	0.091	3.08	—	0.114
2^1B_{3g}	3.38	—	Forbidden	3.31	—	Forbidden

^a Calculated excitation energy in eV using the CASSCF/CASPT2 method.

^b Experimental excitation energy in eV from Ref. 161.

^c Calculated oscillator strength.

^d Experimental excitation energy in eV from Ref. 166.

Schütz et al. (cf. Table XV) agree with experimental data, although the deviations are somewhat larger than for naphthalene⁺.

As indicated by Schütz et al., the CASSCF/CASPT2 calculations on the larger PAH radical cations are at the limit of the current implementation of the method and available resources. Presently, it is not possible to compute the high-energy spectrum of large PAH radical cations, because of the demands on the size of the active space. On the other hand, these calculations illustrate that the CASSCF/CASPT2 method is capable of yielding reliable, quantitative results in areas not accessible to experiment, for example, molecules or molecular ions appearing in low concentrations in stellar atmospheres or in interstellar matter.

B. Electronic Spectroscopy for Transition Metal Compounds

The CASPT2 method has been applied successfully in a number of studies of properties of transition metal atoms and compounds containing one or two metal atoms. Most of these applications have dealt with ground-state properties, such as structure and binding energies [23, 28, 29, 168, 169], but a number of studies of electronic spectra and excited states have also been performed [22, 24, 32, 170, 171]. The first transition metal system for which the CASPT2 approach was applied was the nickel atom. The reason for the interest in this system was an earlier MRCI study, which had shown that it was necessary to include two sets of *d*-type orbitals (*3d* and *4d*) into the reference space for the SD-MRCI wavefunction in order to get accurate results for the splitting between the d^8s^2 , d^9s , and d^{10} states [172]. The CASPT2 study showed that it was indeed possible to obtain accurate relative energies, but only with an

active space comprising 14 orbitals ($3d$, $4d$, $4s$, and $4p$). The results were actually more accurate than those obtained in the earlier MRCI study. The $3d$ double-shell effect was clear: Adding a second $3d$ shell to the active space changes the $d^9s \rightarrow d^{10}$ excitation energy from 0.42 to 1.87 eV (the final result obtained by adding core–valence correlation corrections is 1.77 eV, only 0.03 eV from the experimental value). While it is gratifying that the CASPT2 method is able to compute this notoriously difficult energy difference, it is less satisfactory that such a large active space was needed. The study also pointed to the importance of including $3s$, $3p$ correlation terms. Their effect on the relative energies were on the order of 0.1 eV. As was well known from earlier studies, it is necessary to add an estimate of the relativistic effects by means of first-order perturbation theory.

Below we illustrate how the experience obtained in the nickel study has been transferred to the molecular case. It has been shown in studies of structure and bonding that the $3d$ double-shell effect is important when the number of $3d$ electrons changes. Thus the extra $3d$ shell plays a crucial role for the electronic structure in NiH and CuH, while bonding in transition metal dimers can be described without the second $3d$ shell [23, 168]. However, there is an important modification compared to the atomic case. It was found that a $4d$ orbital is needed only when the doubly occupied $3d$ orbital does not interact directly with ligand orbitals. If it does, it is necessary to have the corresponding ligand orbital active, and the addition of one more orbital does not affect the result. Instead, the active orbital describing the interaction with the ligand will acquire a certain amount of $4d$ character; how much depends on the covalency of the metal ligand bond. Thus one is led to an active space that will comprise 10 orbitals with up to 10 active electrons for all compounds involving a transition metal ion and closed-shell ligands. We shall see that such a binding model will work for many systems and will give an accurate description of the spectroscopy, provided that extra active orbitals are added in the case of charge transfer excitation to ligand orbitals not included in the 10-orbital space. It is actually the first consistent and quantitative model for the bonding in transition metal complexes that is capable of describing the ground-state structure, the metal ligand bond strength, and the spectroscopy simultaneously. The examples given in the following sections illustrate this. There are cases where the model does not work. They are characterized by the need for larger active spaces than the 14-orbital limit set by the present technology. The chromium dimer is an example of a system with a complex metal–metal bond. It is shown that the spectroscopy of this system can be well described within the present model and with an active space

comprising only the valence orbitals $3d$ and $4s$. The nickel and copper dimers have been treated successfully with a similar active space [168] and the same approach has been used for larger di-metal complexes such as cyclobutane–diazadivanadium [169] and dichromium–tetraformate [173].

1. *Special Considerations*

The accurate calculation of molecules containing transition metal atoms or ions requires some special considerations, which are absent (or at least less important) for the lighter elements in most organic molecules. First, care has to be taken in constructing the CASSCF reference wavefunction. For all but the smallest systems it is not possible simply to include all valence electrons into the active space; most often a careful choice of active electrons and orbitals has to be made, based on the knowledge of electronic structure properties. Given the wide variety of different bonding types that can be formed between a transition metal and its surroundings, this choice is not always obvious a priori, and different options may have to be considered. In this section we present an overview of some important near-degeneracy effects that have been encountered during our recent applications of the CASSCF/CASPT2 method in transition metal chemistry.

Another feature specific to the correlation problem in transition metals and their compounds concerns the role played by the $3s, 3p$ semicore electrons. It has been known for a long time [174] that the $3s, 3p$ orbitals in the first-row transition metal atoms cannot be considered truly core orbitals. The $3s, 3p$ core orbitals are confined to the same region of space as the $3d$ valence orbitals and their role in the correlation treatment can therefore not simply be ignored if accurate results are to be obtained. It has been shown [174] that $3s, 3p$ correlation thoroughly affects the energy separation between states, with a different number of $4s$ electrons in transition metal atoms, but more so for the elements at the left side of the series than for Ni and Cu, where its importance becomes small. In transition metal compounds, the importance of the $4s$ orbital decreases as the metal gets surrounded by more ligands, and the lowest electronic transitions most often occur between terms belonging to the same $3d$ configuration. A detailed investigation of the importance of $3s, 3p$ correlation for this type of transitions was performed in a recent CASSCF/CASPT2 study [171] of the lowest excited states in the transition metal ions Ti^{2+} – Ni^{2+} and V^{3+} – Cu^{3+} . It was shown in this systematic study that the core–core correlation contributions were as important as the core–valence contributions. Of special importance were double excitations from the $3p$ shell to the $3d$ shell. The total effect could amount to up to 0.5 eV for relative energies within a given $(3d)^n$

configuration. We refer to the original paper for details [171]. The role of $3s$, $3p$ correlation has been investigated further in all molecular applications presented in this review, including the charge-transfer transitions in $\text{Cr}(\text{CO})_6$ and $\text{Ni}(\text{CO})_4$ (Section III.B.2).

Up to now, applications of the CASSCF/CASPT2 method to transition metal systems have been confined to compounds containing transition metals belonging to the first transition series. Although relativistic effects are most certainly less important here than for the members of the second and third series, they can often not be ignored if accuracy is required. For example, it is well known that including the mass-velocity and Darwin terms from the Pauli equation has a profound effect (up to 0.35 eV) on the relative energy of the $3d^n 4s^2 - 3d^{n+1} 4s^1 - 3d^{n+2}$ states in the heaviest elements Ni–Cu, where they act to stabilize “ s -electron rich” configurations [175]. Since, on the other hand, correlation effects generally favor $3d$ over $4s$ occupation, both effects tend to cancel. Ignoring relativistic effects may, therefore, in combination with an incomplete treatment, easily lead to the right result for the wrong reasons. Relativistic effects are quite often also important for the bonding in transition metal compounds, where they may alter the shape of potential curves, bond distances, and binding energies. The only case where the Darwin and mass-velocity terms may safely be ignored is in the calculation of $3d \rightarrow 3d$ transitions in the spectra of transition metal compounds. However, in this case one may have to deal with the effect of spin-orbit coupling, at least in cases where different states have close-lying energies. In this section we present the results of a recent CASSCF/CASPT2 study on ScCl_2 , CrCl_2 , and NiCl_2 , which may be considered as a case study of relativistic effects in first-row transition metal compounds. Indeed, due to the simultaneous occurrence of a strong $3d$ – $4s$ mixing and a weak ligand field splitting of the M^{2+} ground state, both the mass-velocity and Darwin terms and spin-orbit coupling effects turned out to play a crucial role in the determination of the ground state and the relative energy of low-lying excited states in these systems.

Near-Degeneracy Effects and Choice of the Active Space. Although the emphasis of the present review is on spectroscopy, this section is concerned primarily with the ground state. Indeed, in most organic systems the HF configuration dominates the ground-state and near-degeneracy effects become important only for excited states. The same is no longer true when entering the field of transition metal chemistry. It is well known, for example, that ground-state properties of molecules such as $\text{Cr}(\text{CO})_6$ and ferrocene are hard to describe using single reference methods, due to the presence of large nondynamical correlation effects.

Thus the most elaborate study performed on $\text{Cr}(\text{CO})_6$ using the single-reference CCSD(T) method [176] still captured only 71% of the total binding energy.

One way to look at the problem of nondynamical correlation is to consider the occupation numbers of the natural orbitals resulting from a CASSCF calculation. Such a procedure is not foolproof of course, since it does not reveal any near-degeneracy effects that have not already been included in the CASSCF active space. Additional confirmation of the fact that the chosen active space is indeed adequate for the problem under consideration must therefore be obtained from the results of subsequent CASPT2 treatment, more specifically from the absence of any important intruder states in the final first-order wavefunction. Most of the molecules have been treated successfully with the CASPT2 method, using the active spaces presented in this section [28, 29, 170, 177, 178]. We will, however, also present two examples, CrF_6 and CrO_4^{2-} , for which the CASPT2 method turned out to be less successful, since all nondynamical correlation effects in these molecules could not be captured with an active space of at most 14 orbitals, the limit of the present CASPT2 code.

In Tables XVI and XVII we have collected the natural orbital occupation numbers from different CASSCF calculations on a selection of octahedral and tetrahedral molecules of first-row transition metals. In all cases a CASSCF calculation was performed using a "basic" active space of 10 orbitals. For some of the molecules additional calculations with larger active spaces (up to 14 orbitals) are also presented. Only ground-state results are presented, except for the molecules CrF_6^{3-} , $\text{Cr}(\text{CN})_6^{3-}$, CoF_6^{3-} , and $\text{Co}(\text{CN})_6^{3-}$, for which we have included a selected number of excited states.

For all octahedral molecules presented in Table XVI, the basic 10-orbital active space consists of the metal $3d$ orbitals, residing in the representations $t_{2g}(3d_\pi)$ and $e_g(3d_\sigma)$ as well as their bonding or antibonding counterparts within the same representations. All systems are characterized by a $t_{2g}(3d_\pi)^n$ ground state (where $n = 0, 3, 6$), with a formally empty antibonding $e_g(3d_\sigma)$ shell. Within the e_g representation, the corresponding bonding σ ligand orbitals were therefore included. Within t_{2g} , the included orbitals depend on the character of the ligand concerned: for the π -donor ligands F^- , H_2O , and NH_3 a doubly occupied ligand π shell was added, whereas for the π acceptors CN^- and CO , the included orbitals are the low-lying unoccupied π^* orbitals of t_{2g} symmetry.

For the Cr^{3+} and Co^{3+} compounds, the natural orbital occupation numbers in Table XVI reveal some clear trends, which can be related to the nature of the metal–ligand interaction. First we notice that for the π donors F^- , H_2O , and NH_3 , correlation effects within the t_{2g} representa-

TABLE XVI
 Natural Orbital Occupation Numbers Resulting from Different CASSCF Calculations on Some Representative Octahedral Transition Metal Compounds

Complex	Ligand			Metal 3d			Ligand π^*		
	State	Other	t_{2g}	e_g	t_{2g}	e_g	t_{2g}	e_g	Other
CrF_6^{3-}	$4A_{1g}$	—	5.988	3.998	3.002	0.012	—	—	—
	$4T_{2g}$	—	5.997	3.994	2.002	1.006	—	—	—
	$4A_{2g}$	—	5.998	3.987	3.002	0.013	—	—	—
	$4A_{2g}$	—	6.000	3.969	3.000	0.031	—	—	—
	$4A_{2g}$	—	—	3.947	2.971	0.053	0.029	—	—
CoF_6^{3-}	$4T_{2g}$	—	—	3.969	1.984	1.029	0.018	—	—
	$5T_{2g}$	—	6.000	3.998	4.001	2.001	—	—	—
	$1T_{1g}$	—	5.999	3.989	4.957	1.056	—	—	—
	$1A_{1g}$	—	6.000	3.982	5.901	0.118	—	—	—
	$1A_{1g}$	—	6.000	3.971	5.915	0.082	—	—	—
$\text{Co}(\text{H}_2\text{O})_6^{3+}$	$1A_{1g}$	—	6.000	3.936	5.923	0.096	—	—	—
	$1A_{1g}$	—	—	3.915	5.905	0.099	0.081	—	—
	$1T_{1g}$	—	—	3.939	4.936	1.006	0.059	—	—
	$5T_{2g}$	—	—	3.975	4.970	2.021	0.034	—	—
	$1A_{1g}$	—	—	3.958	5.763	0.049	0.230	—	—
$\text{Cr}(\text{CO})_6$	$1A_{1g}$	—	—	3.945	5.738	0.050	0.226	0.041(t_{1u})	—
	$1A_{1g}$	—	—	3.953	5.751	0.050	0.226	0.020(t_{2u})	—
	$1A_{1g}$	—	—	3.953	5.756	0.051	0.230	0.009(t_{1g})	—
	$1A_{1g}$	—	5.819	3.860	0.183	0.139	—	—	—
	$1A_{1g}$	5.861(t_{1g})	5.796	3.857	0.344	0.142	—	—	—
CrF_6	$1A_{1g}$	5.888(t_{1u})	5.825	3.862	0.214	0.211	—	—	—
	$1A_{1g}$	5.901(t_{2u})	5.803	3.862	0.297	0.137	—	—	—

TABLE XVII
 Natural Orbital Occupation Numbers Resulting from Different CASSCF Calculations on Some Representative Tetrahedral Transition Metal
 Compounds

Complex	State	Ligand				Metal 3d				Ligand π^*			
		a_1	t_1	t_2	e	t_2	e	t_2	e	t_2	e	t_2	e
Ni(CO) ₄	¹ A ₁	—	—	—	—	5.856	3.915	0.145	0.084	—	—	—	—
	¹ A ₁	—	—	—	—	5.855	3.915	0.143	0.084	—	—	—	0.004
Cr(NO) ₄	¹ A ₁	—	—	—	—	0.297	3.773	5.697	0.233	—	—	—	—
	¹ A ₁	—	—	—	—	0.349	3.579	5.264	0.290	—	—	—	0.519
CrF ₄	³ A ₂	—	—	5.896	3.984	0.106	2.013	—	—	—	—	—	—
	³ A ₂	1.988	5.990	5.896	3.984	0.124	2.020	—	—	—	—	—	—
CrO ₄ ²⁻	¹ A ₁	—	—	5.757	3.880	0.243	0.120	—	—	—	—	—	—
	¹ A ₁	1.943	5.885	5.727	3.879	0.360	0.205	—	—	—	—	—	—

tion are unimportant. For the Co^{3+} systems this is self-evident, since in this case both the bonding and antibonding t_{2g} shells are doubly occupied. Yet for Cr^{3+} also, with a half-occupied $t_{2g}(3d_{\pi})$ shell, the occupation numbers of the corresponding ligand orbitals are close to 2 in all cases. The same is not, however, true for the e_g σ lone-pair ligand orbitals. Here we find a strongly decreasing occupation number within the series $\text{F}^- > \text{H}_2\text{O} > \text{NH}_3$, or with a decreasing polarizability of the ligand. For the metals the trend is also clear: Except for CoF_6^{3-} in its ${}^5T_{2g}$ ground state, the Co^{3+} compounds are characterized systematically by a significant lower ligand e_g occupation number than the Cr^{3+} compounds.

The trends observed can also be connected to the covalency of the metal–ligand interaction. Indeed, although the subdivision in either metal or ligand orbitals in Table XVI is essentially correct, some mixing between both types of orbitals does occur in all cases. This mixing reflects the covalent contribution to the bonding—since no mixing would indicate a purely ionic interaction—and looking at the composition of the molecular orbitals, we notice that the mixing increases rather steeply within the series $\text{F}^- < \text{H}_2\text{O} < \text{NH}_3$ and $\text{Cr}^{3+} < \text{Co}^{3+}$. For example, at the RHF level, the ligand e_g orbitals contain a (derived from Mulliken gross populations) $3d$ contribution of 10.9% for CrF_6^{3-} , 12.7% for $\text{Cr}(\text{H}_2\text{O})_6^{3+}$, and 20.5% for $\text{Cr}(\text{NH}_3)_6^{3+}$. For the cobalt compounds the corresponding numbers are 11.4%, 16.3%, and 24.5%. However, it is also clear that the covalency of the bonding is not yet captured to its full extent by the RHF wavefunction. Indeed, as indicated by the natural orbital occupation numbers in Table XVI, the CASSCF wavefunctions contain a significant contribution from excitations out of the predominantly ligand e_g orbitals into the antibonding metal $e_g(3d_{\sigma})$ orbitals. These excitations go together with a transfer of charge density from the ligands into the metal, thus enforcing the covalency of the bonding. Furthermore, from the trends observed in the occupation numbers it is clear that the importance of this effect increases with the inherent covalency of the bonds. In other words, nondynamical correlation effects tend to become more important as the covalency of the metal–ligand bonds increases, while at the same time they serve to reinforce the covalency even further.

The cyanide compounds in Table XVI are no exception to this rule. On the contrary, of all Cr^{3+} and Co^{3+} complexes included, the cyanide complexes are definitely characterized by the most covalent bonds. In these complexes, σ donation from the carbon lone pairs into the formally empty $e_g(3d_{\sigma})$ orbitals is counteracted by π backdonation from the filled $t_{2g}(3d_{\pi})$ orbitals into the CN π^* orbitals. Both bonding types contain a

significant covalent contribution. It should therefore come as no surprise that nondynamical correlation effects are more important for the cyanide compounds than for the other π -donor Cr^{3+} and Co^{3+} complexes in Table XVI. Correlation effects now serve to increase both σ donation and π backdonation. The effect is again largest for the cobalt complex, with 0.085 additional electron transferred from the carbon lone pair into the $3d_{\sigma}$ orbitals and 0.081 electron from $3d_{\pi}$ into the CN π^* orbitals.

The Cr^{3+} and Co^{3+} compounds in Table XVI belong to a group usually referred to as Werner complexes. They constitute a group of complexes treated by spectroscopy [179] and photochemistry [180] with considerable success in the 1970s and the beginning of the 1980s by means of simple semiempirical ligand field models, based on an ionic view of the metal–ligand interaction. The success of these models can be traced back to the fact that the bonding in these systems is indeed primarily ionic. Yet even within the framework of ligand field theory, the presence of covalent effects could not be ignored. They were included into the model by means of the *nephelauxetic effect* [181]. The term *nephelauxetic* is based on the Greek term “cloud expansion,” which indicates its meaning. It was found that the interelectronic repulsion within the metal $3d$ shell (usually expressed in terms of the Racah parameters A, B, C) is reduced significantly in a transition metal complex compared to the free metal ion, as a result of delocalization of the metal $3d$ electrons into the ligand orbitals, and vice versa. The extent of the reduction is dependent both on the nature of the ligands and of the metal, and from a comparison of the ligand field spectra of an extended range of complexes two nephelauxetic series were constructed, classifying either the ligands or the metal ions with respect to their tendency to form covalent bonds. Interestingly, the sequence of covalency/nondynamical correlation found for the metals and ligands included in this study corresponds exactly to their position in the nephelauxetic series [179]: $\text{F}^- > \text{H}_2\text{O} > \text{NH}_3 > \text{CN}^-$ and $\text{Cr}^{3+} > \text{Co}^{3+}$. It is tempting to assume that this correspondence can be extrapolated to the entire range of metals and ligands included in these series and that the nephelauxetic series could actually be used to predict the extent of nondynamical correlation effects to be expected for a specific metal–ligand combination. A more definite confirmation of this surmise can be given only after a larger variety of metals and ligands have been studied.

Carbonyl does not appear in the nephelauxetic series. Indeed, organometallic compounds fall outside the scope of ligand field theory, due to the fact that these systems are usually characterized by stronger covalent bonds than those of the Werner complexes. Yet CO is closely related to CN^- . As CN^- it is a σ donor and a π acceptor, although the

relative importance of both contributions to bond formation is different for both ligands, CN^- being the stronger σ donor and CO the stronger π acceptor. This is also reflected by the natural orbital occupation numbers in Table XVI. Looking at the isoelectronic $\text{Co}(\text{CN})_6^{3-}$ and $\text{Cr}(\text{CO})_6$ molecules, we notice that both the e_g carbon lone pair and the t_{2g} π^* population are significantly higher in $\text{Cr}(\text{CO})_6$ than in $\text{Co}(\text{CN})_6^{3-}$. The most covalent bonding mechanism creates the largest correlation effect also in this case. For $\text{Cr}(\text{CO})_6$ we have included in Table XVI the results from a number of additional CASSCF calculations performed with an active space of 13 orbitals, obtained by extending the original 10-orbital active space with one additional CO π^* shell of different symmetries. The occupation numbers obtained from these calculations clearly confirm the fact that the orbitals that are actually allowed to mix with the metal $3d$ orbitals are by far the most important in the correlation treatment. The occupation numbers of the t_{1u} , t_{2u} , and t_{1g} CO π^* shells all turn out to be manifestly smaller than the t_{2g} occupation number.

We now turn to Table XVII for a comparison of $\text{Ni}(\text{CO})_4$ with $\text{Cr}(\text{CO})_6$. Since $\text{Ni}(\text{CO})_4$ is a formal d^{10} system, CO-to-Ni σ donation is unimportant. The carbon lone pairs were therefore omitted from the $\text{Ni}(\text{CO})_4$ basic 10-orbital active space. Instead, a virtual e and t_2 shell were included, since the CO π^* orbitals now end up in the representations e , t_1 , and t_2 , of which both e and t_2 are allowed to mix with the $3d$ orbitals. However, although the correlating e and t_2 orbitals are designated as CO π^* orbitals in Table XVII, they in fact turn out to contain a considerable amount of Ni $4d$ character. This observation reflects the importance of the $3d$ double-shell effect in transition metals containing a large number of d electrons. It has already been illustrated that the introduction of a second d shell has a major impact on the accuracy of the computed CASPT2 excitation energies in the Ni atom [32] and on the quality of the description of the bonding in the NiH and CuH molecules [168]. Here we find that the second d shell is actually at least as important as the CO π^* orbitals for the electron correlation in $\text{Ni}(\text{CO})_4$. To illustrate this point further, we have plotted the difference of the total density between the CASSCF and the SCF wavefunction for $\text{Ni}(\text{CO})_4$ compared to $\text{Cr}(\text{CO})_6$ (cf. Fig. 6). For $\text{Cr}(\text{CO})_6$ this plot nicely illustrates the effect of correlation on the bonding, with an increased σ donation and π backdonation in the CASSCF treatment compared to SCF (although some $3d$ - $4d$ correlation can also be spotted). On the other hand, the $\text{Ni}(\text{CO})_4$ plot clearly shows the combined effect of radial extension of the $3d$ electrons in the CASSCF treatment and the correlation effects connected with the Ni-CO bonding.

The present results obtained for $\text{Cr}(\text{CO})_6$ and $\text{Ni}(\text{CO})_4$ are a clear

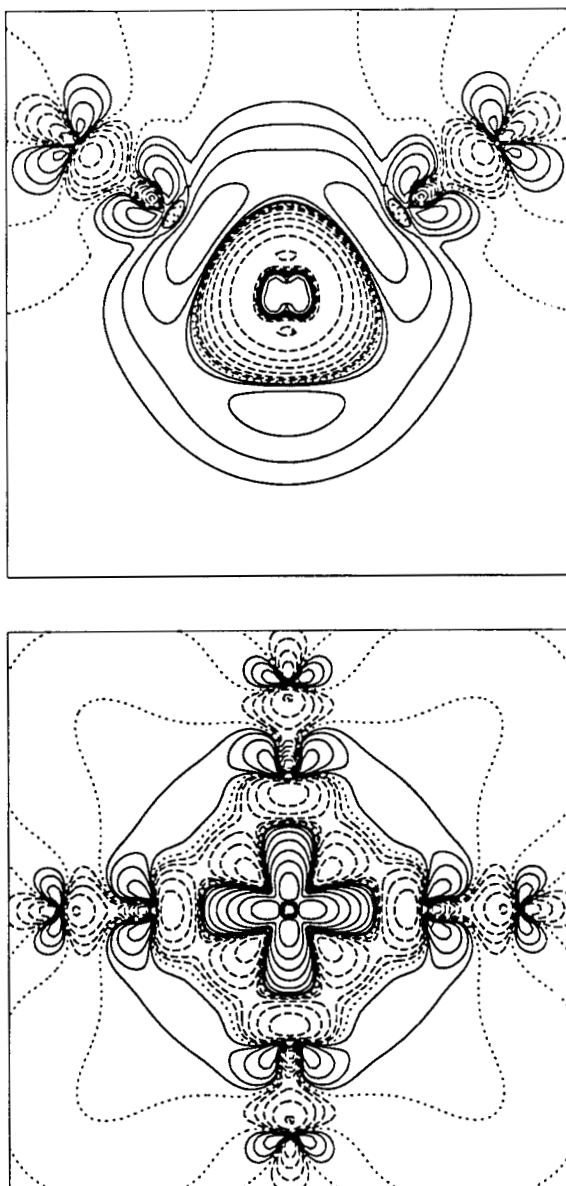


Figure 6. Total density difference plot between the CAS(10/10) wavefunction and the Hartree–Fock wavefunction for $\text{Ni}(\text{CO})_4$ (upper part) and $\text{Cr}(\text{CO})_6$ (lower part). The figure describes the density shifts in a plane containing the central nickel and two CO ligands. Full contours correspond to an increase in electron density and dashed contours to a decrease. At the dotted lines $\Delta\rho = 0$. The values of the $\Delta\rho$ contours are ± 0.00025 , ± 0.0005 , ± 0.001 , ± 0.002 , ± 0.004 , ± 0.008 , ± 0.016 , ± 0.032 , and 0.0 a.u.

indication of the difficulty in treating organometallic compounds with single-reference methods. The presence of strong nondynamical correlation effects in these systems, both the $3d$ double-shell effect and correlation effects on the bonding, severely limits the accuracy of any calculation that does not include these effects from the start. The CASPT2 method has therefore turned out to be more than a feasible alternative for the description of the bonding in these systems. Starting from the 10-orbital active space described here, a CASPT2 treatment of the bonding in $\text{Ni}(\text{CO})_4$ and $\text{Cr}(\text{CO})_6$ [29] has produced results which are far more accurate than the results obtained up to now with any single-reference method. Furthermore, this is also the case for the molecules $\text{Ni}(\text{C}_2\text{H}_4)$ [28], $\text{Ni}(\text{CO})_x$ ($x = 1-3$) [29], $\text{Fe}(\text{CO})_5$ [29], and ferrocene [28], which have not been included here. In all cases, an active space of only 10 orbitals proved to be large enough as a starting point for the CASPT2 treatment. An active space of this size is perfectly manageable for the present CASPT2 code, leading to CPU times that are smaller (less than 1 CPU hour on an IBM RS6000/580) than can possibly be expected from a single-reference configuration interaction or coupled-cluster calculation, considering the large number of electrons [up to 74 for $\text{Cr}(\text{CO})_6$] included in the correlation treatment.

One may therefore ask if CASPT2 has conquered the problems in the difficult field of *ab initio* transition metal chemistry. The answer to this question critically depends on whether or not the 10-orbital-active-space rule observed here turns out to be applicable to all transition metal systems in general. Unfortunately, this is not the case. A few recent CASPT2 studies have indicated that in some special cases it is unavoidable to extend the active space with ligand valence orbitals that are of different symmetries than those of the metal $3d$ orbitals. All cases met up to now have one thing in common: They concern systems that no longer fit nicely into the picture of a transition metal complex being built from the interaction between a metal ion with an incomplete $3d$ shell, on the one hand, and a number of ligands with closed shells, on the other hand. A notorious example is $\text{Cr}(\text{NO})_4$. $\text{Cr}(\text{NO})_4$ is isoelectronic with $\text{Ni}(\text{CO})_4$, and both molecules have an identical ground-state electronic configuration. Yet, trying to fit the bonding pattern in $\text{Cr}(\text{NO})_4$ into the picture of $\text{Ni}(\text{CO})_4$, one ends up with a formal $d^{10} \text{Cr}^{4-}$ ion and four NO^+ ligands. Such a picture is obviously unrealistic, and the natural orbital occupation numbers in Table XVII nicely illustrate this fact. First we have to remark that while subdivision of the molecular orbitals into either ligand or metal orbitals is essentially correct for all other systems in Tables XVI and XVII, it has become completely blurred in case of $\text{Cr}(\text{NO})_4$. The orbitals designated as metal $3d$ in fact each contain only

54% Cr $3d$ character, while we find 37% and 40% $3d$ character in NO π^* orbitals of t_2 and e symmetry, respectively. This already indicates that the bonding in $\text{Cr}(\text{NO})_4$ is purely covalent and should better be viewed as being built from neutral Cr and four NO radicals. Furthermore, looking at the occupation numbers of the natural orbitals resulting from the 10-orbital CASSCF calculation, we notice that the t_2 orbitals with predominant $3d$ character have now become the weakly occupied orbitals, with a population of only 0.297 electron, while most electrons, 5.697, are found in the predominantly NO π^* orbitals. However, it is clear that the remaining NO π^* shell of t_1 symmetry can in this case most certainly not be ignored in the CASSCF treatment. Adding it to the active space gives it an occupation number of as much as 0.519 electron. A CASSCF treatment of $\text{Cr}(\text{NO})_4$ with only 10 active orbitals, as presented recently by Bagus and Nelin [182], simply does not catch all important electronic structure features of this molecule.

In fact, the importance of the $t_1 \pi^*$ shell in $\text{Cr}(\text{NO})_4$ was noted several years ago by Bauschlicher and Siegbahn [183], who called its contribution to the bonding a purely ionic contribution. Although this definition may seem spurious at first in view of the present considerations, it becomes clear if one realizes that the presence of 0.519 electron in the t_1 shell is indeed the result of a purely ionic charge transfer between orbitals which are, for symmetry reasons, not allowed any covalent interaction. An important consequence of this fact is also that any calculation on $\text{Cr}(\text{NO})_4$ using single-reference methods is doomed to fail. Indeed, where an SCF treatment at least partially describes the covalency of the bonding within the t_2 and e representations through mixing at the orbital level, it does not even begin to capture the ionic component of the bonding associated with the t_1 shell. The same remark holds for any multireference treatment with a limited reference space. However, in a recent CASSCF/CASPT2 study [178] on the series $\text{Ni}(\text{CO})_4$, $\text{Co}(\text{CO})_3(\text{NO})$, $\text{Fe}(\text{CO})_2(\text{NO})_2$, $\text{Mn}(\text{CO})(\text{NO})_3$, $\text{Cr}(\text{NO})_4$, we have shown that results of similar accuracy can be obtained for all these molecules, on the condition that the size of the CASSCF active space is gradually increased from 10 to 13 within the series. Although the calculations with 13 active orbitals were, of course, more demanding in terms of computer time (with a maximum of 4 CPU hours), the CASSCF/CASPT2 method also turned out to be successful for $\text{Cr}(\text{NO})_4$, with no further important intruder states appearing in the first-order wavefunction.

However, for two other molecules, CrF_6 and CrO_4^{2-} , the CASSCF/CASPT2 method turned out to be less successful. Textbooks on inorganic chemistry usually give the central chromium in CrO_4^{2-} an oxidation

number (+6), thus describing the molecule as consisting of d^0 Cr^{6+} and four O^{2-} closed-shell ligands. The same reasoning describes CrF_6 as d^0 Cr^{6+} + six F^- . However, this simple picture is, of course, again far from realistic. The results of a Mulliken population analysis point instead to a charge of only +1.7 in CrO_4^{2-} and 1.6 in CrF_6 . Again, this charge reduction is the result of a considerable covalent mixing between the metal $3d$ and ligand $2p$ orbitals as well as from an additional charge transfer from the ligands to the metal at the CASSCF level. However, although the observed charge reorganizations are significantly less severe than for $\text{Cr}(\text{NO})_4$, they are no longer constrained to a limited set of orbitals. This is again illustrated by Tables XVI and XVII, where we have included the results of several CASSCF calculations for both molecules, in which the basic 10-orbital active space was extended with different sets of ligand $2p$ orbitals. As one can see, the additional orbitals do not have occupation numbers close to 2. For comparison, we have also added CrF_4 to Table XVII. As opposed to CrO_4^{2-} , CrF_4 is still a 10-orbital-active-space molecule, even with a formal charge of (+4) on Cr. However, the results obtained for CrF_6 and CrO_4^{2-} indicate that an accurate CASPT2 calculation on these molecules would have to be based on an active space including the Cr $3d$ as well as all ligand $2p$ orbitals, resulting in 17 orbitals for CrO_4^{2-} and 23 orbitals for CrF_6 . Both calculations are obviously impossible at this moment. CASSCF/CASPT2 calculations using smaller active spaces have been tried on both molecules. For CrF_6 , calculation of the barrier for pseudorotation to a trigonal prism using a 10-orbital active space [184] resulted in a barrier height more than twice as high than the result obtained from both a CCSD(T) [185] and DFT study [186] and which should probably be considered as less reliable. On the other hand, calculation of the spectrum of CrO_4^{2-} completely failed, even with 14 active orbitals, due to the appearance of severe intruder states even for the lowest excited states [187].

We end this section with some considerations on spectroscopy. To do so, we return to the Werner systems discussed earlier, in particular to the fluoride and cyanide compounds, for which we have included in Table XVI the results of a few excited states. The excited states were chosen such that each corresponds to a configuration with a different $e_g(3d_\sigma)$ occupation number. Although the different ligand field states are subject to the same type of nondynamical correlation effects, we notice that in some cases the occupation numbers of the ligand orbitals are significantly different for different states. This is especially true for the cyanide complexes, for which correlation effects actually tend to lose importance with each electron transferred from the $t_{2g}(3d_\pi)$ into the $e_g(3d_\sigma)$ orbitals. The ligand field spectrum of these systems was described successfully in a

recent CASSCF/CASPT2 study [170], using an active space of 10 orbitals. In Section III.B.2 we present the results obtained for $\text{Co}(\text{CN})_6^{3-}$ and for the isoelectronic $\text{Fe}(\text{CN})_6^{4-}$ and $\text{Cr}(\text{CO})_6$ systems. The fluoride molecule CrF_6^{3-} is the most ionic system considered, with few or no nondynamical correlation effects on the bonding. A quantitative description of the spectrum of this ion has been obtained in a CASSCF/ACPF study based on an active space containing only the five $3d$ orbitals [188, 189]. The same is true for CrF_6^{2-} and CrF_6^{4-} , the spectra of which have been the subject of a recent CASPT2 study [190]. On the other hand, for the slightly more covalent CoF_6^{3-} it was shown [191] that a significant improvement in transition energies could be obtained by extending the active space with the ligand e_g orbitals.

When considering organometallic systems, a calculation of the charge transfer states may become more of interest. Obviously, an extension of the basic 10-orbital active space can in this case most often not be avoided, since the charge transfer states included in this active space may not be the ones of interest. For example, the active space of 10 orbitals used for the calculation of the ground state of $\text{Cr}(\text{CO})_6$ only includes the $\text{CO } \pi^*$ orbitals of t_{2g} symmetry, while the lowest charge transfer bands in its spectrum are due to transitions to the $\text{CO } \pi^* t_{1u}$ and t_{2u} shells. On the other hand, adding both the t_{1u} and the t_{2u} shells on top of the basic 10 orbitals would result in an active space of 16 orbitals, which is too large. In calculating charge transfer spectra, one may therefore have to compromise by using different active spaces for different excited states. This does not present any serious drawback, as long as there are no strong interactions between excited states treated with different active spaces. CASSCF/CASPT2 calculations on the charge transfer spectra of $\text{Cr}(\text{CO})_6$, $\text{Fe}(\text{CO})_5$, and $\text{Ni}(\text{CO})_4$ have recently been performed with considerable success [29, 177]. The results obtained for $\text{Cr}(\text{CO})_6$ and $\text{Ni}(\text{CO})_4$ are presented in Section III.B.2. More details concerning the active spaces used are given there.

Relativistic Effects: ScCl_2 , CrCl_2 , and NiCl_2 . A nice illustration of the importance of core correlation and relativistic effects to the bonding properties of first-row transition metal compounds was found in a recent systematic CASPT2 study of transition dihalides MF_2 and MCl_2 ($\text{M} = \text{Sc} - \text{Zn}$). Here we review some important results obtained for ScCl_2 , CrCl_2 , and NiCl_2 . The calculations were performed using different active spaces, depending on the metal. Thus for SrCl_2 and CrCl_2 , only the five $3d$ orbitals were included, while for NiCl_2 the σ_g and π_g chlorine valence orbitals and a second d shell were added to account both for the increased covalency of the metal-chlorine bonds and the $3d$ double-shell

effect, thus obtaining 13 active orbitals. Two sets of CASPT2 calculations were performed, one set including all valence electrons ($M\ 3d$, $Cl\ 3s$, $3p$) and a second set including in addition also the metal $3s$, $3p$ electrons. Relativistic effects were taken into account by including the mass-velocity and Darwin terms using first-order perturbation theory at the CASSCF level. Furthermore, the effect of spin-orbit coupling was estimated using an effective one-electron spin-orbital coupling operator, together with a scaling of the metal charge to an effective value that reproduces the spectroscopically observed atomic levels [192].

Fairly large ANO type basis sets were used in this study: $(17s12p9d4f)/[7s6p4d2f]$ for the metal [41] and $(17s12p5d4f)/[6s5p2d1f]$ for chlorine [40]. Even with these basis sets, basis-set superposition errors on the M–Cl bond distances are significant. They were examined in detail for $MnCl_2$ by means of the full counterpoise method. For the valence-only calculations, a correction of $0.005\ \text{\AA}$ was found, due exclusively to the incompleteness of the chlorine basis set. Including the $3s$, $3p$ electrons increases the metal contribution, but not too drastically. A total correction of $0.010\ \text{\AA}$ was now obtained. It was assumed that these results can be extrapolated to the entire series of MCl_2 compounds, and they have been included in all results reported here.

Transition metal dihalides are generally characterized by a weak ligand field splitting of the free M^{2+} ground state. In a $D_{\infty h}$ point group, the $3d$ shell is split into δ_g , π_g , and σ_g orbitals. Simple ligand field arguments indicate the d -orbital energy level sequence $\delta_g < \pi_g < \sigma_g$. This would then give $ScCl_2$ a ${}^2\Delta_g(\delta_g^1)$ and $CrCl_2$ a ${}^5\Sigma_g^+(\delta_g^2\pi_g^2)$ ground state, while for $NiCl_2$ a ${}^3\Pi_g(\delta_g^4\pi_g^3\sigma_g^1)$ ground state should be obtained. However, the results from our CASPT2 study suggest that none of these states in fact correspond to the actual ground state in the molecules considered. In Table XVIII we have collected the results of a CASPT2 geometry optimization of all possible molecular states originating from the ground state in the free M^{2+} ion. In all three molecules, the ground state as predicted from ligand field theory actually shows up as the first excited state, although in the case of $CrCl_2$ the energy difference with the calculated ${}^5\Pi_g$ ground state is small and becomes positive only when both $3s$, $3p$ correlation and relativistic effects are taken into account. Obviously, qualitative ligand field arguments are unable to capture the actual bonding situation in these molecules. In $ScCl_2$, the single d electron clearly prefers the σ_g orbital (which is supposed to be highest in energy) over δ_g and π_g , and also in the other two systems there is a slight preference for σ_g over π_g . This preference for occupying the σ_g orbital can easily be understood when considering the shape of this orbital,

TABLE XVIII
 Ligand Field Splitting of the $\text{Sc}^{2+} \ ^2D$ Ground State, the $\text{Cr}^{2+} \ ^5D$ Ground State, and the $\text{Ni}^{2+} \ ^3F$ Ground State in the Corresponding Dichlorides

	Only Valence Electrons Correlated						Also Metal 3s, 3p Correlated			
	Nonrelativistic			Relativistic ^a			Nonrelativistic		Relativistic ^a	
	Main Conf.	R_e (Å)	T_e (cm ⁻¹)	R_e (Å)	T_e (cm ⁻¹)	R_e (Å)	T_e (cm ⁻¹)	R_e (Å)	T_e (cm ⁻¹)	
ScCl_2	$^2\Sigma_g^+$	2.324	0	2.318	0	2.297	0	2.292	0	
	$^2\Delta_g$	2.404	336	2.401	1126	2.371	1905	2.367	2710	
	$^2\Pi_g$	2.434	6159	2.431	7023	2.402	8170	2.400	9055	
	$^3\Pi_g$	2.205	0	2.198	0	2.183	0	2.175	0	
CrCl_2	$^5\Sigma_g^+$	2.244	-634	2.240	-247	2.230	-11	2.226	408	
	$^5\Delta_g$	2.233	4883	2.224	4875	2.215	5066	2.206	5062	
	$^3\Sigma_g^-$	2.075	0	2.060	0	2.069	0	2.055	0	
	$^3\Pi_g$	2.087	800	2.077	1048	2.091	679	2.080	960	
NiCl_2	$^3\Phi_g$	2.091	3187	2.076	3076	2.086	2713	2.072	2605	
	$^3\Delta_g$	2.122	3130	2.111	3535	2.118	3760	2.108	4177	

^a Including the Darwin and mass-velocity terms from the Pauli equation.

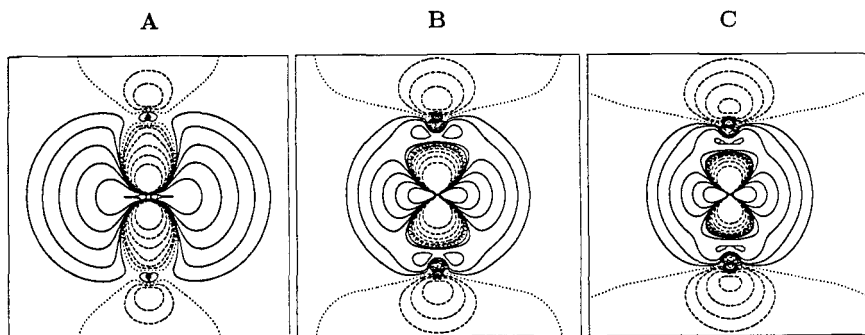


Figure 7. The $9\sigma_g^+$ orbital in ScCl_2 (A), CrCl_2 (B), and NiCl_2 (C). The figure shows the orbitals in a plane containing the central metal and the two chlorine atoms. Values of the contours are ± 0.128 , ± 0.064 , ± 0.032 , ± 0.016 , ± 0.008 , ± 0.004 , and 0.0 a.u.

shown in Fig. 7. These plots clearly indicate a large $3d_\sigma$ - $4s$ mixing in the σ_g orbitals, which serves to construct a $3d$ - $4s$ hybrid in such a way that the maximum density is located in the plane perpendicular to the metal-chlorine bonds, thus minimizing the exchange repulsion with the Cl^- σ electron pair. The mixing is extreme in ScCl_2 and decreases strongly when going to CrCl_2 and further to NiCl_2 .

Apart from leading to a breakdown of the ligand field model, the strong $3d$ - $4s$ mixing in the σ_g orbitals also induces a relativistic contribution to the relative energies of the low-lying states in Table XVIII. Looking at the configurations corresponding to the various states, we notice that in all cases the introduction of Darwin and mass-velocity terms leads to a stabilization of configurations with the highest σ_g occupation number. The effect is small but definitely present. It is largest for ScCl_2 , about 800 cm^{-1} , and decreases when going to CrCl_2 and NiCl_2 , in harmony with the fact that the $4s$ contribution to the σ_g orbital decreases in the same order. Notice also that in CrCl_2 the relativistic contribution to the energy of the transition between the $^5\Pi_g$ and $^5\Delta_g$ states is negligibly small. Both are characterized by the same σ_g occupation number, and the transition between them corresponds to a $\delta_g \rightarrow \pi_g$ transition. This is a confirmation of the fact that relativistic effects are negligible for "pure" $3d$ - $3d$ transitions.

Table XVIII also includes the effect of correlation of the semicore $3s$, $3p$ electrons on the transition energies. As one can see, the effect is substantial, especially for ScCl_2 , where it increases the energy difference between the different states with up to 2000 cm^{-1} . A significantly smaller effect is found for CrCl_2 and NiCl_2 .

Both $3s$, $3p$ correlation and relativistic effects also affect the value of the bond distances in Table XVIII. These distances were obtained from

an individual optimization at the different computational levels. Bond-angle deformations were also considered, and in fact the ${}^5\Pi_g$ state in CrCl_2 was found to be slightly bent, with a Cl–Cr–Cl angle varying between 155 and 165° for the various levels of approximation. For simplicity, the $D_{\infty h}$ notation has been maintained for this state. The effect of 3s, 3p correlation is again largest for ScCl_2 , where it results in a shortening of the bond lengths by around 0.03 Å for all states. Smaller effects are found for CrCl_2 , while for NiCl_2 the effect is almost absent. On the other hand, relativistic corrections to the bond distances are clearly largest for NiCl_2 while almost absent for ScCl_2 .

On the whole it is clear that the combined effect of 3s, 3p correlation and relativistic (mass-velocity and Darwin) corrections has important consequences for both the structure and the relative energy of the low-lying states in the considered molecules. Up to this point the effects of spin-orbit coupling have not yet been considered. However, for both CrCl_2 and NiCl_2 substantial effects can be expected, since in both molecules the first excited state is close in energy to the ground state but is characterized by a different M–Cl bond distance. For example, looking at CrCl_2 we notice that the final bond distances obtained for the ${}^5\Sigma_g^+$ and ${}^5\Pi_g$ states differ by as much as 0.051 Å, while the energy difference between them is only 408 cm^{-1} . It is clear that the actual ground state in this molecule is a mixture of both states, with a flexible structure. The Cr–Cl bond distance in CrCl_2 reported from a gas-phase electron diffraction study [193] is 2.207 Å, in between the values calculated for the two states. In fact, the same study reports CrCl_2 as a highly bent molecule, which is not reproduced by our calculations. However, determination of the CrCl_2 structure was greatly hindered by the presence of dimeric species in the sample. This may explain the discrepancy between the experimental and calculated bond angles.

The effect of spin-orbit coupling was considered in more detail for NiCl_2 . Using the final CASPT2 energies (with 3s, 3p correlation and including the Darwin and mass-velocity terms) as the diagonal elements of the spin-orbit coupling matrix, the resulting Σ_g^+ ground state was found to be composed of 76% ${}^3\Sigma_g^-$ and 24% ${}^3\Pi_g$ configurations. A reoptimization of the Ni–Cl bond distance for this state resulted in a value of 2.062 Å, 0.007 Å longer than the result obtained for the pure ${}^3\Sigma_g^-$ state, and 0.014 Å shorter than the experimental Ni–Cl bond distance of 2.076 Å [194]. The latter agrees with the results obtained for all other MCl_2 systems studied in Ref. 195. It was found that CASPT2 systematically underestimates the M–Cl bond distance in these systems, by 0.01–0.02 Å.

Using the optimized distance for the Σ_g^+ ground state, a calculation of

the spectrum of NiCl_2 was performed, both with and without spin-orbit coupling. $3s$, $3p$ correlation and the Darwin and mass-velocity terms were included in both sets of calculations. The calculations now included all states corresponding to the four lowest 3F , 1D , 3P , and 1G states in Ni^{2+} . The results are shown in Fig. 8. The calculated spectrum with spin-orbit coupling is in agreement with the experimental absorption spectrum of NiCl_2 [196]. In the region $0\text{--}7000\text{ cm}^{-1}$, a broad and complex absorption band is found, corresponding to the series of closely spaced levels originating from the $\text{Ni}^{2+} {}^3F$ ground state. The $\text{Ni}^{2+} {}^3P$ state is split into ${}^3\Pi_g$ and ${}^3\Sigma_g^-$, calculated without spin-orbit coupling at $11,589\text{ cm}^{-1}$ and $21,845\text{ cm}^{-1}$, respectively. The highest ${}^3\Sigma_g^-$ state is clearly unaffected by spin-orbit coupling. This is confirmed by the experimental spectrum, containing a single band at $21,180\text{ cm}^{-1}$. On the other hand, the lowest ${}^3\Pi_g$ state is surrounded by two singlet states, ${}^1\Delta_g$ and ${}^1\Pi_g$. Spin-orbit coupling therefore results in a series of states with considerable ${}^3\Pi_g$ character, calculated between $10,667$ and $13,316\text{ cm}^{-1}$, in perfect agreement with the appearance of a series of sharp bands in the region $11,000\text{--}14,000\text{ cm}^{-1}$ of the experimental spectrum. Furthermore, low-intensity absorption bands occur in the region $14,000\text{--}19,000\text{ cm}^{-1}$ of the experimental spectrum, agreeing with the fact that all states calculated in this region have predominantly singlet character.

As a conclusion, accurate results are obtained with the CASSCF/CASPT2 method for the metal dichlorides. However, this accuracy can be achieved only with a full correlation treatment, including all valence electrons and the metal semicore $3s$, $3p$ electrons. Relativistic effects can also become quite important in some cases and should therefore be included if accuracy is required.

2. Transition Metal Complexes with Cyanide and Carbonyl Ligands

The accurate calculation of excited states and electronic spectra of organometallic systems still remains a major challenge to *ab initio* methods. The simultaneous occurrence of important nondynamical correlation effects and a large number of electrons make these systems virtually impossible to handle with configuration-interaction or coupled-cluster methods unless severe restrictions are imposed on either the size of the reference space or the number of electrons actually included in the correlation treatment. Even if these restrictions are calibrated carefully, it is most often impossible to avoid a substantial loss of accuracy. The fact that the CASSCF/CASPT2 method does not suffer from these restrictions a priori makes it a promising alternative for the calculation of electronic spectra of organometallics and other large transition metal

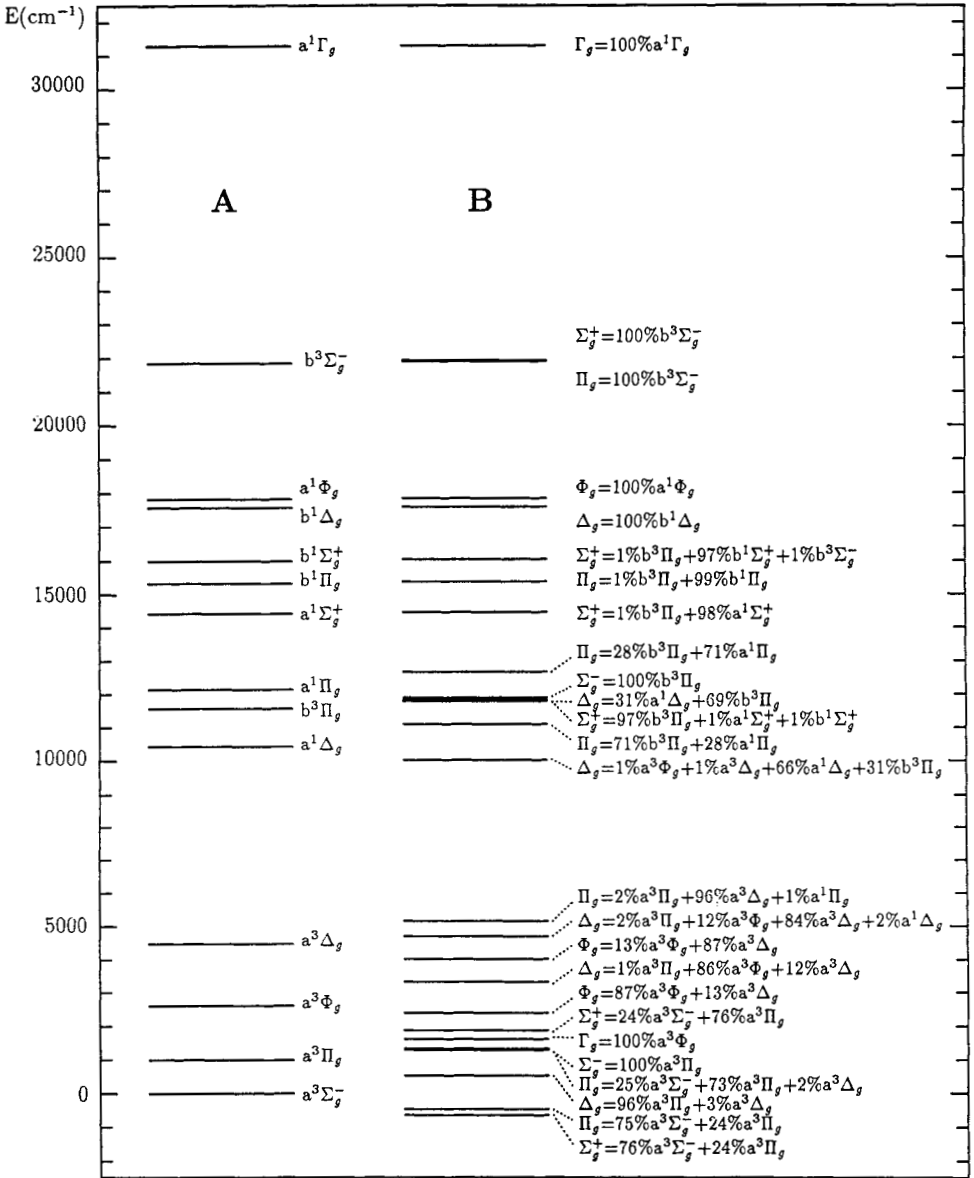


Figure 8. Spectrum of NiCl_2 , calculated without (A) and with (B) spin-orbit coupling.

systems, provided that an appropriate reference active space can be constructed, including all near-degeneracy effects as well as the excited states of interest.

The first application of the CASSCF/CASPT2 method to the spectra of large transition metal systems concerned a systematic study of the ligand field spectra of $M(\text{CN})_6^{n-}$ systems, where $M = \text{V}, \text{Cr}, \text{Mn}, \text{Fe}$, and Co and $n = 3$ or 4 [170]. It was found there that a balanced description of the ground state and all excited ligand field states could be obtained with an active space of 10 orbitals, consisting of the bonding and antibonding combinations of the metal $3d$ and the cyanide σ and π^* valence orbitals (see also Section III.B.1). With this reference space, all calculated CASPT2 transition energies were in excellent agreement with the experimental data available, with errors in the range 0.0–0.35 eV. More recently, the method was applied in a study of the ground-state properties and the electronic spectra of $\text{Cr}(\text{CO})_6$, $\text{Fe}(\text{CO})_5$, and $\text{Ni}(\text{CO})_4$ [29, 177], where the emphasis was now on the calculation of charge transfer states. Since not all relevant excited charge transfer states are contained in the active space of 10 orbitals, appropriate for the ground-state description, it had to be extended for the calculation of the spectra. However, it was found that with an active space of at most 13 orbitals, satisfactory results could be obtained, with an accuracy comparable to the ligand field state calculations.

Some of the most important results obtained from the studies above are reviewed below, including a comparison of the ligand field spectra of the isoelectronic systems $\text{Co}(\text{CN})_6^{3-}$, $\text{Fe}(\text{CN})_6^{4-}$, and $\text{Cr}(\text{CO})_6$, the charge transfer states in $\text{Cr}(\text{CO})_6$, and the spectrum of $\text{Ni}(\text{CO})_4$. Due to the size of the systems considered, rather limited ANO basis sets [41] were used in these studies: $(17s12p9d4f)/[6s4p3d1f]$ for the metal and $(10s6p3d)/[3s2p1d]$ for C, N, and O, resulting in 208 contracted functions for the octahedral systems and 152 contracted functions for $\text{Ni}(\text{CO})_4$. All calculations were performed using experimental geometries. The calculations on the octahedral $\text{Cr}(\text{CO})_6$, $\text{Co}(\text{CN})_6^{3-}$, and $\text{Fe}(\text{CN})_6^{4-}$ systems were done using D_{2h} symmetry, while for the tetrahedral $\text{Ni}(\text{CO})_4$ molecule D_2 symmetry was used. However, in all cases additional symmetry restrictions were imposed in the CASSCF step to prevent mixing between molecular orbitals belonging to different representations in the actual point group (O_h or T_d) of the molecules.

The role of $3s$, $3p$ correlation was investigated in all cases by comparing the results obtained from two sets of CASPT2 calculations, denoted as CASPT2(v) and CASPT2(c-v), respectively. The CASPT2(v) calculations include the metal $3d$ and all valence electrons of the ligands originating from the $2s$, $2p$ orbitals on C, N, and O, while the metal

3s, 3p electrons are included in the CASPT2(c-v) calculations. Thus up to 74 electrons were correlated in $\text{Co}(\text{CN})_6^{3-}$, $\text{Fe}(\text{CN})_6^{4-}$, and $\text{Cr}(\text{CO})_6$ and 58 electrons in $\text{Ni}(\text{CO})_4$. The role of relativistic effects was not investigated but is expected to be small, at least for the ligand field transitions. The effect of spin-orbit coupling on the ligand field spectrum of $\text{Cr}(\text{CO})_6$ was investigated in a recent study by Daniel and Ribbing [197], but turned out to be very small.

In addition to calculated CASSCF/CASPT2 transition energies, results for the oscillator strengths of the spin and orbitally allowed charge transfer transitions in $\text{Cr}(\text{CO})_6$ and $\text{Ni}(\text{CO})_4$ are presented. They were obtained using transition dipole moments obtained by the CASSCF state interaction method (CASSI). CASPT2(c-v) values were used for the excitation energies, appearing in the expression for the oscillator strengths.

Ligand Field Spectrum of $\text{Co}(\text{CN})_6^{3-}$, $\text{Fe}(\text{CN})_6^{4-}$, and $\text{Cr}(\text{CO})_6$. The ligand field spectra of the isoelectronic species $\text{Co}(\text{CN})_6^{3-}$, $\text{Fe}(\text{CN})_6^{4-}$, and $\text{Cr}(\text{CO})_6$ show an analogous structure. All three systems are characterized by a ${}^1A_{1g}$ ($2t_{2g}^6$) ground state, and their ligand field spectrum therefore consists of excitations from the π bonding $2t_{2g}$ orbitals to the σ antibonding $6e_g$ orbitals, giving rise to the following states: ${}^3T_{1g}$, ${}^3T_{2g}$, ${}^1T_{1g}$, ${}^1T_{2g}$. The spectra of the cyanides $\text{Co}(\text{CN})_6^{3-}$ and $\text{Fe}(\text{CN})_6^{4-}$ are simple and well understood [198]. In both cases three bands were located in the ligand field part of the spectrum, well separated from the charge transfer bands, which do not appear below 5.5 eV. They were assigned as transitions to the ${}^3T_{1g}$, ${}^1T_{1g}$, and ${}^1T_{2g}$ states, respectively. However, the same is no longer true for $\text{Cr}(\text{CO})_6$. Due to the stronger π -acceptor character of CO compared to CN^- , the $3d \rightarrow \text{CO } \pi^*$ charge transfer transitions appear at lower wavenumbers, thus obscuring the weaker ligand field transitions. The spectrum of $\text{Cr}(\text{CO})_6$ is dominated by two intense absorption bands at 4.43 eV and 5.41 eV, corresponding to the two orbitally and spin allowed ${}^1A_{1g} \rightarrow {}^1T_{1u}$ transitions [199–201]. Three weak shoulders appearing at 3.60, 3.91, and 4.83 eV were obtained from a Gaussian analysis of the spectrum by Beach and Gray in 1968 [199]. The shoulder at 4.83 eV was assigned as the second spin-allowed transition to ${}^1T_{2g}$, while the two weak shoulders at the low-energy side of the spectrum were assigned as vibrational components of the ${}^1A_{1g} \rightarrow {}^1T_{1g}$ transition. Although this assignment was made rather tentatively, it became widely accepted over the years [179, 200].

Somewhat remarkably, the Beach and Gray assignment was also reproduced almost exactly in a ROHF study of the $\text{Cr}(\text{CO})_6$ spectrum

[202] with calculated transition energies of 3.86 eV and 4.91 eV for the ${}^1A_{1g} \rightarrow {}^1T_{1g}$ and ${}^1A_{1g} \rightarrow {}^1T_{2g}$ transitions, respectively. This is unexpected, because it is known that the Hartree–Fock method systematically tends to underestimate seriously the ligand field strength in first-row transition metal systems. For example, an ROHF calculation on $\text{Co}(\text{CN})_6^{3-}$ [203] resulted in a value of 3.08 eV for the first spin-allowed transition ${}^1A_{1g} \rightarrow {}^1T_{1g}$, which is 0.95 eV lower than the experimental value. Up to now, no other studies including correlation have been reported for the spectrum of $\text{Cr}(\text{CO})_6$ nor for the hexacyanometalate complexes. An INDO/S CI study on $\text{Cr}(\text{CO})_6$ was reported recently by Kotzian et al. [201], who also remeasured the spectrum but made no attempt to locate the ligand field transitions. In this study both spin-allowed ligand field transitions were calculated below the charge transfer bands, at 3.64 eV (${}^1T_{1g}$) and 4.14 eV (${}^1T_{2g}$), and assigned to the shoulders at 3.60 and 3.91 eV in the Beach and Gray spectrum [199].

CASSCF/CASPT2 results obtained for the ligand field transitions in the three complexes are collected in Table XIX. Both CASSCF (with 10

TABLE XIX
Comparison of the CASSCF and CASPT2 Excitation Energies (eV) for the $d-d$ Transitions in $\text{Co}(\text{CN})_6^{3-}$, $\text{Fe}(\text{CN})_6^{4-}$, and $\text{Cr}(\text{CO})_6$

State	$\text{Co}(\text{CN})_6^{3-}$					Expt. ^b
	CASSCF	CASPT2(v)	ω_v^a	CASPT2(c-v)	ω_{c-v}^a	
${}^3T_{1g}$	3.90	3.38	0.569	3.14	0.559	3.22
${}^3T_{2g}$	4.55	3.89	0.567	3.63	0.557	
${}^1T_{1g}$	4.91	4.23	0.567	3.98	0.558	4.03
${}^1T_{2g}$	6.30	5.22	0.564	4.80	0.554	4.86
State	$\text{Fe}(\text{CN})_6^{4-}$					Expt. ^b
	CASSCF	CASPT2(v)	ω_v^a	CASPT2(c-v)	ω_{c-v}^a	
${}^3T_{1g}$	3.37	2.91	0.564	2.67	0.552	2.94
${}^3T_{2g}$	4.02	3.42	0.563	3.14	0.551	
${}^1T_{1g}$	4.38	3.85	0.562	3.60	0.551	3.84
${}^1T_{2g}$	5.73	4.77	0.560	4.33	0.549	4.59
State	$\text{Cr}(\text{CO})_6$					Expt. ^b
	CASSCF	CASPT2(v)	ω_v^a	CASPT2(c-v)	ω_{c-v}^a	
${}^3T_{1g}$	5.07	4.46	0.572	4.28	0.558	
${}^3T_{2g}$	5.57	4.86	0.553	4.64	0.537	
${}^1T_{1g}$	5.66	5.05	0.576	4.85	0.561	
${}^1T_{2g}$	6.48	5.43	0.568	5.13	0.553	

^a Weight of the CASSCF wavefunction in the first-order wavefunction.

^b From Ref. 198.

active orbitals) and CASPT2 results are reported. The weights of the CASSCF wavefunction in the final CASPT2 first-order wavefunctions are almost exactly the same for three complexes and stable for the different excited states. This is an indication that the chosen 10-orbital active space is large enough to include the essential electronic structure features in all three complexes. It also shows that a balanced treatment of all excited states has been achieved.

Calculated transition energies for $\text{Co}(\text{CN})_6^{3-}$ and $\text{Fe}(\text{CN})_6^{4-}$ at the CASSCF level are clearly too high, with errors up to 1 eV and more. This is a general observation for the CASSCF results obtained for all hexacyanometalate complexes studied in Ref. 170, where it could be traced back to the fact that CASSCF tends to overestimate the occupation of the antibonding $3t_{2g}$ and $6e_g$ orbitals included in the active space, but does so more for the ground state than for the excited states. A considerable improvement is obtained at the CASPT2(v) level. All excited states are drastically lowered with respect to the CASSCF results by the perturbational correlation treatment of the valence electrons. However, the contribution of the metal semicore $3s$, $3p$ electrons is most certainly not negligible: The difference between the CASPT2(v) and CASPT2(c-v) results amounts to 0.4 eV for the ${}^1A_{1g} \rightarrow {}^1T_{2g}$ transition in both $\text{Co}(\text{CN})_6^{3-}$ and $\text{Fe}(\text{CN})_6^{4-}$. At the CASPT2(c-v) level, excellent results are obtained. For $\text{Co}(\text{CN})_6^{3-}$, the transition energies calculated agree with the experimental values to within 0.1 eV. The error is in each case slightly negative, implying that the splitting of the various $2t_{2g}^5 6e_g^1$ states is described even more accurately. The same remark holds for $\text{Fe}(\text{CN})_6^{4-}$. The transition energies calculated are slightly less accurate in this case, with a maximum error of 0.27 eV. However, the relative energies of the various $2t_{2g}^5 6e_g^1$ states again agree to within 0.05 eV with the experimental splitting.

In view of the close relationship between both cyanide complexes and $\text{Cr}(\text{CO})_6$, similar accuracy is expected at the CASPT2(c-v) level for the latter molecule. The results for $\text{Cr}(\text{CO})_6$ in Table XIX do show similar trends, in that the transition energies generally decrease as the correlation treatment is improved. However, the CASPT2(c-v) results obtained for the energies of the spin-allowed transitions to ${}^1T_{1g}$ and ${}^1T_{2g}$ do not compare at all well with the values of 3.60, 3.91, and 4.83 eV reported from Gaussian analysis of the spectrum by Beach and Gray [199]. For the second transition, the difference between the calculated result and the band position according to Beach and Gray is 0.30 eV, which is acceptable, but for the first transition a discrepancy of 0.94 eV or more is found. It is highly unlikely that the present CASPT2 method would lead to such a large error for this transition. Furthermore, this would also imply that

the error for the splitting between both states is at least 0.61 eV, which is even more unlikely. Considering the quality of the CASPT2 results obtained for $\text{Co}(\text{CN})_6^{3-}$ and $\text{Fe}(\text{CN})_6^{4-}$, we therefore believe that the weak shoulders at 3.60 eV and 3.91 eV in the spectrum of $\text{Cr}(\text{CO})_6$, if present, should not be assigned as ligand field transitions. The presence of the second band at 4.83 eV conforms better to the present results. Given that the Beach and Gray assignment of this band is correct and that the CASPT2(c-v) result for the ${}^1T_{2g}-{}^1T_{1g}$ splitting in $\text{Cr}(\text{CO})_6$ is as accurate as in the case of the cyanide compounds, we can predict the position of the first transition to ${}^1T_{1g}$ at 4.55 eV, right below the first intense ${}^1A_{1g} \rightarrow {}^1T_{1u}$ charge transfer transition. In the next section, where we present the charge transfer spectrum of $\text{Cr}(\text{CO})_6$, we will show that there are, in fact, plenty of other candidates to take over the assignment of the shoulders at both 3.60 and 3.91 eV.

The results from the present CASPT2 study also explain the abnormal ‘‘accuracy’’ of the results obtained using ROHF for the ligand field states. When comparing the ROHF result for the ${}^1A_{1g} \rightarrow {}^1T_{1g}$ transition to the present CASPT2(c-v) result, we now find a difference of 0.99 eV, a perfectly normal ROHF error, of the same magnitude as the ROHF error obtained for $\text{Co}(\text{CN})_6^{3-}$. We also note the large discrepancy (more than 1 eV) between the present CASPT2 results and the INDO/S CI from Kotzian et al. [201] for the spin-allowed ligand field transitions.

Charge Transfer States in $\text{Cr}(\text{CO})_6$. The electronic spectrum of metal carbonyl compounds is usually dominated by charge transfer (MLCT) transitions from the metal 3d orbitals into the CO π^* orbitals. In the case of $\text{Cr}(\text{CO})_6$, the 12 CO π^* orbitals are found in the molecular orbitals $9t_{1u}$, $2t_{2u}$, $2t_{1g}$, and $3t_{2g}$. The region 3.5–7 eV in its spectrum is therefore built from a broad range of charge transfer transitions [200], of which, however, only two ${}^1A_{1g} \rightarrow {}^1T_{1u}$ transitions are both spin and symmetry allowed. They give rise to two intense and broad absorption bands, with a maximum at 4.43 eV and 5.41 eV and an intensity ratio of 1:9.

Only the $3t_{2g}$ CO π^* shell is included in the active space used for the calculation of the ligand field states. Thus the 10 orbitals should have to be extended with the other three CO π^* shells to be able to calculate the full spectrum using the same active space for all states, ending up with an impossible number of 19 active orbitals. The only alternative is to use different active spaces for different excited states. Denoting the basic (5,6) e_g , (2,3) t_{2g} 10-orbital active space as active space A, we decided in favor of the following options:

1. All charge transfer states of gerade symmetry were calculated with

an active space of 13 orbitals, constructed by extending space A with the $2t_{1g}$ shell. This active space will be denoted as B.

2. To include all charge transfer states of ungerade symmetry, active space A would have to be extended with both the $9t_{1u}$ and $2t_{2u}$ shells, leading to a still unmanageable number of 16 orbitals. In a first calculation, both shells were therefore added in turn, thus constructing active space C1 by adding the $9t_{1u}$ shell and active space C2 by adding $2t_{2u}$. However, this selection of orbitals prevents interaction in the CASSCF step among states belonging to the configurations $2t_{2g}^5 9t_{1u}^1$ and $2t_{2g}^5 2t_{2u}^1$, an interaction that could be important. Therefore, a second set of calculations was performed with an active space of 12 orbitals, denoted as D, in which now both the $9t_{1u}$ and $2t_{2u}$ shells were included, in addition to $(2,3)t_{2g}$. The $(5,6)e_g$ σ orbitals were no longer included, but looking at Table XVI we notice that they are less important than $(2,3)t_{2g}$.

Excitations to all singlet states were included in the calculations, as well as the two ${}^1A_{1g} \rightarrow {}^3T_{1u}$ excitations, which are spin forbidden but orbitally allowed. The ${}^1T_{1g}$ and ${}^1T_{2g}$ ligand field states were now also recalculated using active space B. The results are shown in Table XX. We have included in this table the composition of the CASSCF wavefunction in terms of the different singly excited configurations. For the ungerade states, the composition was taken from the calculations performed with active space D.

The general trends observed in the calculated results are the same as for the ligand field states. The CASSCF transition energies are again definitely too high, with errors amounting up to 2 eV and more. The transition energies are strongly reduced at the CASPT2(v) level. The effect of semicore $3s$, $3p$ correlation turns out to be the least important for the transitions to ungerade charge transfer states, for which the difference between the CASPT2(c-v) and CASPT2(v) results is never larger than 0.1 eV. Significantly larger differences, up to 0.3 eV, are found for some of the gerade states, again including the ${}^1T_{2g}$ ligand field state. At the CASPT2(c-v) level, all charge transfer transitions in $\text{Cr}(\text{CO})_6$ are calculated in the region between 3.5 and 7 eV, which agrees nicely with the experimental spectrum. From the composition of the wavefunctions, we find the following overall energy sequence for the CO π^* orbitals: $9t_{1u} < 2t_{2u} < 3t_{2g} < 2t_{1g}$. The transition energies calculated for the two spin and orbitally allowed ${}^1A_{1g} \rightarrow {}^1T_{1u}$ transitions are satisfactory, with a maximum error of 0.34 eV. There can be no doubt that these two transitions are responsible for the two intense bands in the spectrum.

Both singlet ligand field states are now found between the two strong

TABLE XX
Absorption Spectrum of $\text{Cr}(\text{CO})_6$: CASSCF and CASPT2 Results

Final State	Composition ^a	Active Space	Transition Energy (eV)				Oscillator Strength	
			CASSCF	CASPT2(v)	CASPT2(c-v)	Expt. ^b	Calc.	Expt. ^b
a^1E_u	85%($2t_{2g} \rightarrow 9t_{1u}$)	C_1-D	5.11-5.28	3.49-3.67	3.41-3.59	—	—	—
a^1A_{2u}	85%($2t_{2g} \rightarrow 9t_{1u}$)	C_1-D	5.14-5.32	3.65-3.66	3.58-3.58	—	—	—
a^1T_{2u}	76%($2t_{2g} \rightarrow 9t_{1u}$), 9%($2t_{1g} \rightarrow 2t_{2u}$)	C_1-D	5.18-5.26	3.77-3.64	3.70-3.56	—	—	—
a^3T_{1u}	79%($2t_{2g} \rightarrow 9t_{1u}$), 10%($2t_{2g} \rightarrow 2t_{2u}$)	C_1-D	5.25-5.36	3.97-3.78	3.90-3.69	—	—	—
b^1E_g	2%($2t_{2g} \rightarrow 2t_{1u}$), 82%($2t_{1g} \rightarrow 2t_{2u}$)	C_2-D	5.86-6.16	4.05-4.14	3.97-4.05	—	—	—
a^1A_{1u}	84%($2t_{2g} \rightarrow 2t_{2u}$)	C_2-D	5.92-6.29	4.23-4.20	4.15-4.10	—	—	—
b^1T_{2u}	4%($2t_{2g} \rightarrow 9t_{1u}$), 82%($2t_{1g} \rightarrow 2t_{2u}$)	C_2-D	6.21-6.57	4.39-4.52	4.32-4.43	—	—	—
a^1T_{1u}	66%($2t_{2g} \rightarrow 9t_{1u}$), 21%($2t_{2g} \rightarrow 2t_{2u}$)	C_1-D	6.15-5.97	4.61-4.19	4.54-4.11	4.43	1.33-0.20	0.25
b^3T_{1u}	4%($2t_{2g} \rightarrow 9t_{1u}$), 83%($2t_{1g} \rightarrow 2t_{2u}$)	C_2-D	6.23-5.59	4.59-4.61	4.51-4.51	—	—	—
a^1E_g	86%($2t_{2g} \rightarrow 3t_{2g}$), 2%($2t_{1g} \rightarrow 2t_{1g}$)	B	7.17	4.78	4.58	—	—	—
a^1T_{1g}	5%($2t_{2g} \rightarrow 6e_g$), 83%($2t_{2g} \rightarrow 3t_{2g}$)	B	6.80	5.02	4.82	—	—	—
b^1T_{1g}	88%($2t_{2g} \rightarrow 6e_g$), 1%($2t_{2g} \rightarrow 3t_{2g}$)	B	5.66	5.04	4.85	—	—	—
a^1T_{2g}	74%($2t_{2g} \rightarrow 6e_g$), 14%($2t_{1g} \rightarrow 3t_{2g}$)	B	6.42	5.38	5.08	—	—	—
b^1T_{1u}	13%($2t_{2g} \rightarrow 9t_{1u}$), 77%($2t_{2g} \rightarrow 2t_{2u}$)	C_2-D	7.16-7.75	5.16-5.30	5.07-5.20	5.41	1.63-2.58	2.30
b^1E_g	8%($2t_{2g} \rightarrow 3t_{2g}$), 75%($2t_{1g} \rightarrow 2t_{1g}$)	B	9.09	5.52	5.42	—	—	—
b^1T_{2g}	30%($2t_{2g} \rightarrow 6e_g$), 55%($2t_{2g} \rightarrow 3t_{2g}$), 1%($2t_{1g} \rightarrow 2t_{1g}$)	B	7.47	5.74	5.43	—	—	—
a^1A_{2g}	85%($2t_{2g} \rightarrow 2t_{1g}$)	B	8.01	5.71	5.62	—	—	—
c^1T_{1g}	2%($2t_{2g} \rightarrow 3t_{2g}$), 83%($2t_{1g} \rightarrow 2t_{1g}$)	B	8.41	6.00	5.91	—	—	—
c^1T_{2g}	1%($2t_{2g} \rightarrow 6e_g$), 11%($2t_{2g} \rightarrow 3t_{2g}$), 72%($2t_{1g} \rightarrow 2t_{1g}$)	B	8.41	6.03	5.92	—	—	—
b^1A_{1g}	11%($2t_{2g} \rightarrow 3t_{2g}$), 9%($5e_g \rightarrow 6e_g$)	B	10.81	7.12	6.89	—	—	—

^a For the ungerade charge transfer states, the composition in terms of an excitation to either $9t_{1u}$ or $2t_{2u}$ is obtained from the CASSCF calculation with the active space D.

^b From Ref. 199.

charge transfer bands, at 4.85 eV (b^1T_{1g}) and 5.08 eV (a^1T_{2g}). Comparing these results to the results in Table XIX, we notice that while the $^1T_{1g}$ state is calculated at exactly the same position with active spaces A and B, a small difference between the results is obtained for the $^1T_{2g}$ state. This can be traced back to the composition of the a^1T_{2g} state in Table XX, which now contains 14% $2t_{2g} \rightarrow 3t_{2g}$ charge transfer character. However, the difference is small, only 0.05 eV, giving further credit to the 10-orbital active space A originally chosen for calculation of the ligand field states. With active space B, the difference between the result calculated for the $^1T_{2g}$ state and the shoulder observed at 4.86 eV in the Beach and Gray spectrum is only 0.26 eV. However, from the results in Table XX it seems just as likely that this shoulder is actually due to the first $^1A_{1g} \rightarrow ^1T_{1g}$ ligand field transition, or to a superposition of both. As for the shoulders at 3.60 eV and 3.91 eV, there seems to be little doubt that these should actually be assigned as either the spin-forbidden but orbitally allowed $^1A_{1g} \rightarrow ^3T_{1u}$ transition or to one of the orbitally forbidden singlet-singlet transitions, of which there are plenty in the region 3.6–4.1 eV.

For states with ungerade symmetry, the agreement between the transition energies calculated with active spaces C1–C2 and D is in most cases acceptable, with a maximum difference of 0.2 eV. An exception is the first $^1A_{1g} \rightarrow ^1T_{1u}$ transition. In this case the difference between the results calculated with the active spaces C1 and D amounts to 0.43 eV. We notice, however, that the $^1T_{1u}$ state under consideration is subject to a considerable interconfigurational mixing between the configurations with either $9t_{1u}$ or $2t_{2u}$ occupied. This interaction is significantly larger for this state than for any of the other ungerade states. This may explain the larger discrepancy between the results obtained with active space D, where the interaction is treated variationally at the CASSCF level, and active space C1, where it is treated perturbationally in the CASPT2 step. However, considering that both active spaces C1 and D were in fact chosen as a compromise for the the 16-orbital space that one would really prefer to use for the ungerade states, the results obtained should still be considered as satisfactory.

Neglect of the interaction between both $^1T_{1u}$ states when using the active spaces C1–C2 has more serious consequences for the oscillator strengths calculated, due to the fact that CASSCF wavefunctions are used for this purpose. Indeed, with the active space C1–C2, rather similar transition moments (–2.00 a.u.; –2.09 a.u.) are calculated for the pure $2t_{2g} \rightarrow 9t_{1u}$ and $2t_{2g} \rightarrow 2t_{2u}$ transitions, leading to an intensity ratio of only 1:1.2 for the two orbitally allowed transitions, much smaller than the experimental value of about 1:9. On the other hand, active space D

contains both ${}^1T_{1u}$ states as a combination of the pure transitions, differing only in sign. As a result, the transition moment for the first, negative, combination is weakened, while it is enforced for the second, positive, combination. Although the calculated intensity ratio, 1:12.9, is now slightly too high, the absolute values of the oscillator strengths calculated with active space D are in good agreement with the values given from experiment.

As a final note we add that the recently reported INDO/S CI calculations of the $\text{Cr}(\text{CO})_6$ spectrum resulted in an intensity ratio of 1:400 for the two transitions allowed, due to the fact that with this method the interconfigurational mixing in both ${}^1T_{1u}$ states is grossly overestimated. Although the calculated transition energies reported, 4.60 eV and 5.79 eV, conformed with experiment, both ${}^1T_{1u}$ states were in fact calculated as an almost equal mixture of $2t_{2g}^5 9t_{1u}^1$ and $2_{2g}^5 2t_{2u}^1$.

Spectrum of $\text{Ni}(\text{CO})_4$. Since $\text{Ni}(\text{CO})_4$ is formally a d^{10} system, no ligand field transitions appear in its electronic absorption spectrum, which consists solely of Ni $3d \rightarrow \text{CO } \pi^*$ charge transfer bands. Within the point group T_d , the CO π^* orbitals transform as e , t_1 , and t_2 , and one would a priori expect five bands in the spectrum, corresponding to five spin and orbitally allowed ${}^1A_1 \rightarrow {}^1T_2$ transitions. However, all experimental spectra of $\text{Ni}(\text{CO})_4$, recorded either in solution [204], in a matrix environment [205], or in the gas phase [201], reveal at most three bands. The solution spectrum exhibits a main peak at 6.0 eV with two shoulders at 5.5 eV and 5.2 eV. Of these, only the band at 5.2 eV was detected in a matrix isolation spectrum, where instead a new shoulder appeared at 4.5 eV. Finally, in the most recent recording of the spectrum in the gas phase, the main peak at 6.0 eV and two shoulders at 5.4 eV and 4.6 eV could be discriminated. No experimental oscillator strengths have been reported, but in all cases the intensity of the bands increases steeply with an increasing wavenumber.

The theoretical interpretation of the $\text{Ni}(\text{CO})_4$ spectrum has always been hampered by the absence of a more resolved structure in the experimental spectra. Up to now, a detailed assignment has only been provided in the most recent study of the gas-phase spectrum, where it was based on calculations performed with the INDO/S CI method [201]. To our knowledge, no previous *ab initio* results have been reported for the spectrum of $\text{Ni}(\text{CO})_4$.

As for $\text{Cr}(\text{CO})_6$, a calculation of the complete charge transfer spectrum of $\text{Ni}(\text{CO})_4$, including singlet excited states of all possible symmetries, has been performed in a recent CASSCF/CASPT2 study [177]. Here the results obtained for the symmetry-allowed ${}^1A_1 \rightarrow {}^1T_2$

transitions are reported. Transition energies obtained at the CASSCF and CASPT2 level as well as oscillator strengths obtained using the CASSI method are presented in Table XXI, where we have included the INDO/S CI results for comparison.

Since the number of CO π^* orbitals in Ni(CO)₄ is limited to eight, no selection of different active spaces for different excited states has to be made in this case. Instead all states were calculated using the same active space of 13 orbitals, consisting of the $2e$, $9t_2$ Ni $3d$, and the $3e$, $10t_2$, and $2t_1$ CO π^* orbitals, and including 10 electrons. However, we remember that ground-state CASSCF calculations on Ni(CO)₄ indicate a considerable contribution of Ni $4d$ character in the $3e$ and $10t_2$ orbitals, accounting for the $3d$ double-shell effect (see also Table XVII and Fig. 6). Part of the Ni $4d$ character inevitably gets lost in the CASSCF calculations on excited states containing either a singly occupied $3e$ or $10t_2$ orbital, since the corresponding orbital now turns into an exclusively CO π^* orbital. This situation introduces a slight unbalance in the calculations, which would only be removed at the expense of adding an additional virtual e and t_2 shell. The unbalance is most strongly reflected in the CASSCF results in Table XXI. As usual, all transition energies are calculated too high at the CASSCF level. We notice, however, the large error, up to 3 eV and more, for the three lowest 1T_2 states with either a singly occupied $10t_2$ or $2e$ orbital. Both shells are left unoccupied in the highest two 1T_2 states, which are therefore more in balance with the ground state.

Fortunately, the CASPT2 results do not seem to suffer from the unbalanced CASSCF situation. Indeed, the weights of the CASSCF wavefunction in the first-order CASPT2(v) wavefunction are about the same for all states, indicating a balanced set of calculations. The CASPT2 results are again affected by the inclusion of a $3s$, $3p$ correlation, although the effect is almost negligible for the two highest charge transfer states. The largest effect is found for the a^1T_2 state, for which the difference between CASPT2(v) and CASPT2(c-v) amounts to 0.43 eV. Obviously, correlation of the semicore $3s$, $3p$ electrons cannot be neglected if one wants to get an accurate description of the relative energy of different charge transfer states in organometallic compounds.

Based on the transition energies obtained at the CASPT2(c-v) level, together with the calculated oscillator strengths, the following assignment of the spectral bands in the experimental Ni(CO)₄ spectra is proposed:

1. There can be little or no doubt that the lowest and least intense band observed at 4.5–4.6 eV in the matrix isolation and gas-phase spectra is due to the $9t_2 \rightarrow 10t_2$ transition. According to the

TABLE XXI
Absorption Spectrum of Ni(CO)₄: CASSCF and CASPT2 Results

Final State	Composition	Transition Energy (eV)				Oscillator Strength		
		CASSCF	CASPT2(v)	CASPT(c-v)	INDO/S	CASSI	INDO/S	INDO/S
<i>a</i> ¹ T ₂	92%(9t ₂ → 10t ₂)	7.49	4.72	4.29	4.15	0.29	0.14	0.14
<i>b</i> ¹ T ₂	92%(9t ₂ → 3e)	7.57	5.45	5.19	4.36	0.38	0.11	0.11
<i>c</i> ¹ T ₂	94%(2e → 10t ₂)	7.34	5.75	5.54	4.91	0.29	0.02	0.02
<i>d</i> ¹ T ₂	93%(9t ₂ → 2t ₁)	7.67	6.20	6.17	5.36	0.47	0.45	0.45
<i>e</i> ¹ T ₂	88%(2e → 2t ₁), 6%(9t ₂ → 2t ₁)	8.16	6.90	6.89	6.20	0.83	1.74	1.74

calculations, this transition is well separated from the other transitions. The calculated transition energy, 4.29 eV agrees well with the experimental band position, and the oscillator strength calculated indicates that this is indeed the least intense band in the spectrum.

2. The band positions calculated for the b^1T_2 ($9t_2 \rightarrow 3e$) and c^1T_2 ($2e \rightarrow 10t_2$) states, 5.19 eV and 5.54 eV, are in agreement with the experimental band positions of the two shoulders observed at 5.2 eV and 5.5 eV in the solution spectrum, which should therefore be assigned as such. On the other hand, only one band is observed in this region in the gas-phase spectrum, at 5.4 eV. This band should therefore be related to both the $9t_2 \rightarrow 3e$ and $2e \rightarrow 10t_2$ transitions.
3. According to the results, the most intense band at 6.0 eV in the solution- and gas-phase spectra should be assigned as the $9t_2 \rightarrow 2t_1$ transition. The only possible alternative could be that it is in fact a superposition of both the transitions from $9t_2$ and $2e$ to $2t_1$. However, the calculated splitting between both transitions is more than 0.6 eV, and one would therefore expect them to appear as distinct bands in the spectrum. We also notice that the highest charge transfer transition could just as well fall outside the range measured by the spectra, which never reached below 200 nm (above 6.2 eV).

The present assignment is different from the assignment proposed by Kotzian et al. [201] based on the INDO/S CI results, shown in Table XXI. With that method all allowed charge transfer transitions in $\text{Ni}(\text{CO})_4$ are predicted at significantly lower energies. Consequently, the three bands appearing in the gas-phase spectrum were assigned as follows: the band at 6.0 eV as e^1T_2 , the band at 5.4 eV as d^1T_2 , and the band at 4.6 eV as a superposition of the lowest three transitions. The latter assignment seemed to be justified by the low oscillator strengths calculated for these transitions. However, the relative oscillator strengths of the allowed charge transfer states are quite different with the two methods. As indicated earlier by the results presented for $\text{Cr}(\text{CO})_6$, this observation must be connected to the extent of interconfigurational mixing observed for the different 1T_2 states. Actually, almost no mixing occurs in the CASSCF wavefunctions (see Table XXI), while the INDO/S CI method gives a large mixing. In view of the excellent results obtained with the CASSI method for the oscillator strengths in $\text{Cr}(\text{CO})_6$, we believe that the present CASSI results for the oscillator strengths should also be considered as being closer to the truth than the INDO/S CI results. This then puts some serious doubt on the assignment given by Kotzian et al. [201] for the 4.6-eV band. In view of the low intensity of this band, it

could never be composed of three transitions with a considerable oscillator strength.

Finally, we want to refer to the results of a recent CASSCF/CASPT2 study of the spectrum of $\text{Fe}(\text{CO})_5$ [29]. A comparison with the INDO/S CI results showed that in this case also, CASSCF/CASPT2 gives significantly higher transition energies and quite different oscillator strengths. It is clear that the CASSCF/CASPT2 method is highly superior to INDO/S CI, which, at this moment, seems to represent the only method alternative for calculation of charge transfer spectra of organometallic compounds.

3. Cr_2 Molecule and Its Spectroscopy

As for all transition metal quantum chemistry, the primary difficulty in describing the chromium dimer concerns electron correlation. This is demonstrated clearly by the ground-state properties computed at the RHF-SCF and CASSCF levels of theory. At the experimental bond length the molecular energies given by the two methods are far above that of two separated atoms (more than 20 eV with the RHF-SCF method) [206]. Another difficulty concerns the multiconfigurational character of the wavefunction for the ground state. The weight of the Hartree-Fock configuration in a CASSCF wavefunction based on an active space comprising 12 active orbitals (3d and 4s) is less than 50%. It is clear that single-configurational correlation methods are inappropriate for this particular molecule [207].

In some very recent calculations on the electronic spectrum of the chromium dimer [23, 25] we were able to show how well suited the CASSCF/CASPT2 approach is for this molecule. The plenitude of configurations needed for its description at the zeroth-order level does not lead to prohibitively large expansions at the first-order level. This is one of the advantages with CASPT2 over MRCI techniques. Further, the CASSCF/CASPT2 method allows us to calculate excited electronic states almost as easy as ground electronic states. However, the calculations were not straightforward because of problems with intruder states for some electronic states (cf. Section II.C). The intruder states appear at short internuclear distances (typically between 2.8 and 4.4 a.u.) and they give rise to rather weak singularities in the potential curves. In Fig. 9 the potential energy curves of 18 electronic states of Cr_2 are displayed. Here, only points with reference weights larger than 0.7 were taken into account when constructing the curves. Although the intruder states constitute a problem, in particular for calculating accurate values of vibrational frequencies, they do not destroy the overall picture. With the level shift

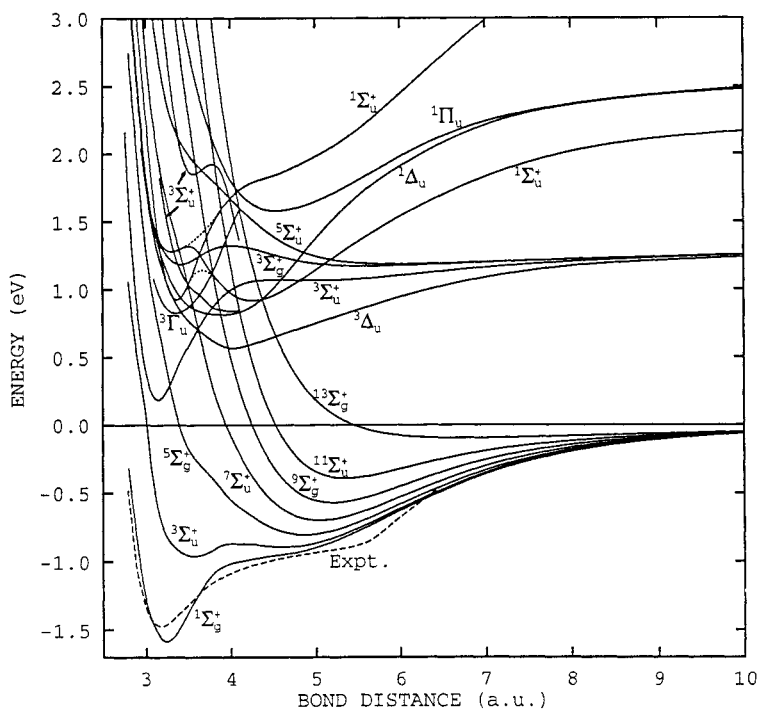


Figure 9. Potential curves for Cr_2 computed using the CASSCF/CASPT2 method. The dashed curve represents the experimental potential for the ground state. The dotted curves indicate avoided crossings.

introduced in Section II.C we will hopefully be able to obtain accurate spectroscopic constants also for the excited states.

An additional difficulty concerns the crossing of the two $1\Sigma_u^+$ states at the CASPT2 level of theory (see Fig. 9). At the CASSCF level of theory these two states are dominated primarily by two configurations. The weight of the two configurations changes heavily with bond distance. At equilibrium, the two configurations are weighted equally in each state, while at somewhat larger distances one configuration dominates. This is a typical situation where a multistate CASPT2 method should be used, treating the two $1\Sigma_u^+$ states simultaneously (see Section II.C).

Despite the problems stated above, we were able to give explanations to some of the experimental data about Cr_2 . Using an ANO basis set of size $8s7p6d4f$ and including $3s$, $3p$ correlation effects and relativistic corrections, the following results were obtained (experimental results in parentheses):

1. The intensity profile of the rotational spectrum for the $A^1\Sigma_u^+ \leftarrow X^1\Sigma_g^+$ 0-0 band is probably due to strong nonadiabatic interactions near the inner walls of the $A^1\Sigma_u^+$ state and another $^1\Sigma_u^+$ state lower in energy.
2. The location of the $A^1\Sigma_u^+$ state is 2.86 eV (2.70 eV) above the ground state, and that of the lower $^1\Sigma_u^+$ state is 2.51 eV (2.40 eV) above the ground state.
3. Spectroscopic constants for the $^3\Sigma_u^+$ state located 1.82 eV (1.76 eV) above the ground state are $r_e = 1.67 \text{ \AA}$ ($1.65 \pm 0.02 \text{ \AA}$) and $\Delta G_{1/2} = 680 \text{ cm}^{-1}$ (574 cm^{-1}).
4. The $^5\Sigma_g^+$ state in the ground-state manifold is a plausible candidate for the metastable state detected in 1985 by Moskovits et al. [216]. The vibrational frequency $\omega_e = 148 \text{ cm}^{-1}$ (79 cm^{-1}) does differ from the experimental value. The difference can be attributed, at least partially, to matrix effects. After populating the metastable state Moskovits et al. [216] observed an intense absorption at 2.11 eV. This absorption may be the vertical transition $^5\Sigma_u^+ \leftarrow ^5\Sigma_g^+$ calculated at 2.07 eV.

In summary, there is agreement between the spectroscopic data computed and available experimental information. The CASSCF/CASPT2 method has thus shown that it is capable of treating not only the ground state but also a large number of excited states for a molecule that has been a frustrating challenge for quantum chemistry for more than 10 years. With the newly implemented level-shift technique, the intruder state problem is also solved, which makes the calculations less involved and the results more stable. The entire field of spectroscopy of transition metal dimers and their ions is therefore open for an accurate theoretical analysis.

IV. SUMMARY

We have in this review presented a number of applications of the CASSCF/CASPT2 method in electronic spectroscopy. The general conclusion to be drawn from these and a large body of other applications is that if the method can be applied, it yields accurate results. The limitations of the approach is set by the possibility to select a small number of active orbitals, which describe the nondynamical correlation. This is almost always possible, but we have seen cases where the smallest acceptable active space is already outside the limits of the program. The CrF_6 molecule is one example, C_{60} is another. The application to

polyaromatic hydrocarbons discussed earlier is an example which shows how the size of the active space can easily outgrow the capacity of the present technology. Extensions of the method to widen the range of applications are, however, possible:

1. The number of active orbitals can be increased by introducing direct calculations of the third-order density matrices without intermediate storing, combined with a new iterative solution to the first-order CI equations, which does not require diagonalization of large matrices (cf. Ref. 7).
2. It is also necessary to increase the capacity of the CASSCF program such that larger CI expansions can be handled. The limit today is about 10^6 CFs. Techniques to do this exist. An alternative is to use a RASSCF instead of a CASSCF reference function, which would allow a considerably larger number of active orbitals. However, the generalization of CASPT2 to RASPT2 is not trivial.
3. A CASPT2 gradient code is under development. It will enable more detailed studies of potential surfaces for excited states.
4. A multistate CASPT2 method, which is also under development, will improve results in cases where several energy surfaces of the same symmetry are close in energy and interact strongly. The most important situations where this occurs are probably close avoided crossings as illustrated for some excited states in Cr_2 [23] and close encounters between valence and Rydberg excited states. These situations are characterized by large modifications of the CASSCF reference function due to dynamic correlation.
5. The search for an improved zeroth-order Hamiltonian continues with the goal to remove the systematic error in binding energies. The methods presented in a previous section work well for cases with no inactive orbitals close in energy to the active orbitals. The correction terms move the orbital energies of the active orbitals closer to the ionization energies, which restores the balance for excitations out of them. To correct simultaneously for the imbalance of excitations into the active orbitals, it seems necessary to introduce two-electron terms in the zeroth-order Hamiltonian, which leads to considerable technical complications for large active spaces.

It is thus clear that there is room for considerable improvement of the CASSCF/CASPT2 approach. However, even at its present level of development it is a very useful and accurate method. We have presented

examples from electronic spectroscopy, but the same method can be used to study energy surfaces for chemical reactions, including geometries of equilibria and transition states. Good examples are recent studies of the Bergmann reaction (autoaromatization of hex-3-ene-1,5-diyne) [208] and the Cope rearrangement [209]. The CASPT2 method has been used to compute vibration energies of ozone and the ozonide anion [210, 211]. It is thus a general method. It has limitations in accuracy, but this drawback is balanced by the generality of the method and the size of the molecules that may be studied.

ACKNOWLEDGMENTS

The research reported in this paper has been supported by a grant from the Swedish Natural Science Research Council (NFR), by IBM Sweden under a joint study contract, by the Cooperación Científico-Técnica (Ministerio de Asuntos Exteriores) of Spain, by projects PB91-0634 and PB94-0986 of Spanish DGICYT, and by the Belgian National Science Foundation (NFWO) together with the Belgian government (DPWB). Luis Serrano acknowledges a postdoctoral grant from the DGICYT of the Ministerio de Educación y Ciencia of Spain. Important contributions to the MOLCAS system, of which CASPT2 is one module, have been given by Roland Lindh, Jeppe Olsen, and Per-Olof Widmark. The authors would like to acknowledge fruitful discussions with Gunnar Karlström and Andrzej Sadlej. The following persons are acknowledged for their contributions to the work on transition metal compounds: Luc G. Vanquickenborne, Erik Van Praet, Eftimios Tsokos, Ralf Åkesson, Carl Ribbing, Kristine Ooms, Birgit Dumez, Rosendo Pou-Amérigo, Joakim Persson, and Nazzareno Re. Apart from the present authors, the following persons have contributed to the work on organic systems: Johan Lorentzon, Mercedes Rubio, Enrique Ortí, and Martin Schütz.

REFERENCES

1. S. R. Langhoff, Ed., *Quantum Mechanical Electronic Structure Calculations with Chemical Accuracy*, Kluwer, Dordrecht, The Netherlands, 1995.
2. B. O. Roos, in *Advances in Chemical Physics; Ab Initio Methods in Quantum Chemistry, II*, K. P. Lawley, Ed., Wiley, Chichester, West Sussex, England, 1987.
3. H. Partridge, S. R. Langhoff, and C. W. Bauschlicher, Jr., in *Quantum Mechanical Electronic Structure Calculations with Chemical Accuracy*, S. R. Langhoff, Ed., Kluwer, Dordrecht, The Netherlands, 1995.
4. M. Perić, B. Engels, and S. D. Peyerimhoff, in *Quantum Mechanical Electronic Structure Calculations with Chemical Accuracy*, S. R. Langhoff, Ed., Kluwer, Dordrecht, The Netherlands, 1995.

5. P.-Å. Malmqvist, B. O. Roos, M. P. Fülscher, and A. Rendell, *Chem. Phys.* **162**, 359 (1992).
6. K. Andersson, P.-Å. Malmqvist, B. O. Roos, A. J. Sadlej, and K. Wolinski, *J. Phys. Chem.* **94**, 5483 (1990).
7. K. Andersson, P.-Å. Malmqvist, and B. O. Roos, *J. Chem. Phys.* **96**, 1218 (1992).
8. B. O. Roos, P. Linse, P. E. M. Siegbahn, and M. R. A. Blomberg, *Chem. Phys.* **66**, 197 (1982).
9. P.-Å. Malmqvist, to be published, 1995.
10. P.-Å. Malmqvist, A. Rendell, and B. O. Roos, *J. Phys. Chem.* **94**, 5477 (1990).
11. K. Andersson, M. P. Fülscher, G. Karlström, R. Lindh, P.-Å. Malmqvist, J. Olsen, B. O. Roos, A. J. Sadlej, M. R. A. Blomberg, P. E. M. Siegbahn, V. Kellö, J. Noga, M. Urban, and P.-O. Widmark, *MOLCAS Version 3*, University of Lund, Lund, Sweden, 1994.
12. K. Andersson and B. O. Roos, In *Modern Electron Structure Theory*, Vol. 1, R. Yarkony, Ed., World Scientific, New York, 1995.
13. B. O. Roos, M. P. Fülscher, Per-Åke Malmqvist, M. Merchán, and L. Serrano-Andrés, In *Quantum Mechanical Electronic Structure Calculations with Chemical Accuracy*, S.R. Langhoff, Ed., Kluwer, Dordrecht, The Netherlands, 1995.
14. K. Andersson, Ph.D. thesis, University of Lund, Lund, Sweden, 1992.
15. K. Andersson and B. O. Roos, *Int. J. Quantum Chem.* **45**, 591 (1993).
16. C. W. Murray and E. R. Davidson, *Chem. Phys. Lett.* **187**, 451 (1991).
17. P. M. Kozłowski and E. R. Davidson, *J. Chem. Phys.* **100**, 3672, (1994).
18. P. M. Kozłowski and E. R. Davidson, *Chem. Phys. Lett.* **226**, 440 (1994).
19. K. G. Dyall, *J. Chem. Phys.*, **102**, 4909 (1995).
20. K. Andersson, *Theor. Chim. Acta* **91**, 31 (1995).
21. J.-P. Malrieu, J.-L. Heully, and A. Zaitsevski, *Theor. Chim. Acta* **90**, 167 (1995).
22. B. O. Roos, in *New Challenges in Computational Quantum Chemistry*, P. J. C. Aerts, R. Broer, and P. S. Bagus, Eds., University of Groningen, Groningen, The Netherlands, 1994.
23. K. Andersson, B. O. Roos, P.-Å. Malmqvist, and P.-O. Widmark, *Chem. Phys. Lett.*, **230**, 391 (1994).
24. K. Andersson, *Chem. Phys. Lett.* **237**, 212 (1995).
25. K. Andersson, *Theor. Chim. Acta* **91**, 31 (1995).
26. B. O. Roos and K. Andersson, *Chem. Phys. Lett.*, **245**, 215 (1995).
27. P.-O. Widmark, P.-Å. Malmqvist, and B. O. Roos, *Theor. Chim. Acta* **77**, 291 (1990).
28. K. Pierloot, B. J. Persson, and B. O. Roos, *J. Phys. Chem.* **99**, 3465 (1995).
29. B. J. Persson, B. O. Roos, and K. Pierloot, *J. Chem. Phys.* **101**, 6810 (1994).
30. J. B. Foresman, M. Head-Gordon, J. A. Pople, and M. J. Frisch, *J. Phys. Chem.* **96**, 135 (1992).
31. A. Balková and R. J. Bartlett, *Chem. Phys. Lett.* **193**, 364 (1992).
32. K. Andersson and B. O. Roos, *Chem. Phys. Lett.* **191**, 507 (1992).
33. B. O. Roos, K. Andersson, and M. P. Fülscher, *Chem. Phys. Lett.* **192**, 5 (1992).
34. J. M. O. Matos, B. O. Roos, and P.-Å. Malmqvist, *J. Chem. Phys.* **86**, 1458 (1987).

35. M. Merchán, E. Ortí, and B. O. Roos, *Chem. Phys. Lett.* **226**, 27 (1994).
36. L. Serrano-Andrés, M. Merchán, I. Nebot-Gil, R. Lindh, and B. O. Roos, *J. Chem. Phys.* **98**, 3151 (1993).
37. R. Lindh, U. Ryu, and B. Liu, *J. Chem. Phys.* **95**, 5889 (1991).
38. R. Lindh and B. Liu, *manuscript* (1991).
39. J. Almlöf and P. R. Taylor, *J. Chem. Phys.* **86**, 4070 (1987).
40. P.-O. Widmark, B.J. Persson, and B. O. Roos, *Theor. Chim. Acta* **79**, 419 (1991).
41. K. Pierloot, B. Dumez, P.-O. Widmark, and B. O. Roos, *Theor. Chim. Acta* **90**, 87 (1995).
42. F. B. van Duijneveldt, *Technical Report RJ945*, IBM Research, 1970.
43. M. P. Fülscher and B. O. Roos, *Theor. Chim. Acta* **87**, 403 (1994).
44. M. P. Fülscher and B. O. Roos, *J. Am. Chem. Soc.* **117**, 2089 (1995).
45. K. Kaufmann, W. Baumeister, and M. Jungen, *J. Phys. B* **22**, 2223 (1989).
46. J. Lorentzon, P.-Å. Malmqvist, M. P. Fülscher, and B. O. Roos, *Theor. Chim. Acta* **91**, 91 (1995).
47. J. Lorentzon, M. P. Fülscher, and B. O. Roos, *J. Am. Chem. Soc.*, **117**, 9265 (1995).
48. L. Serrano-Andrés, M. Merchán, I. Nebot-Gil, B. O. Roos, and M. P. Fülscher, *J. Am. Chem. Soc.*, **115**, 6184 (1993).
49. J. Olsen, B. O. Roos, P. Jørgensen, and H. J. Aa. Jensen, *J. Chem. Phys.* **89**, 2185 (1988).
50. S. Tenno, F. Hirata, and S. Kato, *Chem. Phys. Lett.* **214**, 391 (1993).
51. P. L. Muiño and P. R. Callis, *J. Chem. Phys.* **100**, 4093 (1994).
52. J. Hylton-McCreery, R. E. Christofferson, and G. G. Hall, *J. Am. Chem. Soc.* **98**, 7191, 7198 (1976).
53. O. Tapia and O. Goscinski, *Mol. Phys.* **29**, 1653 (1975).
54. S. Miertuš, E. Scrocco, and J. Tomasi, *Chem. Phys.* **55**, 117 (1981).
55. K. V. Mikkelsen, Ågren, H. J. Aa. Jensen, and T. Helgaker, *J. Chem. Phys.* **89**, 3086 (1988).
56. G. Karlström, *J. Phys. Chem.* **92**, 1315 (1988).
57. C. J. Cramer and D. G. Truhlar, *J. Am. Chem. Soc.* **113**, 8305 (1991).
58. M. M. Karelson and M. C. Zerner, *J. Phys. Chem.* **96**, 6949 (1992).
59. A. Bernhardsson, G. Karlström, R. Lindh, and B. O. Roos, to be published.
60. K. A. Zachariasse, Th. von der Haar, A. Hebecker, U. Leinhos, and W. Kühnle, *Pure Appl. Chem.* **65**, 1745 (1993).
61. J. Lipinski, H. Chojnacki, Z. R. Grabowski, and K. Rotkiewicz, *Chem. Phys. Lett.* **70**, 449 (1980).
62. L. Serrano-Andrés, M. Merchán, B. O. Roos, and R. Lindh, *J. Am. Chem. Soc.* **117**, 3189 (1995).
63. M. Hachey, P. J. Bruna, and F. Grein, *J. Chem. Soc. Faraday Trans.* **90**, 683 (1994).
64. M. R. J. Hachey, P. J. Bruna, and F. Grein, *J. Phys. Chem.* **99**, 8050 (1995).
65. M. Merchán and B. O. Roos, *Theor. Chim. Acta*, **92**, 227 (1995).
66. E. E. Barnes and W. T. Simpson, *J. Chem. Phys.* **39**, 670 (1963).
67. R. McDiarmid and A. Sabljčić, *J. Chem. Phys.* **89**, 6086 (1988).
68. A. Gedanken and R. McDiarmid, *J. Chem. Phys.* **92**, 3237 (1990).
69. J. G. Philips, J. M. Berman, and L. Goodman, *Chem. Phys. Lett.* **167**, 16 (1990).

70. R. McDiarmid, *J. Chem. Phys.* **95**, 1530 (1991).
71. S. N. Thakur, D. Guo, T. Kundu, and L. Goodman, *Chem. Phys. Lett.* **199**, 335 (1992).
72. J. G. Philis and L. Goodman, *J. Chem. Phys.* **98**, 3795 (1993).
73. X. Xing, R. McDiarmid, J. G. Philis, and L. Goodman, *J. Chem. Phys.* **99**, 7565 (1993).
74. V. Galasso, *J. Chem. Phys.* **92**, 2495 (1990).
75. B. Hess, P. J. Bruna, R. J. Buenker, and S. D. Peyerimhoff, *Chem. Phys.* **18**, 267 (1976).
76. M. Merchán, B. O. Roos, R. McDiarmid, and X. Xing, *J. Chem. Phys.*, in press (1995).
77. S. Taylor, D. G. Wilden, and J. Comer, *Chem. Phys.* **70**, 291 (1982).
78. R. Nelson and L. Pierce, *J. Mol. Spectrosc.* **18**, 344 (1965).
79. L. Serrano-Andrés, M. Merchán, M. Fülischer, and B. O. Roos, *Chem. Phys. Lett.* **211**, 125 (1993).
80. B. O. Roos, M. Merchán, R. McDiarmid, and X. Xing, *J. Am. Chem. Soc.* **116**, 5927 (1994).
81. L. Serrano-Andrés, B. O. Roos, and M. Merchán, *Theor. Chim. Acta* **87**, 387 (1994).
82. R. P. Johnson and M. W. Schmidt, *J. Am. Chem. Soc.* **103**, 3244 (1981).
83. J. P. Malrieu and D. Maynau, *J. Am. Chem. Soc.* **104**, 3021 (1982).
84. W. E. Billups, L.-J. Lin, and E. W. Casserly, *J. Am. Chem. Soc.* **106**, 3698 (1984).
85. S. W. Staley and T. D. Norden, *J. Am. Chem. Soc.* **106**, 3699 (1984).
86. B. A. Hess, Jr., D. Michalska, and L. J. Schaad, *J. Am. Chem. Soc.* **107**, 1449 (1985).
87. D. Michalska, B. A. Hess, Jr., and L. J. Shaad, *Intern. J. Quantum Chem.* **29**, 1127 (1986).
88. T. D. Norden, S. W. Staley, W. H. Taylor, and M. D. Harmony, *J. Am. Chem. Soc.* **108**, 7912 (1986).
89. S. W. Staley and T. D. Norden, *J. Am. Chem. Soc.* **111**, 445 (1989).
90. M. Bogey, M. Cordonnier, J.-L. Destombes, J.-M. Denis, and J.-C. Guillemin, *J. Mol. Spectrosc.* **149**, 230 (1991).
91. C. Petrongolo, R. J. Buenker, and S. D. Peyerimhoff, *J. Chem. Phys.* **76**, 3655 (1982).
92. R. Lindh and B. O. Roos, *Intern. J. Quantum Chem.* **35**, 813 (1989).
93. R. González-Luque, M. Merchán, and B. O. Roos, *Z. Physik*, in press (1995).
94. M. Rubio, M. Merchán, E. Ortí, and B. O. Roos, *Chem. Phys. Lett.* **234**, 373 (1995).
95. M. Rubio, M. Merchán, E. Ortí, and B. O. Roos, *J. Chem. Phys.* **102**, 3580 (1995).
96. M. Rubio, M. Merchán, E. Ortí, and B. O. Roos, *J. Phys. Chem.*, in press (1995).
97. M. Rubio, M. Merchán, and E. Ortí, *Theor. Chim. Acta*, **91**, 17 (1995).
98. R. M. Hochstrasser, R. D. McAlpine, and J. D. Whiteman, *J. Chem. Phys.* **58**, 5078 (1973).
99. R. M. Hochstrasser and H. N. Sung, *J. Chem. Phys.* **66**, 3265 (1977).
100. A. Baca, R. Rossetti, and L. E. Brus, *J. Chem. Phys.* **70**, 5575 (1979).
101. J. Murakami, M. Ito, and K. Kaya, *J. Chem. Phys.* **74**, 6505 (1981).
102. T. G. McLaughlin and L. B. Clark, *Chem. Phys.* **31**, 11 (1978).
103. B. Dick and G. Hohlneicher, *Chem. Phys.* **94**, 131 (1985).
104. B. Nordén, R. Håkansson, and M. Sundbom, *Acta Chem. Scand.* **26**, 429 (1972).

105. J. Sagiv, A. Yogev, and Y. Mazur, *J. Am. Chem. Soc.* **99**, 6861 (1977).
106. P. Swiderek, M. Michaud, G. Hohlneicher, and L. Sanche, *Chem. Phys. Lett.* **187**, 583 (1991).
107. O. Bastiansen and S. Samdal, *J. Mol. Struct.* **128**, 115 (1985).
108. L. O. Edwards and W. T. Simpson, *J. Chem. Phys.* **53** 4237 (1970).
109. E. Ortí, P. Viruela, J. Sánchez-Marín, and F. Tomás, *J. Phys. Chem.*, **99**, 4955 (1995).
110. J. E. Chadwick and B. E. Kohler, *J. Phys. Chem.* **98**, 3631 (1994).
111. R. H. Abu-Eittah and F. A. Al-Sugeir, *Bull. Chem. Soc. Japan* **58**, 2126 (1985).
112. D. Birnbaum and B. E. Kohler, *J. Chem. Phys.* **96**, 2492 (1992).
113. D. B. Wetlaufer, in *Advances in Protein Chemistry*, Vol. 17, C. B. Anfinsen, M. L. Anson, K. Bailey, and J. T. Edsall, Eds., Academic Press, New York, 1962.
114. A. P. Demchenko, *Ultraviolet Spectroscopy of Proteins*. Springer-Verlag, Berlin, 1986.
115. L. Serrano-Andrés and B. O. Roos, *J. Amer. Chem. Soc.*, in press (1995).
116. L. Serrano-Andrés, M. P. Fülcher, B. O. Roos, and M. Merchán, *J. Phys. Chem.*, in press (1995).
117. L. Serrano-Andrés, Ph.D. thesis, University of Valencia, Valencia, Spain, 1994.
118. R. Pariser, *J. Chem. Phys.* **24**, 250 (1956).
119. J. R. Platt, *J. Chem. Phys.* **17**, 489 (1949).
120. A. Weissberger and E. C. Taylor, Eds., *The Chemistry of Heterocyclic Compounds*, Vol. 25, Wiley-Interscience, New York, 1972–1983.
121. J. M. Hollas, *Spectrochim. Acta* **19**, 753 (1963).
122. P. Ilich, *Can. J. Spectrosc.* **67**, 3274 (1987).
123. E. H. Strickland, J. Horwitz, and C. Billups, *Biochemistry* **4914**, 25 (1970).
124. A. A. Rehms and P. R. Callis, *Chem. Phys. Lett.* **140**, 83 (1987).
125. D. M. Sammeth, S. Yan, L. H. Spangler, and P. R. Callis, *J. Phys. Chem.* **94**, 7340 (1990).
126. T. L. O. Bartis, L. I. Grace, T. M. Dunn, and D. M. Lubman, *J. Phys. Chem.* **97**, 5820 (1993).
127. M. Rubio, M. Merchán, E. Ortí, and B. O. Roos, *Chem. Phys.* **179**, 395 (1994).
128. A. Z. Britten and G. Lockwood, *Spectrochim. Acta* **32A**, 1335 (1976).
129. H. Lami, *Chem. Phys. Lett.* **48**, 447 (1977).
130. W. Caminati and S. Di Bernardo, *J. Mol. Struct.* **240**, 253 (1990).
131. C. T. Chang, C. Y. Wu, A. R. Muirhead, and J. R. Lombardi, *Photochem. Photobiol.* **19**, 347 (1974).
132. H. Lami and N. Glasser, *J. Chem. Phys.* **84**, 597 (1986).
133. B. Albinsson and B. Nordén, *J. Phys. Chem.* **96**, 6204 (1992).
134. T. G. Fawcett, E. R. Bernarducci, K. Krogh-Jespersen, and H. J. Schugar, *J. Am. Chem. Soc.* **102**, 2598 (1980).
135. D. S. Caswell and T. G. Spiro, *J. Am. Chem. Soc.* **108**, 6470 (1986).
136. P. E. Grebow and T. M. Hooker, *Biopolymers* **14**, 871 (1975).
137. F. B. C. Machado and E. R. Davidson, *J. Chem. Phys.* **97**, 1881 (1992).
138. D. Christen, J. H. Griffiths, and J. Sheridan, *Z. Naturforsch.* **37A**, 1378 (1982).

139. E. Clar, *Polycyclic Hydrocarbons*, Academic Press, New York, 1964.
140. T. Shida, *Electronic Absorption Spectra of Radical Ions*, Elsevier, Amsterdam, 1988.
141. L. Serrano-Andrés, R. Lindh, B. O. Roos, and M. Merchán, *J. Phys. Chem.* **97**, 9360 (1993).
142. R. C. Dunbar, *Chem. Phys. Lett.* **32**, 508 (1975).
143. R. C. Dunbar, *Anal. Chem.* **46**, 723 (1976).
144. R. C. Dunbar and H. H.-I. Teng, *J. Am. Chem. Soc.* **100**, 2279 (1978).
145. T. Bally, S. Nitsche, K. Roth, and E. Haselbach, *J. Am. Chem. Soc.* **106**, 3927 (1984).
146. T. Bally, S. Nitsche, K. Roth, and E. Haselbach, *J. Chem. Phys.* **89**, 2528 (1985).
147. T. Bally, S. Nitsche, and K. Roth, *J. Chem. Phys.* **84**, 2577 (1986).
148. M. Beez, G. Bieri, H. Bock, and E. Heilbronner, *Helv. Chim. Acta* **56**, 1028 (1973).
149. M. Allan, J. Dannacher, and J. P. Maier, *Chem. Phys.* **73**, 3114 (1980).
150. T. B. Jones and J. P. Maier, *Intern. J. Mass. Spectrom. Ion Phys.* **31**, 287 (1979).
151. M. P. Fülischer, S. Matzinger, and T. Bally, *Chem. Phys. Lett.* **236**, 167 (1995).
152. F. Salama and L. J. Allamandola, *Nature* **358**, 42 (1992).
153. M. Schütz, M. P. Fülischer, and B. O. Roos, to be published.
154. R. Gschwind and E. Haselbach, *Helv. Chim. Acta* **62**, 941 (1979).
155. M. O. Delcourt and M. J. Rossi, *J. Phys. Chem.* **86**, 3233 (1982).
156. T. Shida and W. H. Hamill, *J. Chem. Phys.* **44**, 2375 (1966).
157. T. Shida and S. Iwata, *J. Am. Chem. Soc.* **95**, 3473 (1973).
158. A. Kira, M. Imamura, and T. Shida, *J. Phys. Chem.* **80**, 1445, (1980).
159. A. Kira, I. Nakamura, and M. Imamura, *J. Phys. Chem.* **81**, 511 (1977).
160. L. Andrews, B. J. Kelsall, and T. A. Blankenship, *J. Phys. Chem.* **86**, 2916 (1982).
161. P. A. Clark, F. Brogli, and E. Heilbronner, *Helv. Chim. Acta* **55**, 1410 (1972).
162. W. Schmidt, *J. Chem. Phys.* **66**, 828 (1977).
163. R. C. Dunbar and R. Klein, *J. Am. Chem. Soc.* **98**, 7994 (1976).
164. M. S. Kim and R. C. Dunbar, *J. Chem. Phys.* **72**, 4405 (1980).
165. F. Salama and L. J. Allamandola, *J. Chem. Phys.* **94**, 6964 (1991).
166. L. Andrews, R. S. Friedman, and B. J. Kelsall, *J. Phys. Chem.* **89**, 4016 (1985).
167. N. Otha and M. Ito, *Chem. Phys.* **20**, 71 (1977).
168. R. Pou-Américo, M. Merchán, I. Nebot-Gil, P.-Å. Malmqvist, and B. O. Roos, *J. Chem. Phys.* **101**, 4893 (1994).
169. N. Re, A. Sgamellotti, B. J. Persson, and B. O. Roos, *Organometallics* **14**, 63 (1995).
170. K. Pierloot, E. Van Praet, L. G. Vanquickenborne, and B. O. Roos, *J. Phys. Chem.* **97**, 12220 (1993).
171. K. Pierloot, E. Tsokos, and B. O. Roos, *Chem. Phys. Lett.* **214**, 583 (1993).
172. C. W. Bauschlicher Jr., P. E. M. Siegbahn, and L. G. M. Pettersson, *Theor. Chim. Acta* **74**, 479 (1988).
173. K. Andersson, B. J. Persson, and B. O. Roos, to be published.
174. C. W. Bauschlicher, S. P. Walch, and H. Partridge, *J. Chem. Phys.* **76**, 1033 (1982).
175. R. L. Martin and P. J. Hay, *J. Chem. Phys.* **75**, 4539 (1981).
176. L. A. Barnes, B. Liu, and R. Lindh, *J. Chem. Phys.* **98**, 3978 (1993).

177. K. Pierloot, E. Tsokos, and L. G. Vanquickenborne, to be published.
178. R. Åkesson, K. Pierloot, and L. G. Vanquickenborne, to be published.
179. A. B. P. Lever, *Inorganic Electronic Spectroscopy*, Elsevier, Amsterdam, 1984.
180. L. G. Vanquickenborne and A. Ceulemans, *Coord. Chem. Rev.*, **48**, 157 (1983).
181. C. K. Jørgensen, *Modern Aspects of Ligand Field Theory*, North-Holland, Amsterdam, 1971.
182. P. S. Bagus and C. J. Nelin, in *New Challenges in Computational Quantum Chemistry*, P. J. C. Aerts, R. Broer and P. S. Bagus, Eds., University of Groningen, Groningen, The Netherlands, 1994.
183. C. W. Bauschlicher and P. E. M. Siegbahn, *J. Chem. Phys.* **85**, 2802 (1986).
184. K. Pierloot and B. O. Roos, *Inorg. Chem.* **31**, 5353 (1992).
185. C. J. Marsden, D. Moncrieff, and G. E. Quelch, *J. Phys. Chem.* **98**, 2038 (1994).
186. L. G. Vanquickenborne, A. E. Vinckier, and K. Pierloot, *Inorg. Chem.*, in press (1995).
187. K. Pierloot, unpublished results, 1995.
188. K. Pierloot and L. G. Vanquickenborne, *J. Chem. Phys.* **93**, 4154 (1990).
189. K. Pierloot, E. Van Praet, and L. G. Vanquickenborne, *J. Chem. Phys.* **96**, 4163 (1992).
190. K. Pierloot, E. Van Praet, and L. G. Vanquickenborne, *J. Chem. Phys.* **102**, 1164 (1995).
191. L. G. Vanquickenborne, K. Pierloot, and E. Duyvejonck, *Chem. Phys. Lett.* **224**, 207 (1994).
192. C. Ribbing and C. Daniel, *J. Chem. Phys.* **100**, 6591 (1994).
193. M. Hargittai, O. V. Dorofeeva, and J. Tremmel, *Inorg. Chem.* **24**, 3963 (1985).
194. M. Hargittai, *Inorg. Chim. Acta* **180**, 5 (1991).
195. K. Pierloot, B. Dumez, K. Ooms, C. Ribbing, and L. G. Vanquickenborne, to be published.
196. C. W. DeKock and D. M. Gruen, *J. Chem. Phys.* **44**, 4387 (1966).
197. C. Daniel, private communication, 1995.
198. J. J. Alexander and H. B. Gray, *J. Am. Chem. Soc.* **90**, 4260 (1968).
199. N. A. Beach and H. B. Gray, *J. Am. Chem. Soc.* **90**, 5713 (1968).
200. C. F. Koerting, K. N. Walzl, and A. Kupperman, *J. Chem. Phys.* **86**, 6646 (1987).
201. M. Kotzian, N. Rösch, H. Schröder, and M. C. Zerner, *J. Am. Chem. Soc.* **111**, 7687 (1989).
202. K. Pierloot, J. Verhulst, P. Verbeke, and L. G. Vanquickenborne, *Inorg. Chem.* **28**, 3059 (1989).
203. L. G. Vanquickenborne, M. Hendrickx, I. Hyla-Kryspin, and L. Haspeslagh, *Inorg. Chem.* **25**, 885 (1986).
204. A. F. Schreiner and T. L. Brown, *J. Am. Chem. Soc.* **90**, 3366 (1968).
205. A. B. P. Lever, G. A. Ozin, A. J. L. Hanlan, W. J. Power, and H. B. Gray, *Inorg. Chem.* **18**, 2088 (1979).
206. A. D. McLean and B. Liu, *Chem. Phys. Lett.* **101**, 144 (1983).
207. G. E. Scuseria, *J. Chem. Phys.* **94**, 442 (1991).

208. R. Lindh and B. J. Persson, *J. Am. Chem. Soc.* **116**, 4963 (1994).
209. D. A. Hrovat, K. Morokuma, and W. Thatcher Borden, *J. Am. Chem. Soc.* **116**, 1072 (1994).
210. P. Borowski, K. Andersson, P.-Å Malmqvist, and B. O. Roos, *J. Chem. Phys.* **97**, 5568 (1992).
211. P. Borowski, B. O. Roos, S. C. Racine, T. J. Lee, and S. Carter, *J. Chem. Phys.* **103**, 266 (1995).
212. K. P. Huber and G. Herzberg, *Molecular Spectra and Molecular Structure*, Vol. 4, *Constants of Diatomic Molecules*, Van Nostrand Reinhold, New York, 1979.
213. V. E. Bondybey and J. H. English, *Chem. Phys. Lett.* **94**, 443 (1983).
214. S. M. Casey and D. G. Leopold, *J. Phys. Chem.* **97**, 816 (1993).
215. K. Hilpert and K. Ruthardt, *Ber. Bunsenges, Phys. Chem.* **91**, 724 (1987).
216. M. Moskovits, W. Limm, and T. Mejean, *J. Chem. Phys.* **82**, 4875 (1985).
217. H. Im and E. R. Bernstein, *J. Chem. Phys.* **88**, 7337 (1988).
218. D. Birnbaum and B. E. Kohler, *J. Chem. Phys.* **95**, 4783 (1991).